

Copyright Warning & Restrictions

The copyright law of the United States (Title 17, United States Code) governs the making of photocopies or other reproductions of copyrighted material.

Under certain conditions specified in the law, libraries and archives are authorized to furnish a photocopy or other reproduction. One of these specified conditions is that the photocopy or reproduction is not to be “used for any purpose other than private study, scholarship, or research.” If a user makes a request for, or later uses, a photocopy or reproduction for purposes in excess of “fair use” that user may be liable for copyright infringement,

This institution reserves the right to refuse to accept a copying order if, in its judgment, fulfillment of the order would involve violation of copyright law.

Please Note: The author retains the copyright while the New Jersey Institute of Technology reserves the right to distribute this thesis or dissertation

Printing note: If you do not wish to print this page, then select “Pages from: first page # to: last page #” on the print dialog screen



The Van Houten library has removed some of the personal information and all signatures from the approval page and biographical sketches of theses and dissertations in order to protect the identity of NJIT graduates and faculty.

ABSTRACT

CONTINUITY OF BRIDGES COMPOSED OF SIMPLE-SPAN PRECAST PRESTRESSED CONCRETE GIRDERS MADE CONTINUOUS

**by
Libin Yin**

Bridges composed of simple-span, precast, prestressed concrete girders made continuous via cast-in-place decks and diaphragms are continuous only for live loads and superimposed dead loads. The continuity diaphragms often crack due to time dependent effects in the girders. These cracks not only impair bridge aesthetics and durability, but also reduce “degree of continuity”. A related issue is that joint construction is time consuming and expensive due to reinforcement congestion. This dissertation presents a series of field tests, analytical studies, and laboratory experiments concerning the design and performance of this type of bridge.

Based on a survey of the state departments of transportation in the U.S. and a literature review, the current practice is evaluated. Three bridges in New Jersey were instrumented and tested. Results show that the degree of continuity ranges from 0% to 90%. A comparison of the support detail suggests that anchor bolts be sheathed to allow free rotation of the girders.

A computer program called “CONTINUITY” is developed to analyze the restraint moments and the degree of continuity of bridges up to four continuous spans. The program takes into account concrete creep and shrinkage and strand relaxation. For concrete creep and shrinkage, users can choose from three different models: ACI-209 (American Concrete Institute), CEB-FIP (European) and HPC (High Performance Concrete). Support details and cracking of the composite girder and diaphragm sections

are also considered in the program.

Three-dimensional finite element analyses have been carried out to further study factors affecting restraint moments. The study confirms that the girder age at continuity plays a vital role in developing the restraint moments and that the amount of positive moment reinforcement at the support has a negligible effect on the resultant mid-span moment.

As part of this research a new continuity connection is developed using Carbon Fiber Reinforced Polymer (CFRP) composites. By making the girders continuous for slab self-weight as well, the additional negative moment over the continuity support will counteract the positive restraint moment and limit it below the cracking moment. Thus, cracks will not form and positive moment reinforcement is not needed in the diaphragm. Total 20 laboratory tests were carried out to validate the new connection. Results show that CFRP is effective for improving the continuity and performance of bridges of this type. Recommendations for the use of CFRP reinforcement and a design example are also presented.

**CONTINUITY OF BRIDGES COMPOSED OF SIMPLE-SPAN PRECAST
PRESTRESSED CONCRETE GIRDERS MADE CONTINUOUS**

**by
Libin Yin**

**A Dissertation
Submitted to the Faculty of
New Jersey Institute of Technology
In Partial Fulfillment of the Requirements for the Degree of
Doctor of Philosophy in Civil Engineering**

Department of Civil and Environmental Engineering

August 2004

Copyright © 2004 by Libin Yin

ALL RIGHTS RESERVED

APPROVAL PAGE

CONTINUITY OF BRIDGES COMPOSED OF SIMPLE-SPAN PRECAST PRESTRESSED CONCRETE GIRDERS MADE CONTINUOUS

Libin Yin

M. Ala Saadeghvaziri, Dissertation Advisor
Professor of Civil and Environmental Engineering, NJIT

Date

William R. Spillers, Dissertation Co-Advisor
Distinguished Professor of Civil and Environmental Engineering, NJIT

Date

John R. Schuring, Committee Member
Professor and Chair of Civil and Environmental Engineering, NJIT

Date

Walter Konon, Committee Member
Professor and Associate Chair of Civil and Environmental Engineering, NJIT

Date

Bala Sivakumar, Committee Member
Chief Engineer of Lichtenstein Consulting Engineers, Inc.

Date

BIOGRAPHICAL SKETCH

Author: Libin Yin
Degree: Doctor of Philosophy
Date: August 2004

Undergraduate and Graduate Education:

- Doctor of Philosophy in Civil Engineering,
New Jersey institute of Technology, Newark, NJ, 2004
- Master of Science in Civil Engineering,
Northern Jiaotong University, Beijing, P. R. China, 1995
- Bachelor of Science in Civil Engineering,
Northern Jiaotong University, Beijing, P. R. China, 1992

Major: Civil Engineering

Publications:

Libin Yin, M. Ala Saadeghvaziri And William R. Spillers, "Simple-Span Precast Prestressed Concrete Girders Made Continuous", ASCE Structures Congress - 2005, New York, NY. (Will be published in 2005)

M. Ala Saadeghvaziri, Libin Yin and William R. Spillers, "New Continuity Connection Using Fiber Reinforced Composites", 4th International Conference on Advanced Composite Materials in Bridges and Structures, Alberta, Canada, Jul. 2004.

Libin Yin, Structural Analysis of Bridges: 3-D Beam Elements and Truss Elements with Rigid Arms and Mode Shape Analysis Based on the Improved Lanczos Method, Northern Jiaotong University, Beijing, China, Mar. 1995.

Daotang Wang, Jin Wang and Libin Yin, "The General Preprocessing System for Structural Analysis", the Third National Conference of Computer Applications, Beijing, China, Apr. 1995.

To my beloved family

ACKNOWLEDGMENT

I would like to express my cordial appreciation to my advisors, professor M. Ala Saadeghvaziri and professor William R. Spillers for their consistent and insightful input to this research. I would also like to express my sincere gratitude to the distinguished committee members: professor John Schuring, professor Walter Konon and chief engineer Bala Sivakumar. Their invaluable suggestions and comments have greatly improved the quality of this dissertation.

Funding for this research is provided by the New Jersey Department of Transportation. This is appreciated by the author. Special thanks are given to Mr. Allyn Luke and my friends: Xiaobin Lu, Jian Chen and Sun Punurai for their help with the experiments.

Finally, I would like to thank my parents, my wife and my son for their understanding and consistent support. Without them, this dissertation couldn't come true.

TABLE OF CONTENTS

Chapter	Page
1 INTRODUCTION.....	1
1.1 Background	1
1.2 Literature Review	3
1.2.1 Time Dependent Effects	3
1.2.2 Different Connections	8
1.3 Results of Survey	14
1.4 Objectives	20
1.5 Originality of Research	21
1.6 Organization of the Dissertation	22
2 FIELD TESTS	23
2.1 Introduction	23
2.2 I-287 N.B. over Skyline Drive	24
2.2.1 Bridge Description	24
2.2.2 Instrumentation	25
2.2.3 Test Results	26
2.3 I-287 N.B. over Darlington Ave	29
2.3.1 Bridge Description	29
2.3.2 Instrumentation	33
2.3.3 Results and Analysis	35
2.3.4 Degree of Continuity	37

TABLE OF CONTENTS
(Continued)

Chapter	Page
2.4 Rt. 1&9 S.B. Section 2AG	39
2.4.1 Bridge Overview	39
2.4.2 Crack Patterns	40
2.4.3 Test Procedures	44
2.4.4 Test Results	46
2.4.5 Degree of Continuity	49
2.5 Analysis of Support Details	55
2.6 Conclusions and Recommendations	62
3 FINITE ELEMENT ANALYSES	64
3.1 The Finite Element Model	65
3.1.1 Material Models	65
3.1.2 Finite Element Model	68
3.2 Comparison with PCA Tests and Other Analytical Methods	70
3.2.1 PCA Test Outline	70
3.2.2 Comparison of Results	72
3.3 Parametric Study	77
3.3.1 Girder Age at Deck Casting	77
3.3.2 Amount of Positive Moment Reinforcement	81
4 THE COMPUTER PROGRAM - CONTINUITY	84
4.1 Introduction	84

TABLE OF CONTENTS
(Continued)

Chapter	Page
4.2 Concrete Creep and Shrinkage Models	85
4.2.1 ACI-209 Model	85
4.2.2 CEB-FIP Model	85
4.2.3 Creep and Shrinkage Models for High Performance Concrete	90
4.3 Algorithm	93
4.4 Verification	97
4.5 The Graphical User Interface	98
4.6 Menu Commands	108
4.7 Getting Results	109
5 THE NEW CONTINUITY CONNECTION	110
5.1 Concept	110
5.2 Why CFRP?	111
5.3 Lab Tests	112
5.3.1 Introduction	112
5.3.2 Properties of CFRP and Epoxy Resin	116
5.3.3 Group I Tests	117
5.3.4 Group II Tests	127
5.3.5 Conclusions on Lab Tests	138
5.4 A Design Example	138
5.5 Standard Drawings and Construction Procedure	145

TABLE OF CONTENTS
(Continued)

Chapter	Page
6 CONCLUSIONS	148
6.1 Summary	148
6.2 Conclusions	149
6.3 Recommended Research	150
REFERENCES	152

LIST OF TABLES

Table	Page
1.1 A Cost Comparison of Different Connections	14
2.1 Gage Readings when DOT Truck Passed I-287 NB over Skyline Drive	29
2.2 Comparison of Midspan and Diaphragm Stresses	57
3.1 Material Properties of PCA Specimens	72
5.1 Summary of Beam Geometry and Materials	115
5.2 Properties of CFRP Strips	116
5.3 Properties of Epoxy Resin Used with CFRP Strips	116
5.4 Properties of Cured CFRP Sheets	116
5.5 Properties of Epoxy Resin Used with CFRP Sheets	116
5.6 Summary of Group I Tests	127
5.7 Summary of Group II Tests	137
5.8 Amount Needed for Different Types of CFRP Fabric Sheet	141

LIST OF FIGURES

Figure	Page
1.1 Formation of positive restraint moment under time dependent effects	2
1.2 Keyed scarf connection	8
1.3 Partial post-tensioned connections	9
1.4 Bishop's post-tensioning method	10
1.5 Post-tensioning of pre-strands	12
1.6 Positive connections investigated by PCA	13
1.7 Connection details of different states	18
2.1 Support details	23
2.2 Layout and instrumentation of I-287 NB over Skyline Dr, Mahwah, NJ	25
2.3 Instrumentation on girders (I-287 NB over Skyline Drive)	26
2.4 Diaphragm bottom crack, I-287NB over Skyline Drive	27
2.5 Response of gages NB and SB	28
2.6 Girder cross section (from design drawing)	30
2.7 Strand layout of girders (from design drawing)	30
2.8 Positive moment connection over piers (from design drawing)	31
2.9 Diaphragm detail (from design drawing)	32
2.10 Instrumentation on I-287 NB over Darlington Ave, Mahwah, NJ	33
2.11 Instrumentation on girders	34
2.12 Typical readings (all gages)	35
2.13 Readings of bottom gages when a truck is passing over	36

LIST OF FIGURES
(Continued)

Figure	Page
2.14 Theoretical strains at mid-spans and girder ends	38
2.15 Rt. 1&9 S.B. section 2AG, Newark	40
2.16 Diaphragm crack at fascia beam (Rt. 1&9, Newark)	41
2.17 Typical diaphragm crack at inner beams (Rt. 1&9, Newark)	41
2.18 A close-up of the crushed concrete at fascia beam (Rt. 1&9, Newark)	42
2.19 Diaphragm details at fixed piers (Rt. 1&9 design drawings)	43
2.20 Installing strain gage at mid-span and monitoring responses	45
2.21 Instrumentation layout of Rt. 1&9 tests (Elevation)	45
2.22 Girder top gages near supports	46
2.23 Bottom gages near supports	47
2.24 Strain history of mid-span gages from test	48
2.25 LVDT and DCDT readings	49
2.26 Model 1 support detail	50
2.27 Reaction in anchor rods from model 1	51
2.28 Model 2 support detail	52
2.29 Analytical mid-span strains from model 2	53
2.30 Analytical mid-span strains from model 3	54
2.31 2-D finite element model of a 2-span bridge	56
2.32 Comparison of horizontal stresses at midspan	59
2.33 Comparison of horizontal stresses at the support	60

LIST OF FIGURES
(Continued)

Figure	Page
2.34 Comparison of vertical stresses at the support	62
3.1 Finite element model	70
3.2 Cross section of PCA specimens	71
3.3 Comparison of central support reaction of beam3/4	73
3.4 Comparison of central support reaction of beam1/2	74
3.5 Variation of central support moment with load at different girder ages	76
3.6 Variation of mid-span moment with girder age at deck casting	79
3.7 Variation of central support moment with girder age at deck casting	80
3.8 Variation of mid-span moment with amount of +M reinforcement	82
3.9 Variation of support moment with amount of +M reinforcement	83
4.1 Flow chart of CONTINUITY	98
4.2 Verification with beam3/4	99
4.3 Verification with beam1/2	100
4.4 I-girder dimensions	101
4.5 Box-girder dimensions	102
4.6 The Span tab	103
4.7 The Time tab	104
4.8 The Reinforcement tab (span 1)	105
4.9 The Reinforcement tab (span 3)	106
4.10 The Girder Concrete tab	107

LIST OF FIGURES
(Continued)

Figure	Page
4.11 The Output tab	108
4.12 The Results tab	109
5.1 New connection	112
5.2 Beam 1 details	119
5.3 Details of beams 2, 1R and 2D	119
5.4 Test setup of beams 1, 2, 1R and 2D	120
5.5 Testing of beam 2	120
5.6 Test results of beams 1, 2, 1R and 2D	121
5.7 Failure mode of beam 2 (left) and beam 2D (right)	122
5.8 Test setup of beams 3 and 4	123
5.9 Test setup and failure mode of beams 3 and 4	123
5.10 Test results of beams 3 and 4	124
5.11 Beam 5 setup	125
5.12 Beam 5 under test	126
5.13 Test results of beam 5	127
5.14 Details of beams 6 to 11	130
5.15 Load-deflection of beams 6 to 11	131
5.16 Failure modes of beams 7 to 11	132
5.17 Details of beams 12 to 16	133
5.18 Test setup and failure modes of beams 12 to 16	134

LIST OF FIGURES
(Continued)

Figure	Page
5.19 Load-deflection curves for beams 12 to 14 with different bonding length	135
5.20 Load-deflection curves for beams 15 and 16 with different bonding length	136
5.21 Detail of beams 17 and 18	137
5.22 CFRP rupture of beams 17 (left) and 18 (right)	137
5.23 Analytical and test results of beams 17 and 18.....	138
5.24 Cross-sectional Analysis	142
5.25 Comparison of midspan moments ($C=3.25$, $\epsilon=600 \times 10^{-6}$ in/in)	144
5.26 Comparison of support moments ($C=3.25$, $\epsilon=600 \times 10^{-6}$ in/in)	145
5.27 Comparison of midspan moments ($C=2.0$, $\epsilon=600 \times 10^{-6}$ in/in)	146
5.28 Comparison of support moments ($C=2.0$, $\epsilon=600 \times 10^{-6}$ in/in)	146
5.29 The proposed new continuity connection	148

CHAPTER 1

INTRODUCTION

1.1 Background

Bridges composed of simple-span precast prestressed concrete girders made continuous through cast-in-place decks and diaphragms have been widely used in the United States since 1960's. These bridges are typically simply supported for deck and girder self-weight, and continuous for live loads and super-imposed dead loads. The design of this type of bridge is based on a series of experimental and analytical studies conducted by Portland Cement Association (PCA)^[2~8].

The construction of this kind of bridge includes the following steps:

1. Erecting and aligning precast prestressed girders.
2. Connecting positive moment reinforcement.
3. Installing diaphragm and deck reinforcement.
4. Casting diaphragm and deck concrete.

The advantage of this kind of construction is that it achieves continuity under live load and secondary dead loads (overlay, parapets etc.). It is still simply supported under girder, deck self-weight and construction loads. Due to time dependent effects (mainly creep of concrete), the girders tend to camber upward even after continuity is established. The established continuity tends to keep the girder ends from rotating, which results in positive restraint moment in the girders over the piers (see Figure1.1). Because the positive moment reinforcement in the diaphragms is not designed properly, cracks usually develop at the bottom of the diaphragms. These cracks not only impair

bridge aesthetics, but also cause corrosion of the reinforcement in the diaphragms, leading to maintenance problems.

For the negative moment to grow, the diaphragm cracks must close first, which needs relatively large live loads. As a result, the continuity of such bridges ranges from 0% to 100%, depending on the loading condition, construction sequence, material properties of the concrete and reinforcement, and structural parameters such as span length, girder geometry, etc.

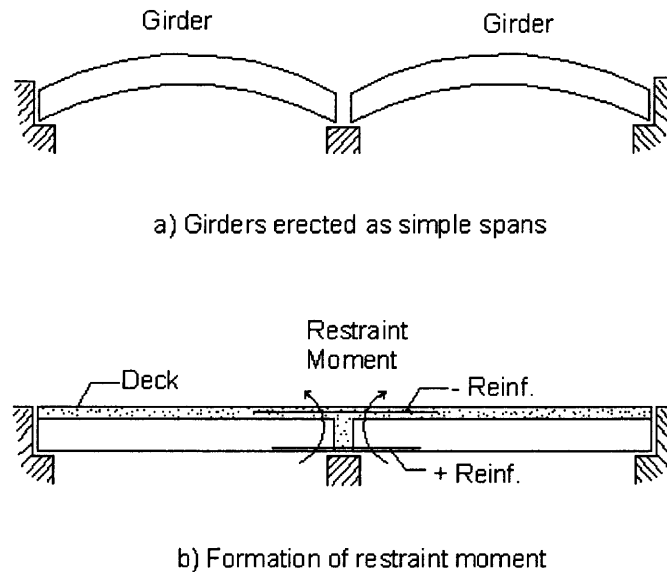


Figure 1.1 Formation of positive restraint moment under time dependent effects.

From a maintenance perspective, continuous spans are more advantageous than simple spans since they eliminate expansion joints. If designed properly, continuous concrete bridges can be maintenance free, while bridges composed of simple spans need regular inspection and maintenance. From a structural point of view, it is desirable to achieve continuity not only for live loads, but also for girder and slab dead loads. More continuity means shallower sections or longer spans, which in turn will reduce the total

cost of the bridge.

Continuity under girder self-weight requires temporary supports shoring within the spans if girders are made continuous on top of piers, or more complex erection procedures if they are made continuous on the ground. Either case could be expensive or even impossible when crossing traffic lanes or bodies of water. But continuity under slab self-weight is relatively easy to achieve through moment connections of the girders at their supports prior to deck and diaphragm castings. Actually, many connection methods have been investigated since 1960's. These connections will be discussed in part 2 of the literature review.

Another issue concerning this type of bridge is the support detail. Because the girders are first erected as simply supported, two bearing pads are typically provided over each continuity pier. Many states including New Jersey also provide anchor rods in the diaphragm to prevent uplifting. These complications make the support behave differently than a conventional pin support. The effects of these support details on the performance of the bridge need to be studied.

1.2 Literature Review

1.2.1 Time Dependent Effects

Time dependent effects include creep of concrete, differential shrinkage between the girder and deck concrete, and relaxation of prestressing strands. These effects will not develop restraint moments in simply supported structures, but in continuous structures, restraint moments will develop at interior supports. Basically, creep of concrete can cause positive restraint moments, while differential shrinkage and strand relaxation cause

negative restraint moments at inner piers.

In the 1960's, the Research and Development Laboratories of PCA carried out a series of extensive experimental and analytical studies of precast prestressed I-shaped girders with a continuous in-situ cast deck slab ^[2~8]. A series of half-scale and even full size specimens was tested both at service and ultimate load levels. Long-term observations were carried out to investigate the time dependent effects. The negative moment connection was provided by steel reinforcement in the deck slab. Two types of positive moment connection were investigated: hooked bar connection and welded bar connection. It was concluded that the welded bar connection was more reliable both from strength and serviceability points of view.

The studies also concluded that “the deformations due to creep and differential shrinkage do not influence the ultimate load carrying capacity of a continuous girder”, and “the influence of creep and shrinkage is restricted to deformations and the possibility of cracking at service load level”^[6]. Estimates of restraint moments due to creep and differential shrinkage based on the rate of creep and the effective modulus methods were presented. Because of the limited information about creep and shrinkage at that time, the same properties were used for deck concrete and girder concrete. Besides, shrinkage was assumed to be proportional to creep. Construction details like girder age at deck casting, girder age at live load application, and the casting sequence of deck and diaphragm were not considered in the study. Due to computational limits, only elastic analyses were carried out.

In the late 1980's, the Construction Technology Laboratories (CTL) investigated the time dependent effects of this type of bridge. A computer program, PBEAM,

developed by C. Suttikan^[9] was used. The PBEAM utilized both the rate of creep and the superposition method for concrete creep, and incorporated an incremental analysis to obtain the time history of the girder response. Based on parametric studies using PBEAM, two simplified computer programs called BRIDGERM and BRIDGELL were developed as design tools for this type of bridge. These programs were actually based on the PCA method, but incorporated ACI-209 concrete creep and shrinkage models. Finally, they concluded that "the presence of positive moment connection in the diaphragms has negligible effect on the reduction of resultant mid-span service moments"^[10] and no positive moment reinforcement should be used in the connection. Design examples and recommended specifications were also included, but they were not adopted by AASHTO because there were no experiments to support their conclusions. Besides, large cracks will form in the continuity diaphragm due to live load and time dependent effects if no positive moment reinforcement is provided. These cracks can impair the aesthetics of the bridge and cause corrosion of the diaphragm reinforcement.

The latest research on this subject was conducted in 2003 by R. A. Miller^[28] (et al.) in NCHRP (National Cooperative Highway Research Program) Project 12-53. The first phase of this research included a survey on the use and type of the negative and positive moment connections and an analytical study carried out by Mirmiran and Kulkarni. A computer program called RESTRAINT was developed. It considered the nonlinear stress-strain response of the materials and the stiffness change of the structure under time dependent effects. The program was verified with PCA and CTL methods and a parametric study was carried out to investigate the factors affecting time-dependent restraint moments. The study confirmed CTL's statement that positive moment

reinforcement has negligible effect on reducing the resultant mid-span moments. But also concluded that “a minimum amount of positive moment reinforcement equivalent to $1.2M_{cr}$ ”^[11] should be used to limit the crack width in the diaphragm and to avoid significant loss of continuity, where M_{cr} is the cracking moment of the diaphragm section.

The second phase included an experimental study of eight full-scale specimens: six 32' long specimens with AASHTO Type II girders and two 100' long specimens with AASHTO Type III girders. Each specimen was composed of two girders connected by a 10" diaphragm and a composite slab.

Each of the six 32' long specimens incorporated a positive moment connection detail: extended strand, extended bar, extended strand with girder ends embedded 6" into the diaphragm, extended bar with girder ends embedded 6" into the diaphragm, extended bar with girder ends embedded 6" into the diaphragm and additional stirrups in the diaphragm, and extended bar with girder ends embedded 6" into the diaphragm and horizontal bars placed through the web of the girders. Results showed that “both the extended strand and the extended bar connections developed sufficient strength. Embedding the girders into the diaphragm seemed to improve the connection performance, but the improvement was difficult to quantify. Adding additional stirrups in the diaphragm area did not improve strength, but did improve ductility and may be beneficial in seismic applications. Placing horizontal bars through the webs of the girders improved strength, stiffness and ductility, but the failure mode was cracking of the girders”^[28]. No particular positive moment connection detail was recommended.

The two 100' specimens were 2-span continuous with a 10" diaphragm between

the girders. For the positive moment connection, the first specimen utilized extended bars while the second used extended strands. All had a strength of $1.2M_{cr}$, where M_{cr} is the positive cracking moment of the composite section. Time-dependent effects were simulated by post-tensioning the girders and jacking up the girder ends. After cracking the positive moment connection, the beams were tested for live load continuity. The second specimen was also tested for negative moment capacity. It was concluded that the connections maintained continuity even when cracked. Based on the study, changes to the AASHTO LRFD Specifications were proposed. The major change was to provide an amount of positive moment reinforcement equivalent to $1.2 M_{cr}$.

The degree of continuity depends on the level of the time dependent effects and the level of live load. First, if small time dependent effects develop while the live load is relatively large, the diaphragm cracks will be closed and continuity is maintained. Second, if a large positive restraint moment develops and the live load is relatively small, continuity is also maintained because the negative live load moment over the support is not big enough to counteract the positive restraint moment. For the two 100' long specimens, the positive moment applied to the connection was 795 kip-ft and 1,250 kip-ft, respectively. The negative live load moment was only 365 kip-ft, much smaller than the positive moment.

1.2.2 Different Connections

Basically, the connections that make simple spans into continuous ones can be divided into two categories: connections over the piers and connections off the piers. From structural point of view, the connections should be placed at the inflection points of continuous beams, where moments are zero, and only shears need to be transferred. A. G. Bishara ^[12] implemented this idea in 1972. He designed and tested a 110' long, two-span continuous beam, composed of three precast prestressed segments joined together near the inflection points. He confirmed the feasibility of the "Keyed Scarf Connection" and concluded that the beam was "continuous at all load levels". See Figure 1.2.

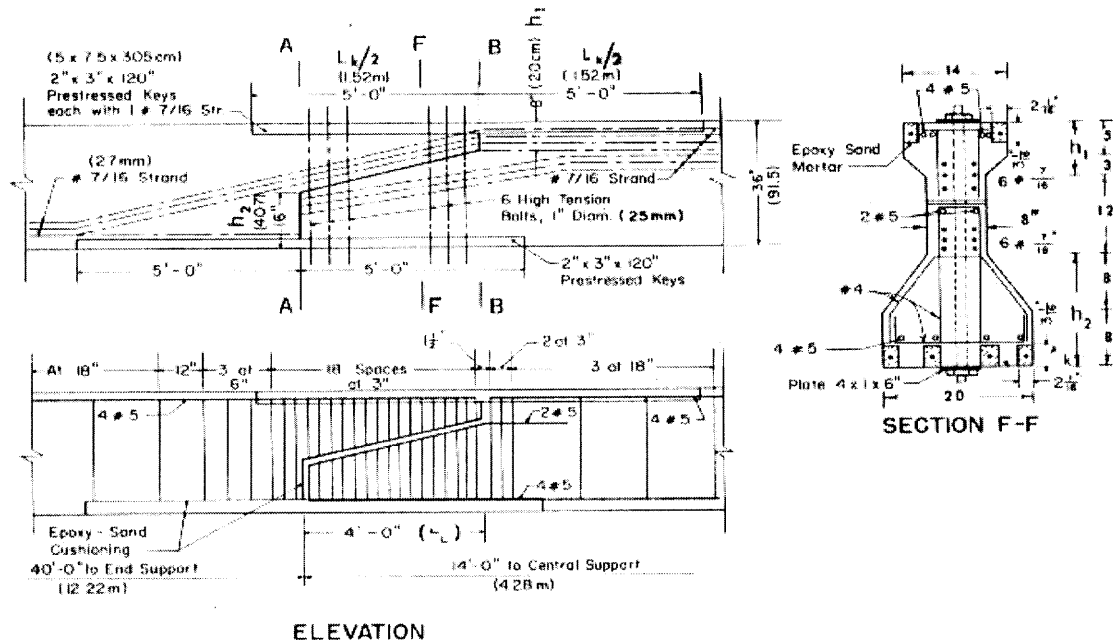


Figure 1.2 Keyed scarf connection ^[12].

The only disadvantage of this method is that it needs additional temporary supports or more cranes during construction, which could be difficult and costly when crossing rivers or traffic. Probably this is the reason for its lack of widespread application.

All the following connections are located over the piers. They can further be divided into two sub-groups: prestressed versus normal reinforced concrete connections. For prestressed connections, there are whole length post-tensioned and partial post-tensioned connections.

Full length post-tensioning can achieve full continuity but it “requires full length ducts and usually necessitates widening the girder webs.” It also “requires end blocks to resist stress concentrations at the anchorage zones” and “special contractors to perform the post-tensioning and grouting”^[14].

Partial post-tensioned connections can achieve the same continuity and avoid the need for professional post-tensioning contractors. Several such methods are illustrated in Figure 1.3.

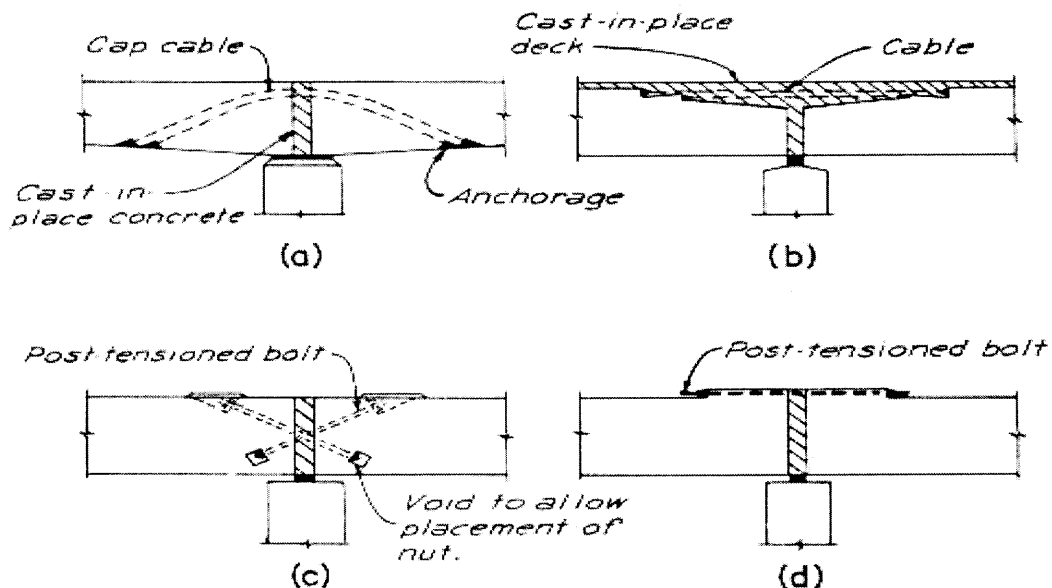


Figure 1.3 Partial post-tensioned connections.

E. D. Bishop proposed a plate connection in 1962^[13]. It includes the following steps (see Figure 1.4):

- All beams are erected as simple spans.
- The end of one beam is jacked upward a calculated amount at the first support.
- The beams are connected at the second support by welding together plates cast into the ends of the top and bottom flanges.
- The raised end is lowered to its final position, thus developing a bending moment at the support equal to that caused by the self-weight of the continuous beam.
- Repeat the above steps as required.

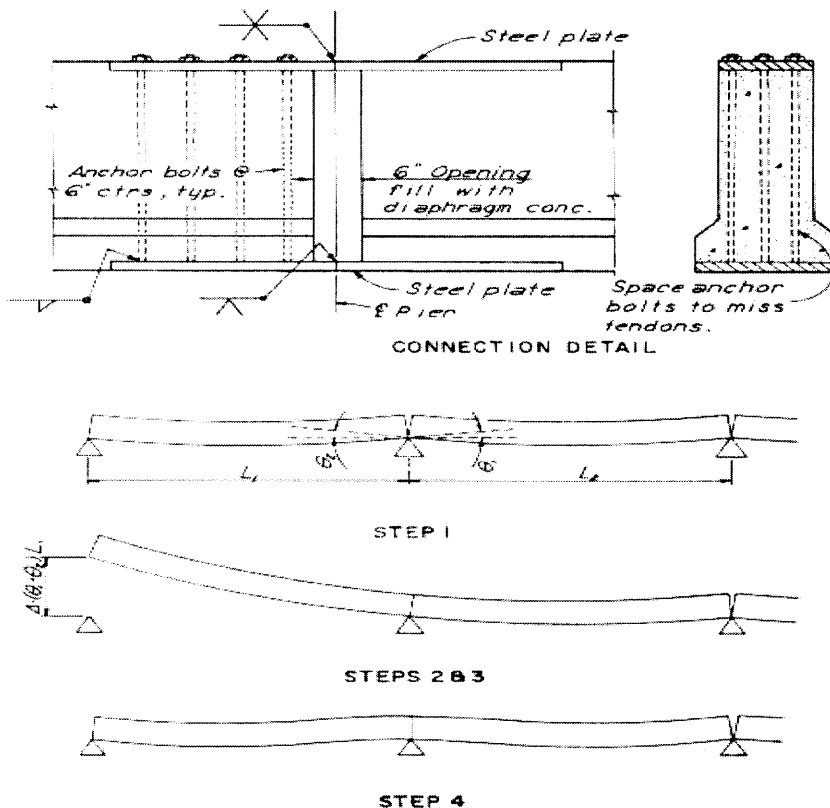


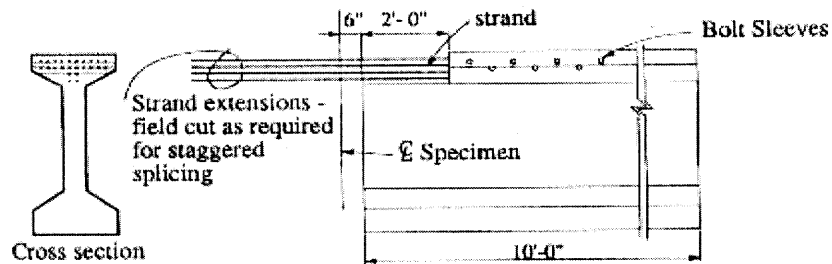
Figure 1.4 Bishop's post-tensioning method.

It's a very smart solution, but there are some drawbacks. First, this method changes the loading condition under beam self-weight from simply supported to a cantilever. This requires additional reinforcements in the upper part of the beams. Second, it's difficult to construct. The steel plates, especially the bottom ones are not easy to weld because of the limited space, and the welded plates can affect the diaphragm concrete casting.

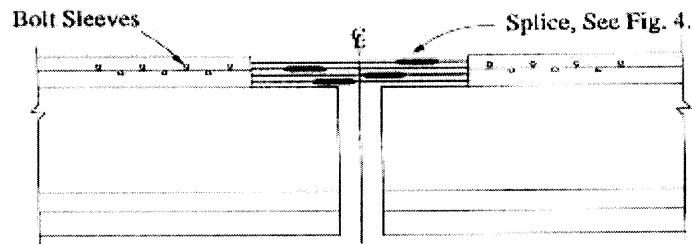
Another partial post-tensioning method, which utilized the pre-tensioning strands in the beams, was developed by M. K. Tadros in 1993 ^[15]. It involves the following steps: 1) bend the bottom prestressing strands to the top at girder ends, 2) splice the bent strands with special anchors, 3) jack the girders away from the support to obtain prestress in the strands, and 4) pour diaphragm concrete (see Figure 1.5). This method requires post-tensioning contractors and special splice manufacturers.

Reinforced concrete connections are common in practice. Current AASHTO Specification falls into this category. Many states including New Jersey use this type of connection. It was first investigated by PCA ^[2-8]. Both negative and positive moment connections were studied. For negative moment connection, it was concluded that conventional deformed rebars in the deck slab could develop adequate resistant moment both for static and dynamic loads "if this type of connection is designed so that its static ultimate strength is 2.5 times the design moment including impact effects"^[4]. Two types of positive connections were investigated (see Figure 1.6). The study showed that welded connections performed well under positive moments caused by time dependent effects, while the hook connections were not as satisfactory with respect to ultimate strength, deflection and crack control. However, the hooked rebar could develop its yield

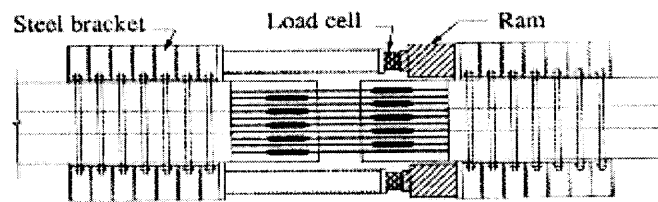
strength “if the inside radius of the hook is not less than the diameter of the bar, and if the distance from the end face of the precast girder to the inside face of the hook is equal to at least 12 times the bar diameter” [4].



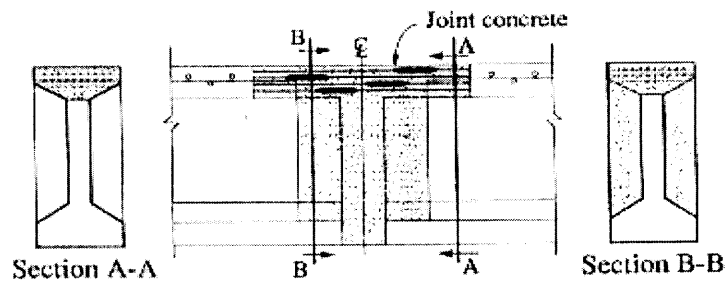
a) Precast girder, side view



b) Strands spliced and all slack removed, side view

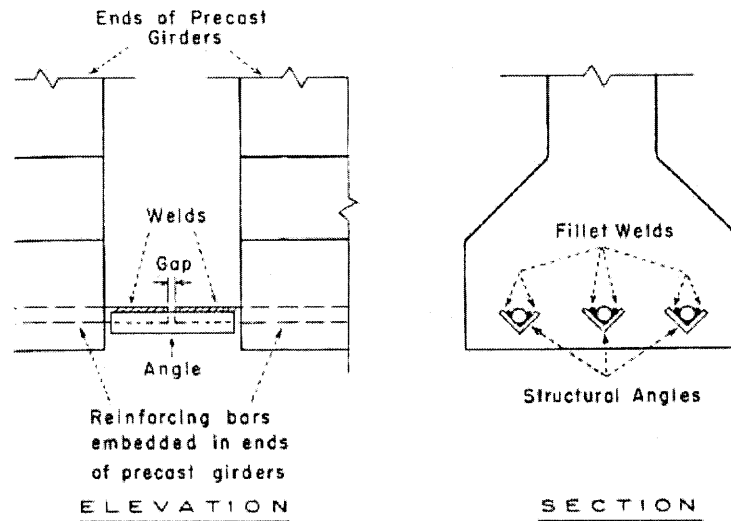


c) Jacking operation, top view

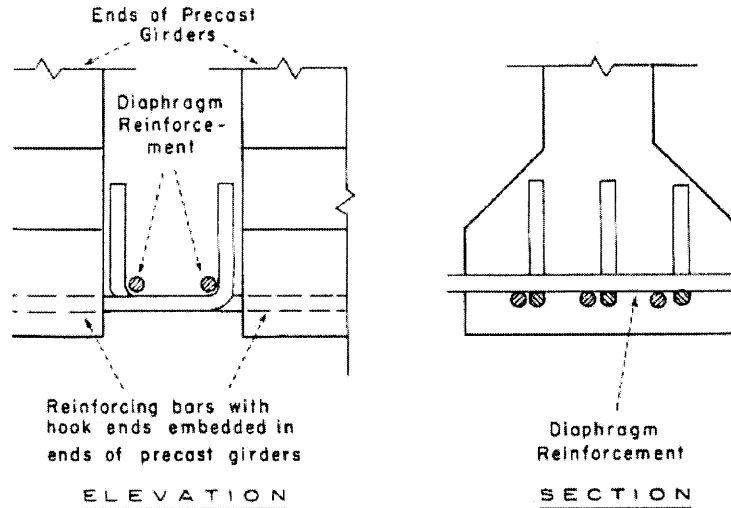


d) Joint is complete, side view

Figure 1.5 Post-tensioning of pre-strands.



(a) Welded bars connection.



(b) Hooked bar connection.

Figure 1.6 Positive moment connections investigated by PCA.

Z. Ma, X. Huo, M. K. Tadros and M. Baishya^[16] proposed another attractive reinforced concrete connection using threaded rods. These rods are embedded in the top flange of the girders and are coupled together in the field by a steel hardware. After coupling the threaded rods, the diaphragm and deck concrete are cast. One great advantage of this method is that it can achieve continuity not only for live load and

superimposed dead load, but also for the dead load of the slab. The added continuity can reduce the number of strands in the girders and save cost. Besides, it is relatively easy to construct. For the positive moment reinforcement, Ma (et al.)^[16] recommended extending and bending strands at the bottom of the girders. One possible problem with this design is that the bulky steel hardware may aggravate the reinforcement congestion in the diaphragm.

A cost comparison of different connections was made by M. A. Saleh, A. Einea and M. K. Tadros^[14]. Four methods were investigated: current practice, full length post-tensioning, threaded rods, and pretensioned strand splicing (Table 1.1). The current practice was selected as a base for comparison. The threaded rod connection is found to be the most economical. Moreover, it needs no special contractors, and it's the easiest to construct, except for the above mentioned reinforcement congestion.

Table 1.1 A Cost Comparison of Different Connections^[14]

Connection Type	Incremental Cost (\$/ft ²)
Current practice	0.00
Full length post-tensioning	+0.90
Threaded rods	-0.15
Strand splicing	+0.10

1.3 Results of Survey

To gage the experience of other highway agencies with the design of continuity connections and to determine their practice vis-à-vis the NCHRP Report 322 recommendations, a survey was developed and distributed to the Department of

Transportation of all states. Twenty-seven states responded (AK, AL, CA, CO, CT, GA, HI, ID, IA, IL, KS, LA, ME, MI, MT, NE, NH, NJ, NV, NY, PA, SC, TN, TX, UT, WA and WI). The survey and all the responses are included in the CD-ROM. Here are some general conclusions from the survey:

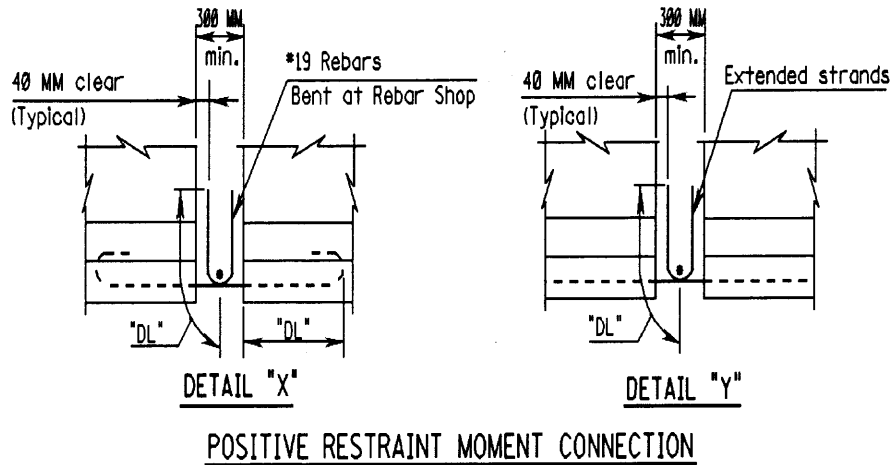
- **Usage.** This kind of construction (providing negative moment reinforcement in the deck and positive moment reinforcement at the diaphragm bottom) is widely used all across the United States. 25 out of 27 states use it, among which 17 states built more than 10 such bridges in the past 5 years.
- **Maintenance.** Many states use it as a measure to eliminate deck joints and save on maintenance costs.
- **Constructability.** Many of the responses cite difficulty in making the continuity connections when they have to deal with projecting reinforcing bars or prestressing strands.
- **Satisfaction.** In general most are happy with this type of construction. On the other hand, Alabama, with some 200 bridges experience, says that they no longer use this type of construction. They cite serious thermal stress problems that led to cracking of the continuous joints. It has been suggested that Alabama's problems are the result of poor detailing.
- **Cracks.** 10 out of 27 states that use this kind of construction experience cracking in the continuity diaphragm because of time dependent effects and live load combinations.
- **Analysis.** In the 25 states that use this kind of construction, 10 states design girders as simply supported for all loads, essentially not taking the advantage of structural continuity. This reinforces the fact that the connection is used more to eliminate a joint than anything else.
- **Degree of continuity.** None of the states have conducted any experimental work to determine the actual degree of continuity.
- **Positive moment reinforcement.** Many of those states that employ the continuity connection use a minimum amount of positive moment reinforcement ($1.2M_{cr}$, where M_{cr} is the positive cracking moment of the composite section). However, this reinforcement is not designed for any specific load. It is believed that it will enhance "structural integrity" and provide "redundancy."
- **Seismic issues.** Several states cite the continuity connection as helping them with seismic problems.

In general, the detail of the positive moment reinforcement, if used, is similar to that used by the New Jersey Department of Transportation. However, the State of New York uses welded bars for I-Beam connections. New York also places the anchor bolts in the girder ends using prefabricated holes. A couple of states (Connecticut and Texas) do not use this type of bridge at all, while several other states (GA, HI, ME, NH, NV) have only one or two bridges with continuity connections. It should be noted that there are states such as Michigan and Utah that do not use positive moment reinforcement in their continuity joints at all and are satisfied with their performance. However, both Michigan and Utah design their bridges as simply supported for all loads. The States of Alabama, Colorado, Illinois, Michigan, Pennsylvania, South Carolina, Tennessee, and Wisconsin have the most experience with this type of bridge. Of these states, Alabama reports dissatisfaction with the connection due to cracking. Alabama practice now is not to provide any positive moment reinforcement. To eliminate open joints, some spans are designed as “only the slab poured continuous with no connection of the girder ends.”

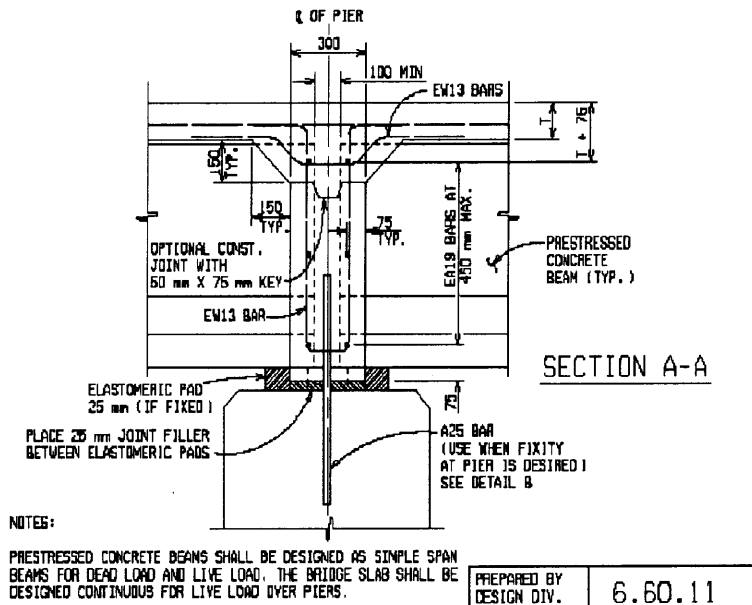
The State of Georgia limited the use of continuity connections because of difficulty in construction and cracking of “the end of the heavily reinforced areas of beams (about ten feet from the beam ends on either side of the joint).” The State of Iowa extends and bends the top reinforcement too in order to increase the integrity of the structure. But they too still design the beams as simply supported for all loads because of “some problem with cracking” and “because of concerns about how much continuity” is achieved. The State of Tennessee is among the most experienced states with very satisfactory experience with this type of bridge. Tennessee uses a wider diaphragm in order to prevent overlap of the positive moment reinforcement and to not embed the

girders. They explicitly design the anchor bolts for seismic loads, however, they do sheath the bolts to prevent bonding with diaphragm concrete and to allow rotation. Tennessee does not agree with NCHRP Report 322 recommendations. On the other hand, the Michigan DOT, which also has extensive experience with the use of this kind of bridge, does agree with those recommendations and does not provide positive moment reinforcement in the continuity diaphragm. But as mentioned, they design the beams as simple span for both dead and live loads. Tennessee also specifies a minimum age of 90 days for the girders prior to continuity establishment to minimize the creep effect.

In summary, despite general similarity, the design approach and details of the continuity connection varies significantly among various states. Figure 1.7 shows several examples of the positive moment connection.

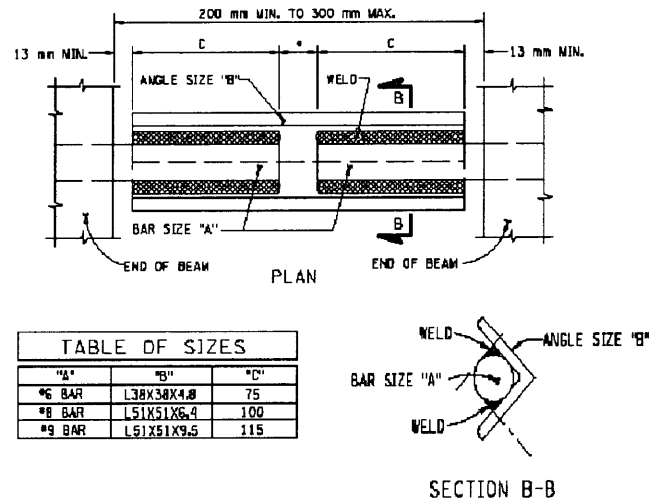


(a) New Jersey

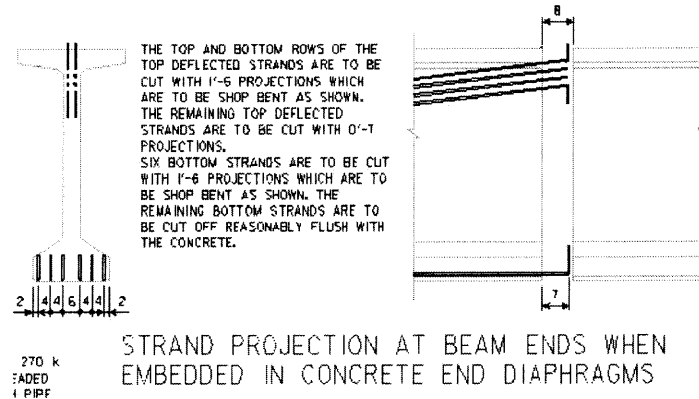


(b) Michigan

Figure 1.7 Connection details of different states.



(c) New York



(d) Iowa

Figure 1.7 Connection details of different states (continued).

From the above discussion, it is clear that the current design and construction of this type of bridge varies considerably, especially for the positive moment reinforcement. Studies done in this area don't agree with one another. Some are even contradictory. For example, PCA^[4] and Mirmiran^[11] recommended providing positive moment reinforcement, while CTL concluded that the positive moment reinforcement had no structural advantage^[10]. Although many negative moment connections were available to

achieve more continuity none of them became popular. Current AASHTO Specification regarding bridges composed of simple-span precast prestressed girders made continuous is vague. Article 9.7.2.1 states that “when structural continuity is assumed in calculating live load plus impact and composite dead load moments, the effects of creep and shrinkage shall be considered”^[18], but it doesn’t specify how. Probably that is the reason why current practices vary dramatically. Further studies are necessary to evaluate the performance of this kind of bridge, to improve the current design and to develop a new continuity connection that can achieve more continuity yet is easy to construct.

1.4 Objectives

The objectives of this research are to:

1. Perform field tests of bridges composed of simple-span precast prestressed concrete girders made continuous under service live loads.
2. Evaluate the responses of this kind of bridge under live load using computer models. Define and determine the degree of continuity using both analytical and field test results.
3. Perform three-dimensional finite element analyses for this kind of bridge and study factors affecting the degree of continuity.
4. Develop a computer program to help engineers evaluate the restraint moments and determine the degree of continuity of the “continuous” bridges.
5. Develop and test in the laboratory a new type of continuity connection using Carbon Fiber Reinforced Polymer (CFRP) composites that achieves more continuity and is relatively easy to construct.

1.5 Originality of Research

Compared with previous studies performed on this subject, the original contributions of this research include the following:

1. Supports with two bearings and anchor bolt(s) act differently from idealized pins / rollers. Basically, the bearings and the anchor bolts can form couples under live loads, which will redistribute moments between the support and the mid-span. This research investigates the influence of the support details on the performance of the bridge.
2. Although many analytical studies (mainly by CTL^[10] and Mirmiran^[11]) have been done to determine the time dependent effects, they are based on a beam theory and they are all two-dimensional. This research utilizes three-dimensional finite element models to furnish a more accurate time history of bridge response.
3. No previous attempts have been made to measure the degree of continuity of a real bridge. The field tests in this study provide insight about the in-situ performance of simple span girders made continuous.
4. Compared with existing analytical computer programs, the program developed in this research, called CONTINUITY, expands design capacity remarkably. For example, PBEAM (developed by Suttikan^[9]) is a general computer program for the analysis of prestressed structures. The use of PBEAM on the particular problem of simple span girders made continuous is cumbersome and time-consuming. BRIDGERM (by CTL^[10]) takes into account the finite length of the diaphragm, but it only does elastic analysis and all spans are simplified to a single span with one or two diaphragm attached. RESTRAINT (by Mirmiran et al. ^[11]) considers the two bearings at each support and the moment-curvature of the girder and diaphragm sections, but it is limited to two equal spans. The CONTINUITY improves upon these existing computer programs by taking into account the two bearings at each support and the cracking of the girder and diaphragm sections, also it can analyze bridges up to four spans with unequal span lengths.
5. External CFRP strengthening has been used widely in this country and around the world because of its lightweight, high strength, corrosion resistance and easy installation. However, it is mainly used for repair and rehabilitation. This study investigates the application of CFRP for new construction to improve the continuity of simple-span girders made continuous. Test results suggest that the new CFRP connection is more advantageous than the threaded rod connection tested by Ma and Tadros^[16] because it alleviates the reinforcement congestion in the diaphragm and girder ends, and it has the potential to narrow the continuity diaphragm.

1.6 Organization of the Dissertation

This chapter introduced the background, literature, survey and objectives of this research. The rest of this dissertation is organized as follows. Chapter 2 describes three field tests performed in New Jersey, including analyses of the test data. Chapter 3 focuses on the finite element analyses. Two important factors, the amount of positive moment reinforcement and girder age at continuity, are studied using the finite element model. Chapter 4 describes the algorithm, verification and usage of the computer program – CONTINUITY. Chapter 5 introduces a new type of continuity connection using carbon fiber reinforced polymer. Also, a series of laboratory tests is presented and a design example is given to validate the new continuity connection. The last chapter summarizes the findings and conclusions of this dissertation and suggests further research needs.

CHAPTER 2

FIELD TESTS

2.1 Introduction

According to the literature review and survey replies, the degree of continuity of bridges composed of simple-span precast prestressed concrete girders made continuous can vary from zero to one hundred percent, depending on factors such as girder age at erection, positive moment reinforcement in diaphragms over piers, creep and shrinkage properties of girder and deck concrete, construction sequence of deck and diaphragm, live load level, etc. Since the girders are first erected as simply supported, continuous girders usually have two supports over each pier (See Figure 2.1). One would not ordinarily build a continuous beam in this fashion since it becomes difficult to control the reactions.

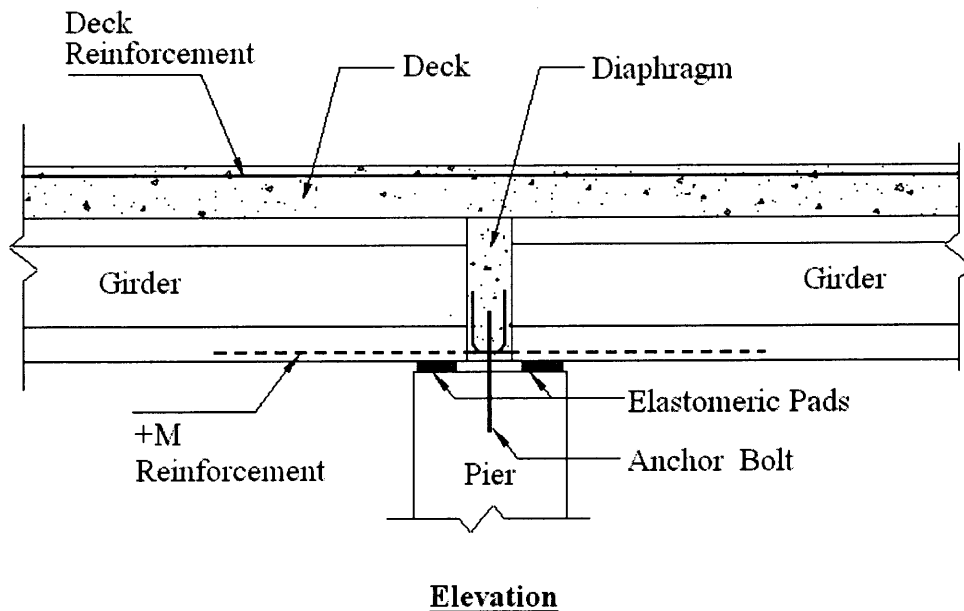


Figure 2.1 Support details.

In some cases, matters are made even more complicated by the use of additional vertical anchor rods, which a) prevent the joint from acting as an expansion joint under thermal loads; b) tend to add additional fixity to the support. In the latter case, these additional anchor rods can lead to splitting and cracking of diaphragms. In any case, the question remains regarding how bridges of this type function, particularly when there is cracking. That is what drives this field investigation.

Many bridges of this type were visited in New Jersey. Some of the bridges had severe cracks in the diaphragms while others didn't. Three typical bridges were selected for testing. Two of them are on Interstate-287. One is over Skyline Drive, which has visible cracks in the diaphragms. Another is over Darlington Avenue, which doesn't have visible cracks. The third bridge is on Routes 1&9 section 2AG in Newark. Here some of the diaphragms have cracked, but others have not. In some cases, the diaphragm concrete is even crushed.

The rest of this chapter presents the experimental investigation of these continuous bridges and an analytical study of the support details.

2.2 I-287 N.B. Over Skyline Drive

2.2.1 Bridge Description

This bridge is located in Oakland, Bergen County, New Jersey. It is a two-span bridge with a continuity connection at the center pier. The first span is 85' long and the second span is 83'. Both north bound and south bound have three traffic lanes and an acceleration ramp. The girders are AASHTO Type IV girders (54"). Each girder has 46 prestressing strands (270 ksi, 1/2" diameter). The average girder spacing is 8'.

Continuity is provided by casting an 8.5" deck on top and an 8" diaphragm between the girders. Positive moment connection is provided by extending and bending the bottom row of prestressing strands (10). A 1.25" dowel is put in each girder line between the two span girders to prevent uplift.

2.2.2 Instrumentation

North bound bridge was chosen to be instrumented. Due to access limitations, it was not possible to install strain gages at the center of either of the two spans. For the same reason, it was not possible to instrument internal girders, leaving the shoulder girder to be instrumented. It should be added that there was an acceleration ramp at this level, further distancing the shoulder girder from the center of the roadway where there was heavy traffic. Thus, instrumentation included strain gages at the ends of the girders on both sides of the center pier and on the diaphragm between B19 and B20 (Figure 2.2).

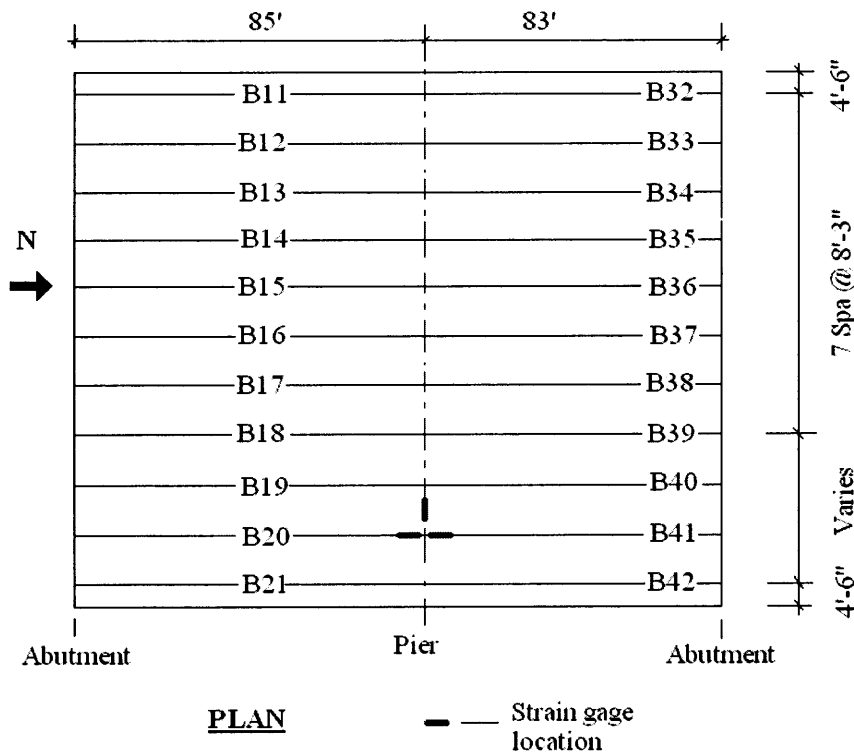


Figure 2.2 Layout and instrumentation of I-287 NB over Skyline Dr, Mahwah, NJ.

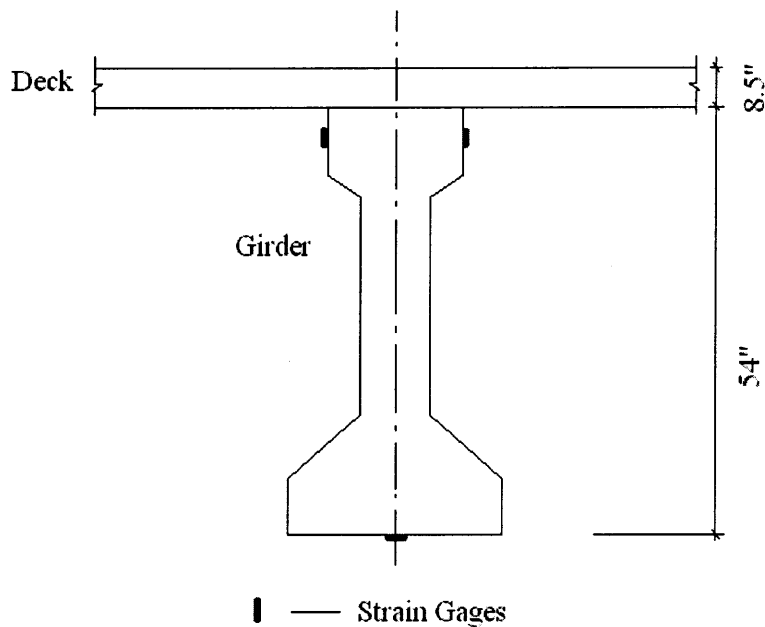


Figure 2.3 Instrumentation on girders (I-287 NB over Skyline Drive).

A total of three strain gages were installed at each end section: one on the bottom of the girder and two attached to the opposite sides of the girder top flange (Figure 2.3). Gage SB (south bottom) was on the bottom of beam 20, gage NB (north bottom) was on the bottom of beam 41, STL (south top left) was on the left side of the top flange of beam 20, STR (south top right) was on the right side of the top flange of beam 20, NTL (north top left) was on the left side of the top flange of beam 41 and NTR (north top right) was on the right side of the top flange of beam 41. A Rosette gage was installed on the diaphragm between B19 and B20. Strain readings were collected by 6 data acquisition units (P3500) and recorded on a computer.

2.2.3 Test Results

As shown in Figure 2.4, the diaphragm at the continuity joint cracks right through the middle. This is consistent with what is typically expected to happen when the time-dependent positive moment exceeds the cracking moment of the cross section.

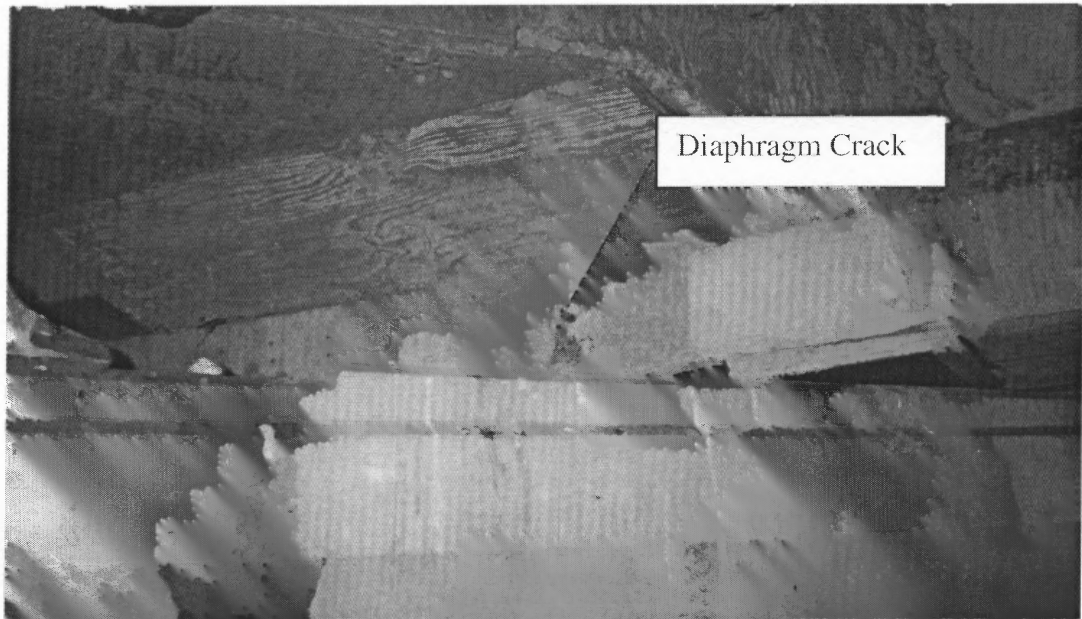
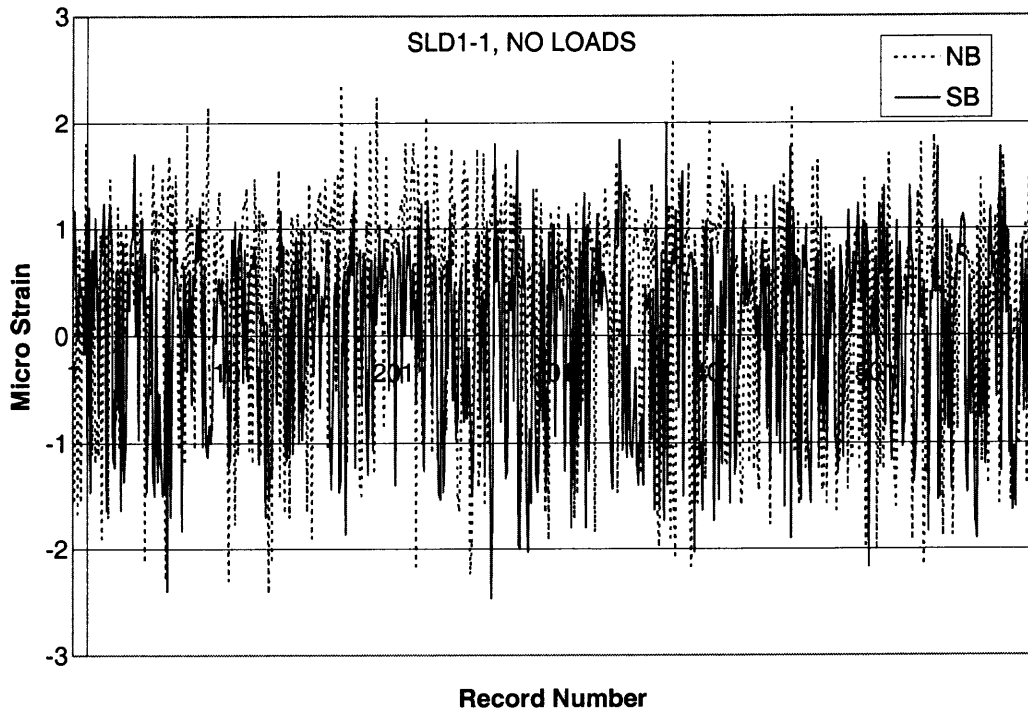
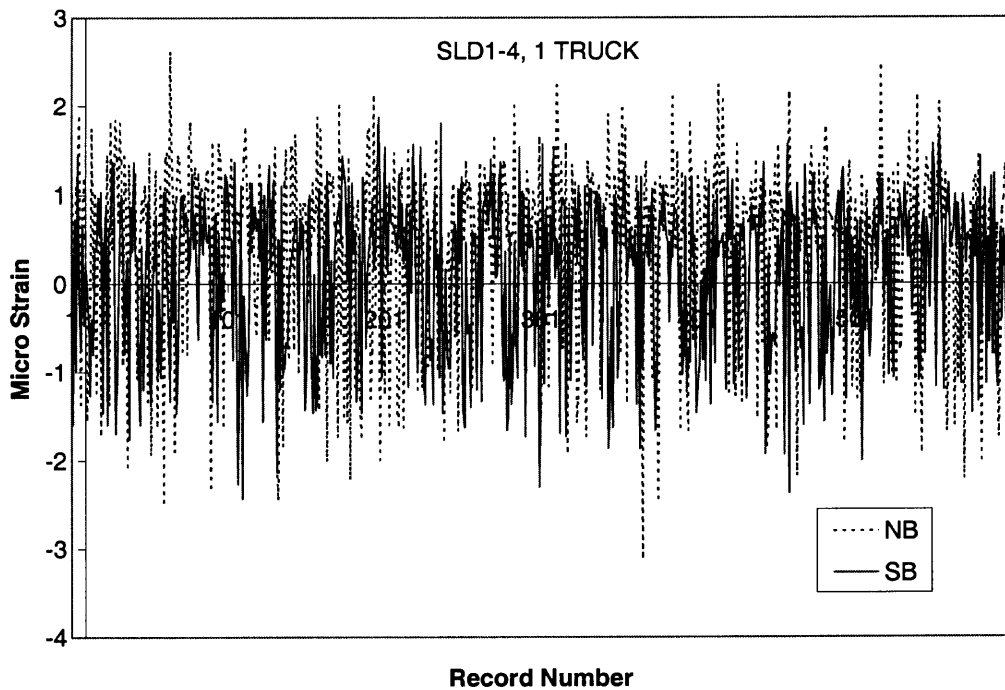


Figure 2.4 Diaphragm bottom crack, I-287 NB over Skyline Drive.

Despite several attempts, no significant output was measured in any of the strain gages (Figure 2.5 only shows the response of the gages at the bottom of the girders, readings of top gages were even smaller). This could be either due to a lack of any continuity (i.e., no bending strain at the ends of a simply supported beam) or it could be due to the fact that the shoulder girder does not carry much of the roadway service load. Additional measurements were made while driving a NJDOT truck right over the girder instrumented. Data were read directly from P3500 when the truck stopped at each location. Table 2.1 lists the response of the gages when the truck was at the midspan of span 1, over the center support and at the midspan of span 2. Still there were no significant readings. These combined with visible wide cracks at the joint indicate that this connection provides little or no continuity under service load.



(a) Responses of gages NB and SB when there was no load.



(b) Response of gages NB and SB when there was a truck passing.

Figure 2.5 Response of gages NB and SB.

Table 2.1 Gage Readings when DOT Truck Passed I-287 NB over Skyline Drive

Gage	Midspan of Span 1	South of Support	North of Support	Midspan of Span 2	North Abutment
NB	2	0	0	0	0
SB	-0.5	-1.5	1.5	8.5	-0.5
NTR	3	2	-2	4	5
STL	-2.5	-1.5	1.5	2.5	-0.5
ROSETTE	-1	0	0	-1	0
STR	4.5	0.5	-0.5	0.5	0.5

Note: N-north (span 2), S-south (span1), B-girder bottom, T-girder top, L-left side of girder top flange and R-right side of girder top flange.

2.3 I-287 N.B. Over Darlington Ave

2.3.1 Bridge Description

This bridge is located in Mahwah, Bergen County, New Jersey. It is a continuous multi-span precast prestressed concrete bridge made continuous through a cast-in-place concrete deck. The southbound bridge has four spans and the northbound one has three spans. The northbound bridge was instrumented. It is 44.5' wide from parapet to parapet and has two 12' traffic lanes and two shoulders of 5' and 12' wide.

Each span has six AASHTO Type VI girders spaced 8.5' on center. A typical girder section is shown in Figure 2.6. The first span girders have 30 seven-wire 270 ksi pre-stressing strands; the second span girders have 58 strands, and the third span girders have 56 strands. All the pre- strands are bent up at third points, as shown in Figure 2.7.

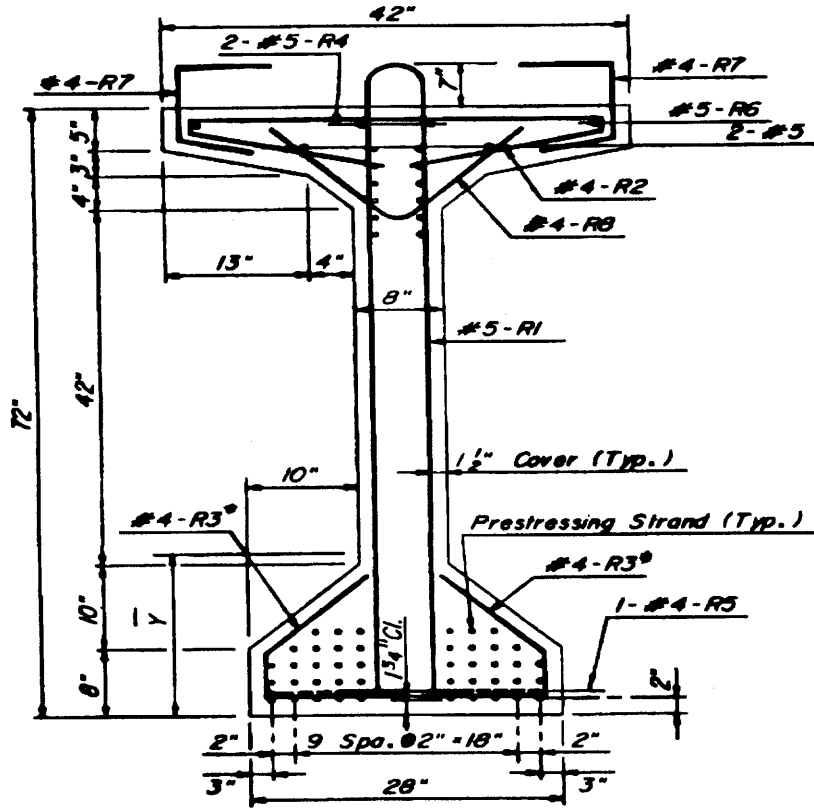


Figure 2.6 Girder cross section (from design drawing).

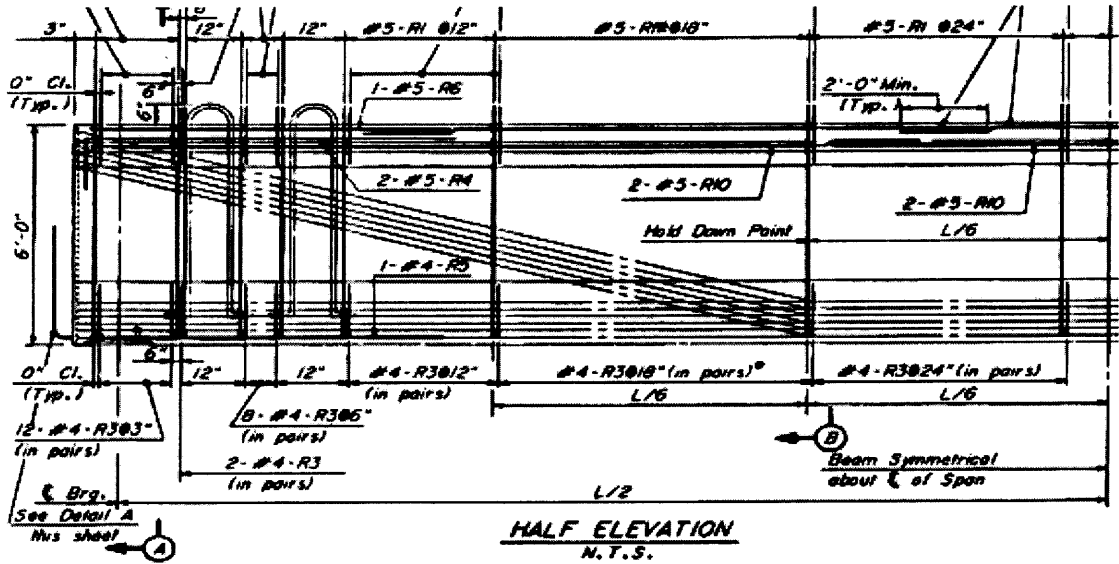


Figure 2.7 Strand layout of girders (from design drawing).

Continuity is established by providing negative and positive moment reinforcement in the deck and diaphragm. The negative moment reinforcement is #7 bars at 7.5" plus #7 bars at 15". The positive moment connection is provided by extending eight prestressing strands from girder ends (Figure 2.8). No anchor bolts are provided in each girder line. Instead, 6" diameter posts are used in the diaphragm between the stringers. These posts are separated from the diaphragm via a compressible joint material (Figure 2.9).

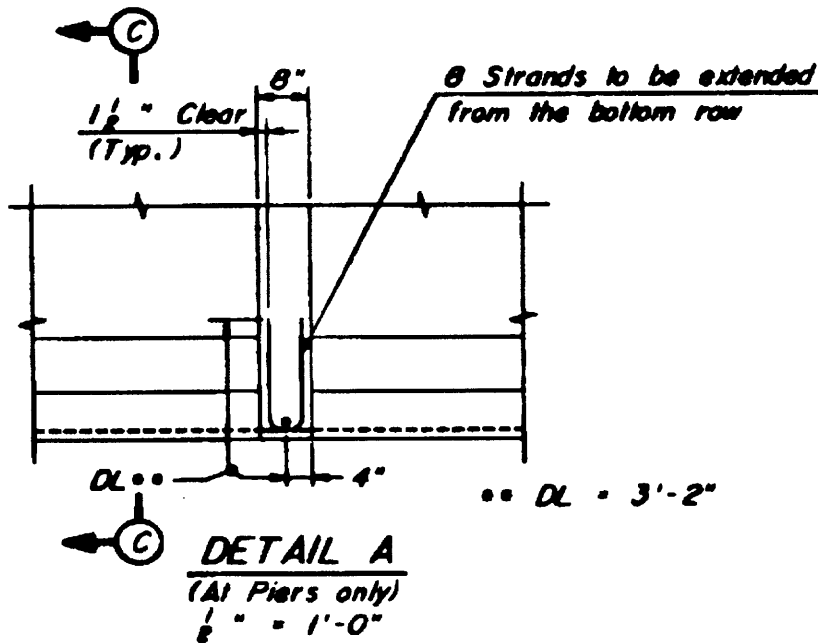
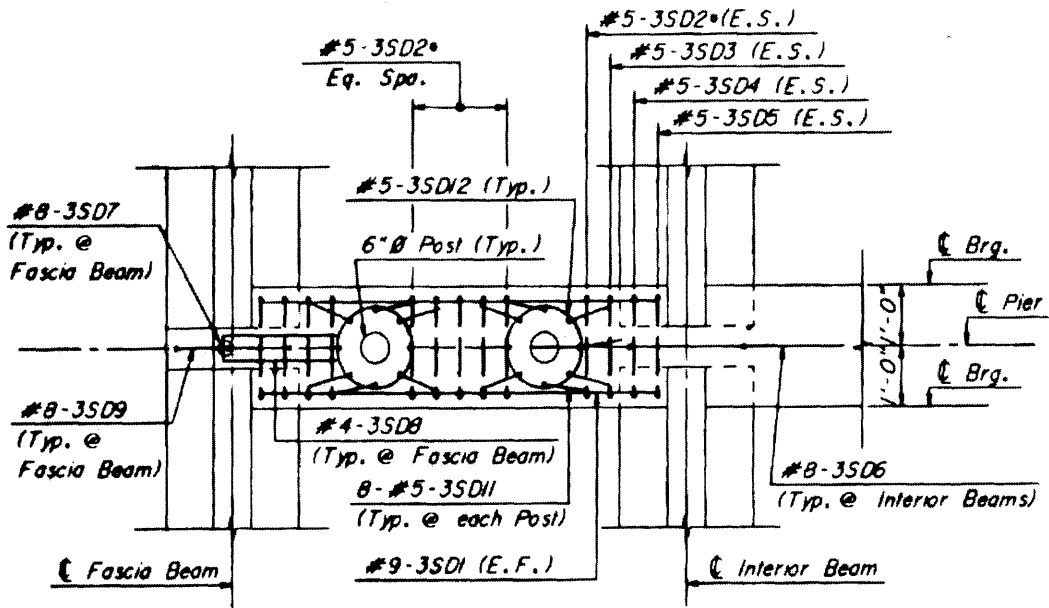
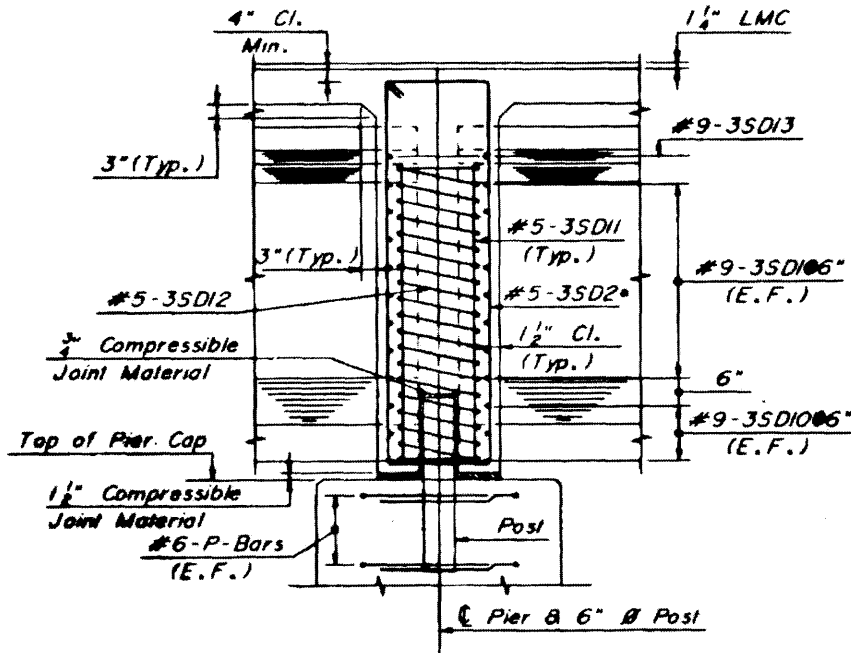


Figure 2.8 Positive moment connection over piers (from design drawing).



(a) Top View



(b) Section

Figure 2.9 Diaphragm detail (from design drawings).

2.3.2 Instrumentation

For this bridge, span 1 is simply supported. Span 2 and 3 are continuous. A girder line from span 2 and 3 was instrumented, as shown in Figure 2.10.

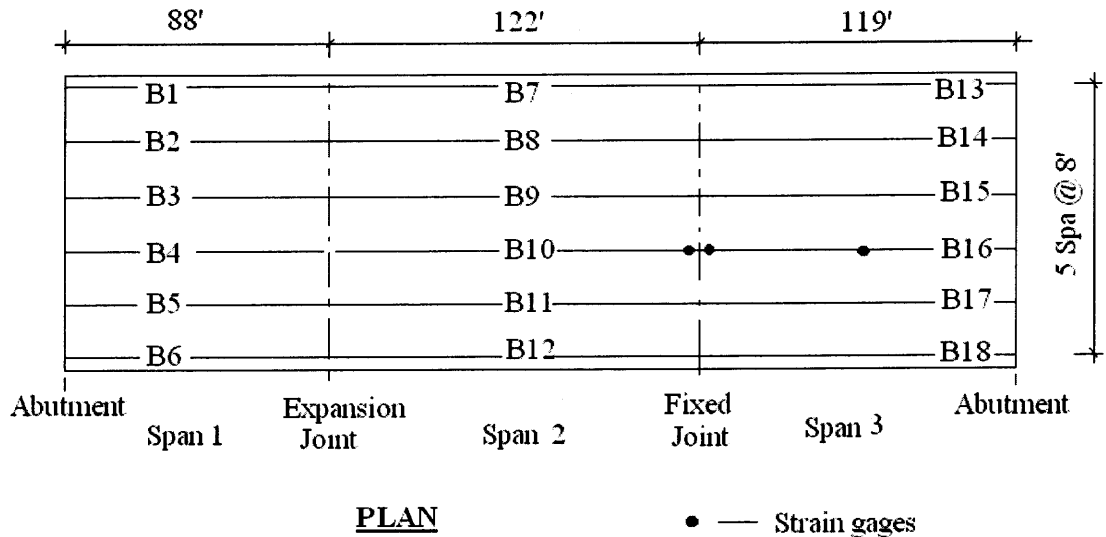


Figure 2.10 Instrumentation on I-287 NB over Darlington Ave, Mahwah, NJ.

Girders B10 and B16 were instrumented. The strain gages at beam end were located 2' from the diaphragm face. Three gages were installed at each end location: top flange left, top flange right and center of the beam bottom (see Figure 2.11). These gages were supposed to give information about the moment transferred from one girder end to the other. Another strain gage was installed near the mid-span of B16 to further verify presence of live load. Because of access limitations, no gages could be installed at the exact center of either span.

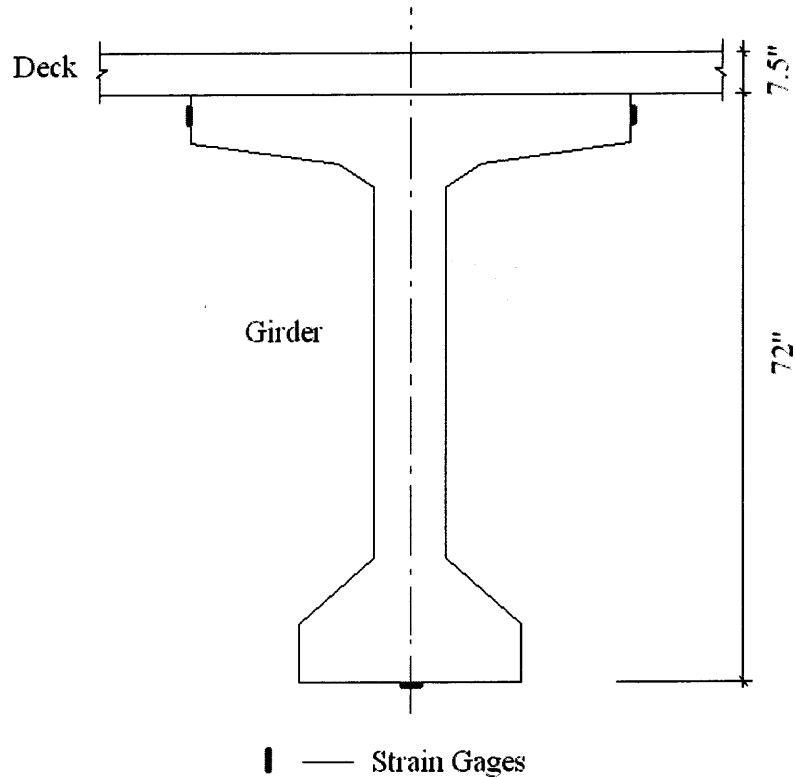


Figure 2.11 Instrumentation on girders.

Two-inch long strain gages were used. They were connected to a data acquisition system (StrainSmart 5000) via special noise-proof wires. The system can take up to 50 readings in a second. An observer was sent onto the bridge to watch the traffic and give instructions for when to record and when to stop the data acquisition.

2.3.3 Results and Analyses

More than 40 measurements were taken from the above setup. Figure 2.12 shows a typical plot of the strain gage readings.

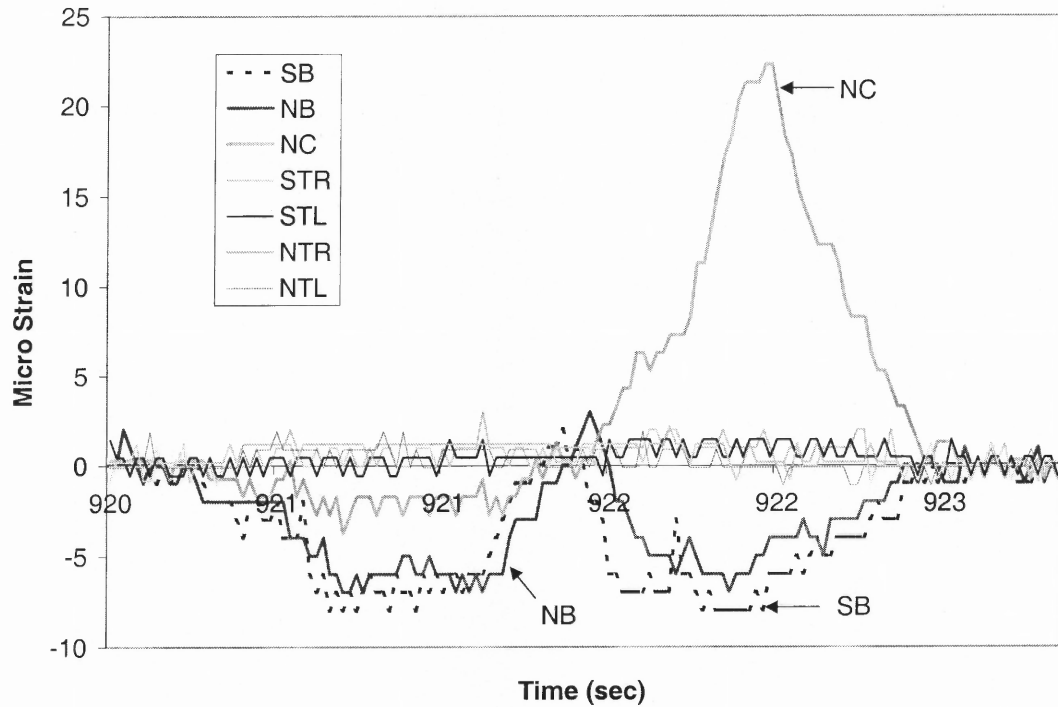


Figure 2.12 Typical readings (all gages).

where S – B10 (South span)

N – B16 (North span)

T – Top Flange

B – Bottom

L – Left

R – Right

C – Mid-span of B16

All top gage readings are within the range of -2 to $+2$ micro-strain. The reason is that these top gages are located near the neutral axis of the composite girder-deck section. For clarity, top readings are eliminated in the following diagrams. Figure 2.13 shows typical readings with one truck traversing the bridge.

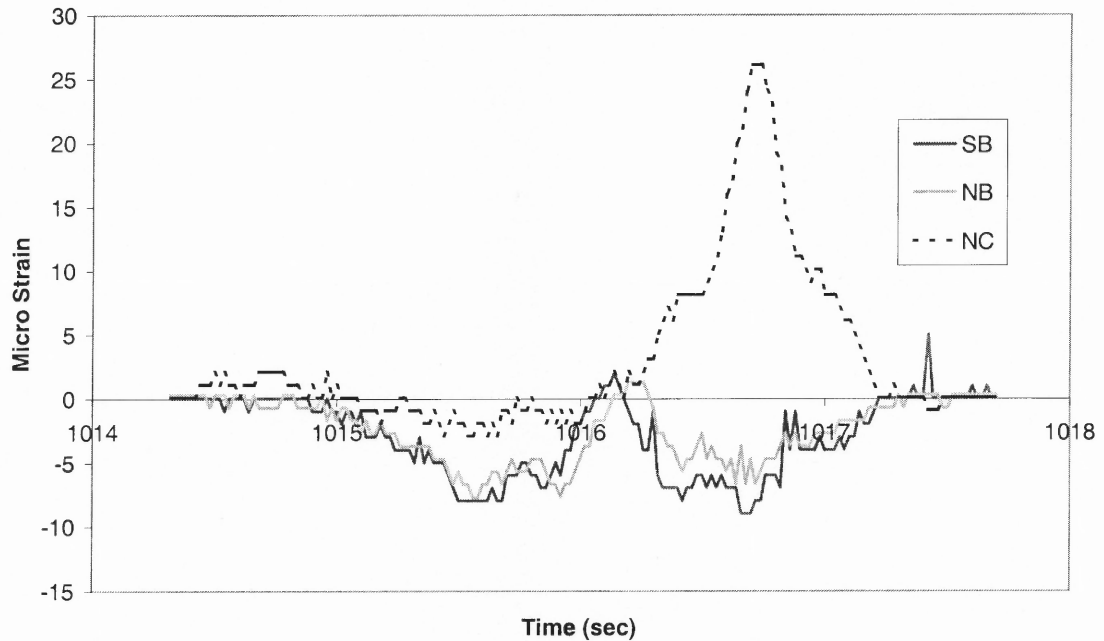


Figure 2.13 Readings of bottom gages when a truck is passing over.

Gages SB (south bottom) and NB (north bottom) are in compression and they follow each other well. The maximum difference between the two is about 20%. This shows that there is good continuity in the connection, which confirms our observation that no cracks were found in the diaphragm. SB and NB would behave differently if no or low continuity was the case.

There were two peaks on NB while there was only one truck passing over. The first peak occurred when the truck was at mid-span of the south beam (B10). The second peak corresponded to the situation when the truck was at mid-span of the north beam

(B16). Another observation is that these two peaks have approximately the same value, which also indicates that good continuity was established.

Response of gage NC (mid-span of north beam) first goes down about 3 micro-strains, and then bounces up to +26 micro-strains. The negative peak appeared when the truck was at mid-span of B10, which coincided with the first peak of NB and SB. If no continuity were established, the negative peak of NC gage would not appear when the truck is in the other span. The positive peak occurred when the truck was right above the NC gage.

2.3.4 Degree of Continuity

In his analytical study, Mirmiran et al.^[11] defined “continuity index” as the ratio of live load moment at the support (or midspan) obtained from analysis to the corresponding elastic moment assuming full continuity. Thus, the continuity indices for supports are smaller than one and those for midspans are larger than one. Because there was no way to stop traffic, the exact values of the live load were not known. This makes it impossible to follow this definition for continuity index.

To determine the degree of continuity of this bridge, an analytical study was performed. The velocity of the vehicle was calculated from the test data. The live load level was calibrated by matching the analytical mid-span strain with that from the test. Figure 2.14 shows the results of the theoretical dynamic analysis.

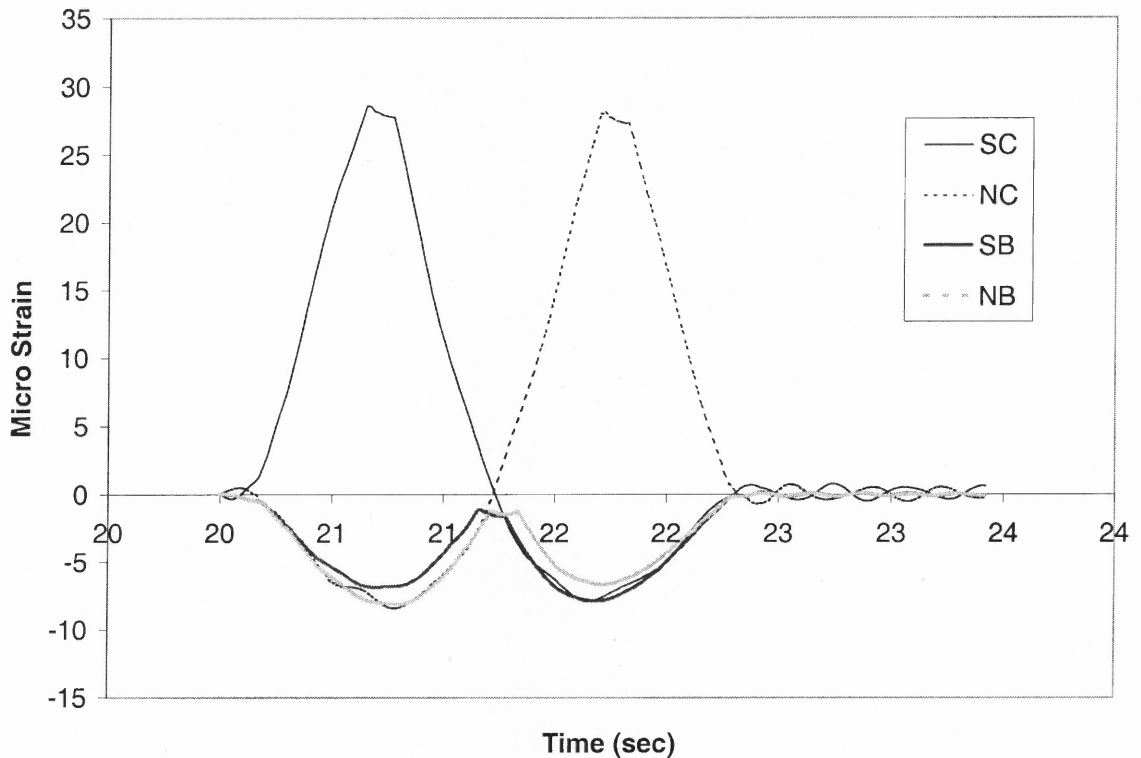


Figure 2.14 Theoretical strains at mid-spans and girder ends.

Continuity can be defined as the moment-transfer capacity of a joint. Since gage NC was not at the exact center of span 3, girder end gages were used to calculate the degree of continuity. Because the live load was unknown, relative values instead of absolute values are used to determine the *degree of continuity*, which is defined as:

$$\text{D.O.C.} = R_{\text{test}} / R_{\text{theo.}}$$

where D.O.C. – degree of continuity.

R_{test} – equals the maximum strain in NB (span 3 near support) divided by the maximum strain in SB (span 2 near support), when the truck is in the middle of span 2, from test data.

$R_{\text{theo.}}$ – theoretical value, equals the maximum strain in NB (span 3 near support) divided by the maximum strain in SB (span 2 near support), when the truck is in the middle of span 2, from elastic analysis assuming full continuity.

For Darlington bridge, $R_{\text{test}} = 7.949/7.665$, $R_{\text{theo.}} = 8.126/6.762$. Thus, the degree of continuity, $\text{D.O.C.} = R_{\text{test}} / R_{\text{theo.}} = 80\%$. Applying similar calculation to the case when the truck was on span 3 yields a D.O.C. of 100%. The average degree of continuity of I-287 NB over Darlington Ave is 90%. This agrees with the fact that there are no visible cracks in the continuity diaphragm.

The good performance of this bridge comes from its support detail. There are no anchor bolts in the continuity diaphragm. Although posts are provided, they are off the girder lines and are separated from the diaphragm by compressible materials.

2.4 Rt. 1&9 S.B. Section 2AG

2.4.1 Bridge Overview

Field tests were also carried out to examine the degree of continuity of the bridge on Rt. 1&9 Section 2AG over Wilson Avenue, Newark, New Jersey (Figure 2.15). This bridge has 52 spans. The southbound bridge is composed of two parts, express and local, each has two traffic lanes and a shoulder. Spans 10 to 13 are 4-span continuous with equal span length of 102 feet. The girders are 63" AASHTO Type V girders, and the deck slab is 7.75" thick.

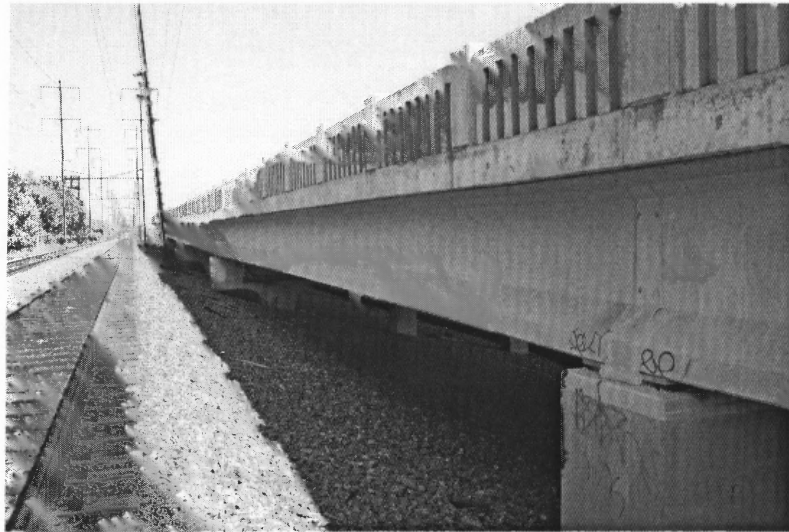


Figure 2.15 Rt. 1&9 S.B. section 2AG, Newark.

2.4.2 Crack Patterns

Girder Top Cracks

Fine cracks were found in the top flanges of span 10 girders. The reason for this will be explained later in the concluding remarks of this chapter.

Diaphragm Cracks

A thorough inspection of the bridge showed that many of the diaphragms over the supports had cracked. Most of the cracks initiated from the interface between the girder and the diaphragm and were located at 45° relative to the center of the diaphragm, and then up. Some others formed between the diaphragm and the girder ends (see Figure 2.16 and Figure 2.17). At one location of west fascia, diaphragm concrete was crushed (Figure 2.18).



Figure 2.16 Diaphragm crack at fascia beam (Rt. 1&9, Newark).



Figure 2.17 Typical diaphragm crack at inner beams (Rt. 1&9, Newark).

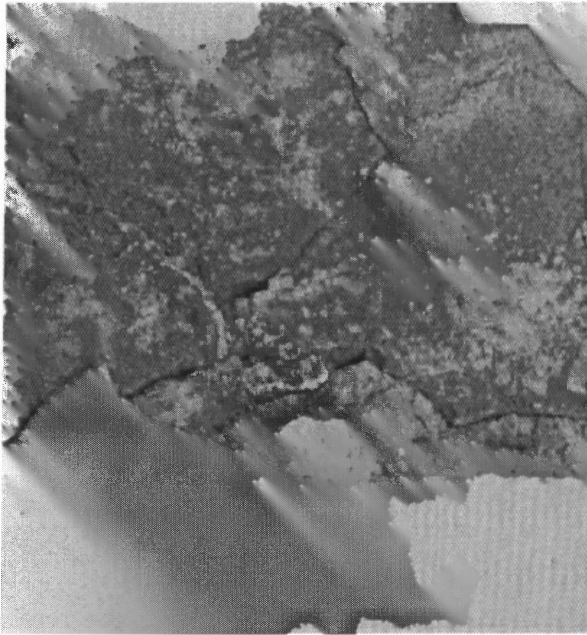
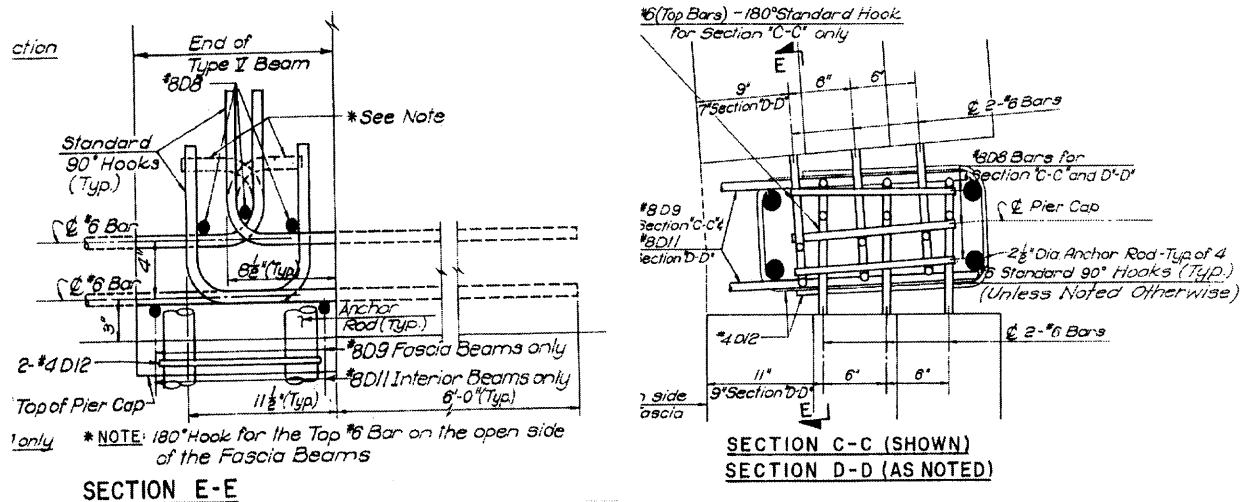


Figure 2.18 A close-up of the crushed concrete at fascia beam (Rt. 1&9, Newark).

One reason for diaphragm cracking comes from the fixed supports. These continuity supports are designed to be fixed in the longitudinal direction by providing thin elastomeric bearings and four anchor rods at the piers. This fixity might cause cracks in the diaphragm when the bridge is subjected to temperature loads and axial creep of the prestressed girders.

A review of the connection detail also sheds some light on possible reasons for these damages. Figure 2.19 is taken from the original plan. When the section is under positive moment due to creep of the prestressed girders, the positive moment reinforcement is put into tension. The cracks initiate at the bottom of the diaphragm and develop upward. The concrete between the U shaped positive moment reinforcement is in compression. When the positive moment is large enough, the concrete in between crushes. PCA tests showed the same failure pattern in the continuity diaphragm^[4].

The four 2.5" diameter anchor rods in the continuity diaphragm plus the two bearings at each pier may form couples, which add to the fixity of the joints. The pull-out forces in the anchor rods also have played a role in the diaphragm cracking. Section 2.5 discusses this issue in detail.



(a) Elevation

(b) Top View

Figure 2.19 Diaphragm details at fixed piers (Rt. 1&9 design drawings).

The last observation regarding the original design is about the horizontal development length of the positive connection. The PCA design method, which is the base for the current AASHTO specification for the design of simple girders made continuous, specifies that the distance between the girder end and the inner surface of the hook should be at least 12 times the bar diameter to develop the yield strength of the positive moment reinforcement. For #6 bars, this distance should be 9 inches. From Figure 2.19 one can see that there are two layers of positive moment reinforcement. The horizontal development length for the bottom layer is 10.75 inches while it is only 7.75 inches for the top layer, which is less than the required 9 inches. The PCA tests also

showed that the hook connections were not as satisfactory as the welded connections with respect to ultimate strength, deflection and crack control. The maximum crack width of the hook connections was 54% larger than that of the welded connections, and the crack opening rates were 50%, 120% and 400% faster than those of welded connections for the three specimens tested by PCA.

2.4.3 Test Procedures

The third stringer (counting from West) of the local lanes was instrumented. In addition to what was done for Darlington, all four mid-span strains were measured. Furthermore linear variable displacement transducers (LVDT) and direct current displacement transducers (DCDT) were used to measure the deflection at the girder ends. Figure 2.20 shows pictures of strain gage installation and the data acquisition system.

Figure 2.21 shows the instrumentation layout. Gage numbers are shown at their corresponding locations. Gage #1, #2, #5 and #16 were at mid-spans. They were mounted to the bottom of the girders. Gage #10 and #11 were on the top flange of span 10 girder, one to the left and the other to the right. Gage #12 and #13 were on the top flange of span 11 girder. All the top gages were located one foot from the diaphragm edge. "a" and "b" were DCDTs mounted to the girder ends. "c" and "d" were LVDTs. In some tests, gages 3, 4, 6 and 7 were mounted to the bottom of the girders, 1' from the diaphragm edge.



Figure 2.20 Installing strain gage at mid-span and monitoring responses.

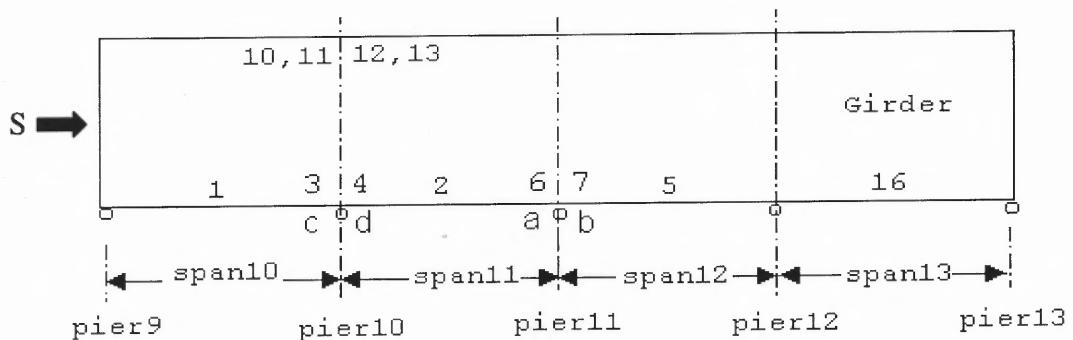


Figure 2.21 Instrumentation layout of Rt. 1&9 tests (Elevation).

After all the gages and transducers were set up, they were connected to a data acquisition system (StrainSmart 5000) through special cards. After zeroing and calibrating all the channels, the system started to monitor the response of all the sensors. The scan rate was 50 times per second. Since a trigger was programmed in advance, the system could automatically record 3 seconds before and 5 seconds after the trigger was activated. This way, the system was able to record automatically when the readings exceeded a certain value.

2.4.4 Test Results

Top Gages at Girder Ends

Figure 2.22 shows typical strain readings in the top gages #10~#13. As can be seen, strains in gage #12 and gage #13 are negligible. Gages 10 and 11 have significant readings, especially gage 10, which is right across a visible crack. Although no visible cracks were found under gage 11, micro cracks might form under the concrete, because gage 10 and 11 were on the same girder. Gage 10 was on the west side of the top flange and gage 11 was on the east side.

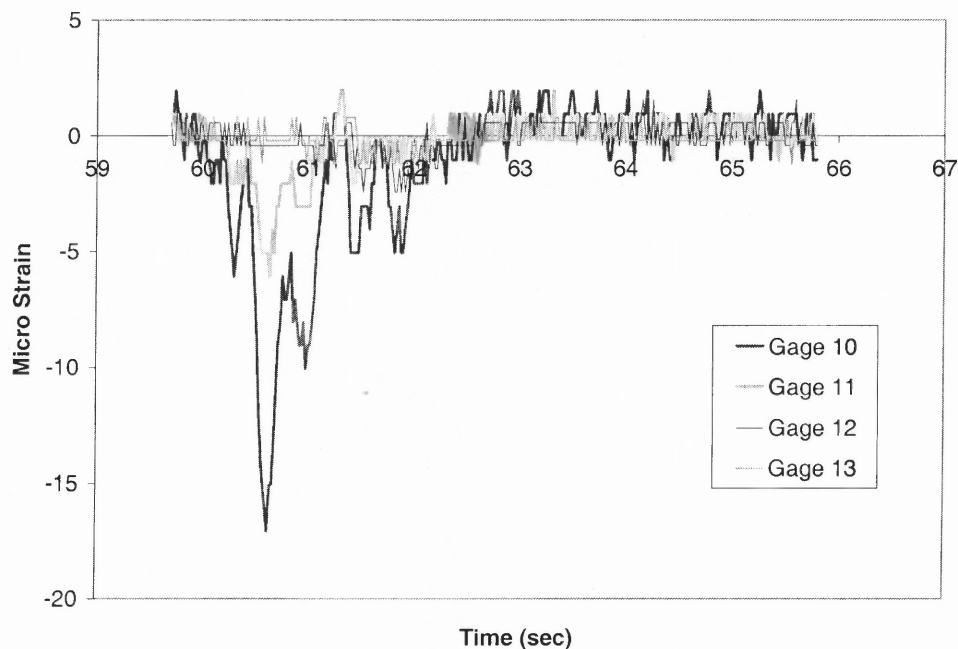


Figure 2.22 Girder top gages near supports.

Similar to I-287N over Darlington, it is believed that these top gages were near the neutral axis of the composite section. No more top gages were installed.

Bottom Gages at Girder Ends

Gages 3 and 4 are near pier 10. Gages 6 and 7 are near pier 11. It can be seen that gages near the same support follow the same trend, showing some degree of continuity. When the truck is at the mid-span, the negative peaks of these gages reach 3~4 micro strains. The positive peaks are due to the bridge vibration.

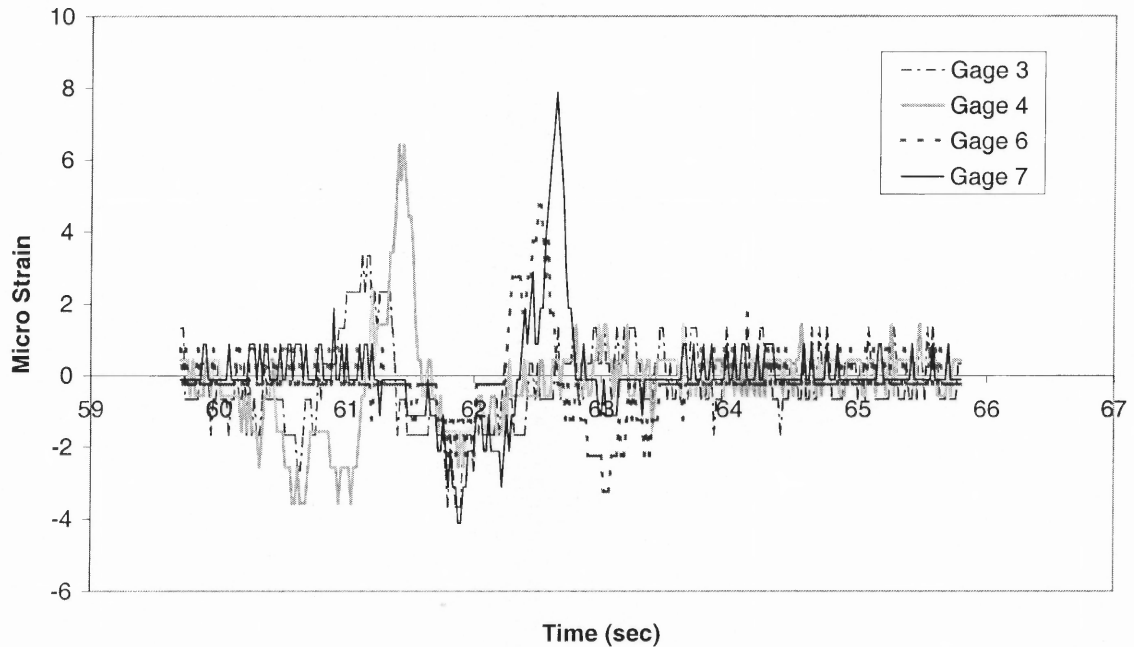


Figure 2.23 Bottom gages near supports.

Mid-span Gages

Theoretically, for a four-span continuous beam, the maximum strains at the center of exterior spans should be larger than those of the interior spans because exterior spans are only continuous at one support while interior spans are continuous at both supports. Figure 2.24 shows a typical strain history of the gages at mid-spans when a truck was passing over. For positive strains, span 10 and 13 were at the same level; span 11 was the

largest while span 12 was the smallest. This was different from expected. Apparently, span 11 had the least continuity and span 12 had the most.

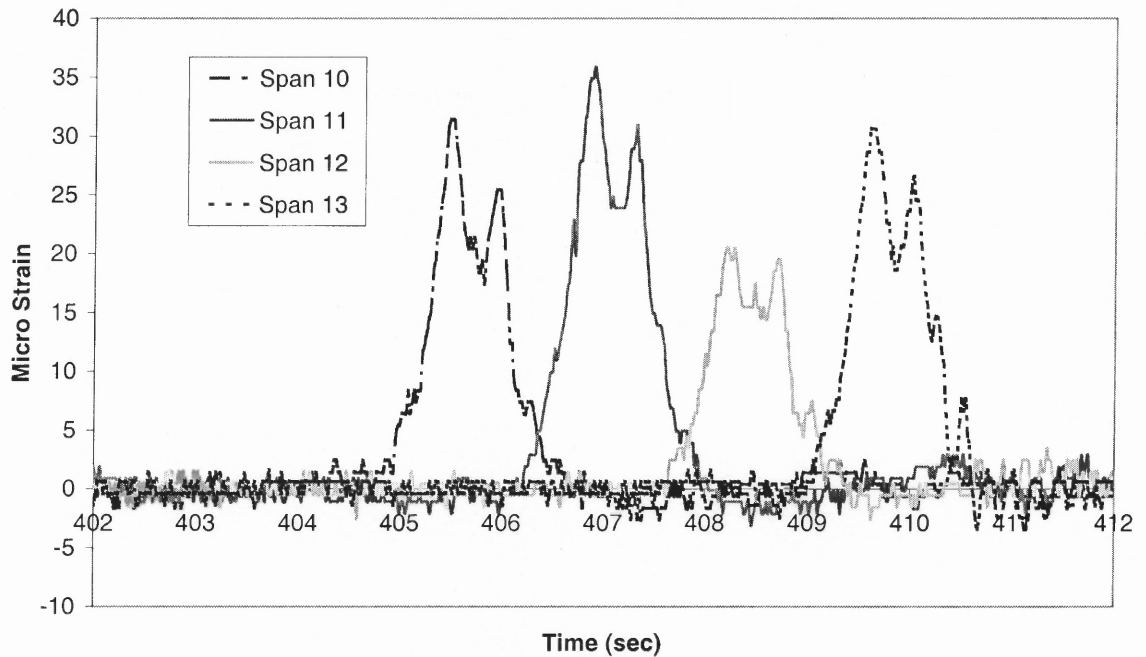


Figure 2.24 Strain history of mid-span gages from test.

LVDTs and DCDTs

The LVDTs and DCDTs were placed near supports, 1.5' from the bearing center line, to measure the deflection at those points. Typical readings are shown in Figure 2.25. Take LVDT 1 and LVDT 2 for an example. When the truck was on span 10, LVDT 1 read maximum downward deflection while LVDT 2 read maximum upward deflection, which suggested some degree of continuity but the values were too small to quantify. These values are mainly used to estimate the live load.

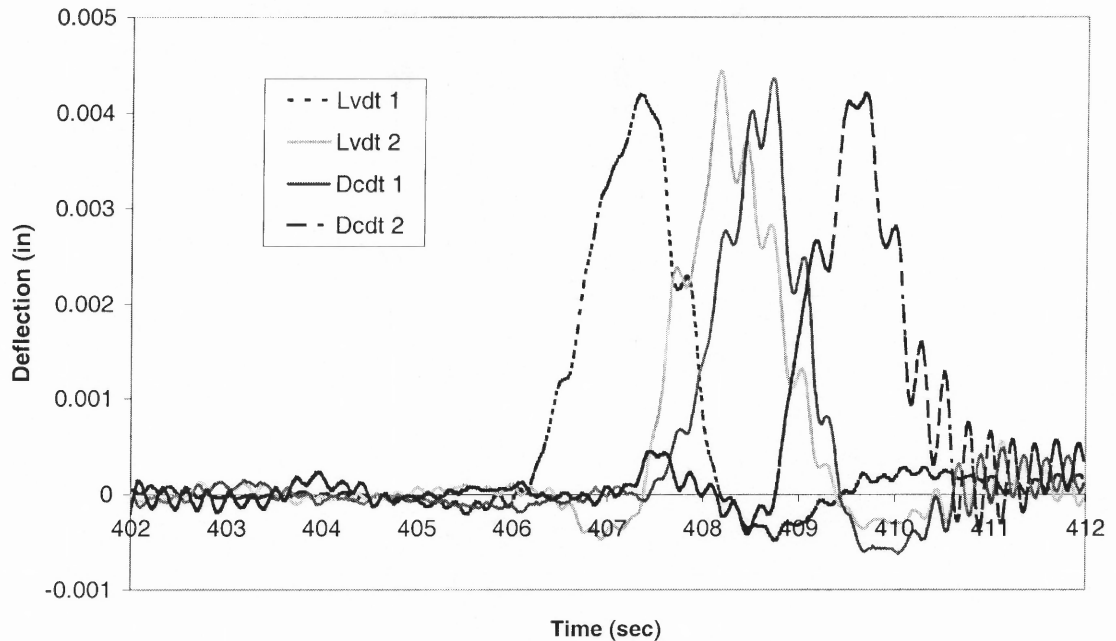


Figure 2.25 LVDT and DCDT readings.

2.4.5 Degree of Continuity

Comparing mid-span strains from tests with those from analyses, one can expect that span 12 has the highest degree of continuity while span 11 has the lowest. But it is inappropriate to define “degree of continuity” the same way as was done for the bridge on I-287 NB over Darlington Ave. For Darlington bridge, “degree of continuity” is defined as the moment-transfer capacity of a joint. It is appropriate for Darlington because there are no anchor bolts in the girder lines. Moments do get transferred fully from one side of the joint to the other. But for Rt. 1&9 bridge, there are four 2.5” diameter anchor rods in each girder line. Moments not only get transferred to the other side, but also get transferred to the pier. Therefore, the negative strain values for support and mid-span gages are relatively small (only 2~3 micro strains after deduction of noise). Degree of continuity must be defined in another way to account for the fixity exerted by

those anchor rods.

If the live load is known, one can determine the degree of continuity of the bridge by comparing the test strain to the theoretical strain either at midspan or at support. Since it was impossible to close the bridge or even stop traffic, there was no way to get the exact location and weight of the truck when strain measurements were made. One possible way of estimating the live load is to simulate the bridge response using computer models. Efforts are first made to study the response of this bridge by modeling those anchor rods and bearing pads at each support.

Figure 2.26 shows the support detail of the first model. Each girder is modeled with 20 beam elements. The elastomeric bearing pads are modeled with compression-only elements. The anchor rods are modeled with spring elements. I_0 and I_1 are moment of inertia of the composite section at mid-span and at the diaphragm, respectively. Element birth and death features are utilized to simulate the staged construction, i.e. girders are simply supported for dead loads and continuous for live loads and superimposed dead loads. Thus, only live loads and superimposed dead loads will introduce reactions in the anchor rods.

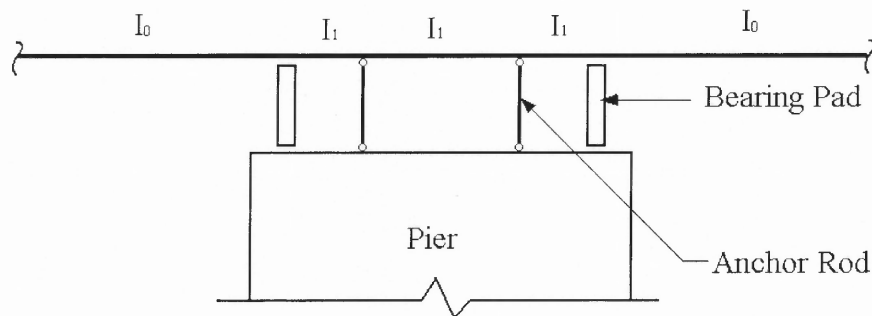


Figure 2.26 Model 1 support detail.

Figure 2.27 shows the reactions in those anchor rods from the 1st model. F1 to F6 represent the forces in the six anchor rods from left to right (compression is negative and tension is positive). The peaks coincide with mid-span strain peaks when the truck is at the middle of each span. Observe that when the truck is at the middle of span 10, the second rod (F2) goes to maximum tension, while the first rod is in compression. This holds for all other cases. Depending on crack patterns of the diaphragm, the effective anchorage of these anchor rods could be different at different piers or even at a same pier. For example in Figure 2.16, more damage is done to the left of the diaphragm, making the left rods less reliable than the right ones. As a result, each pier could provide different restraints to the left span than to the right span.

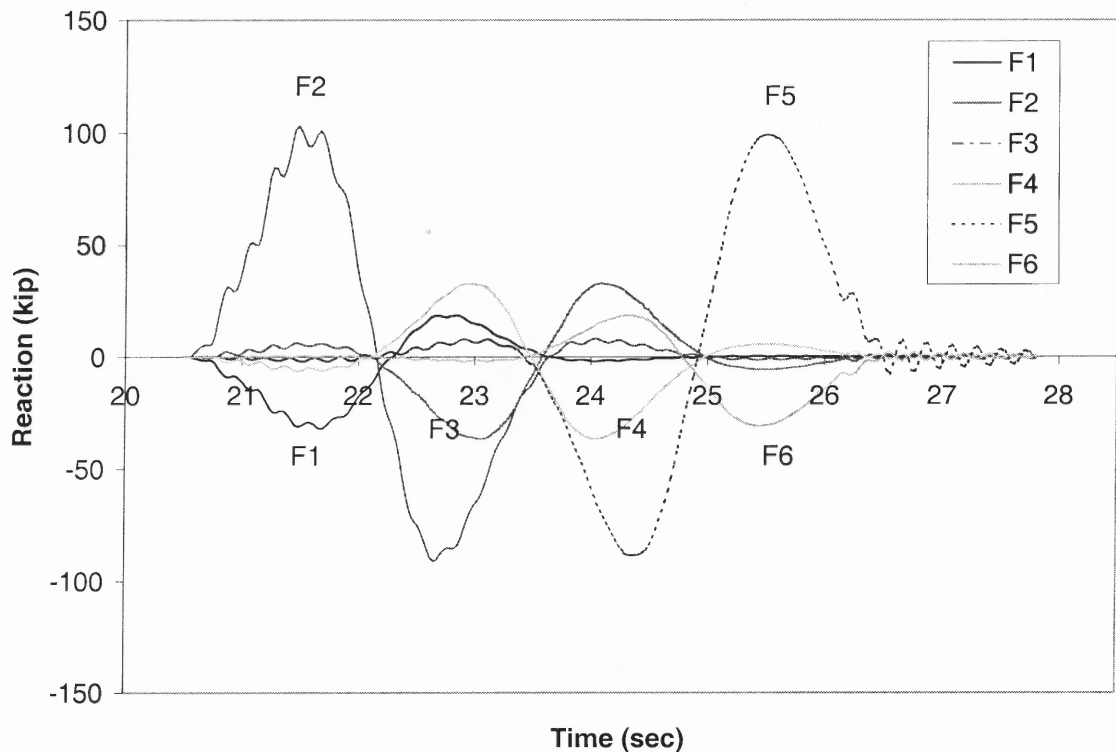


Figure 2.27 Reaction in anchor rods from model 1.

The 2nd model is then developed based on the above elastic model to simulate the responses of the bridge. Three different moments of inertia are given to each continuity diaphragm (one for the left, one for the right and their average for the center) to reflect different levels of restraint applied by the complex support system to the left span and to the right span. Total 6 moments of inertia are given to the beam portions over the three supports. The moment of inertia of the girder is I_0 , same as that in model 1. Figure 2.28 shows the support detail of the second model.

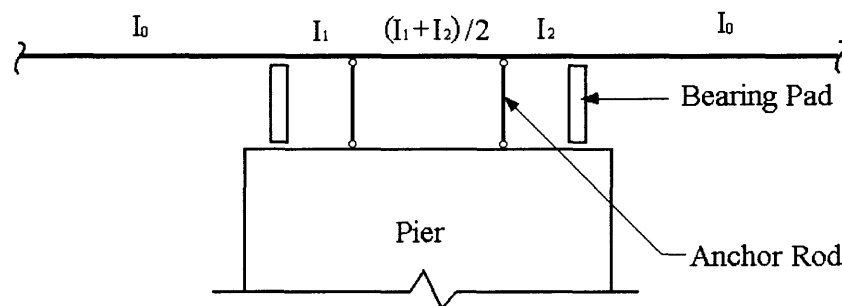


Figure 2.28 Model 2 support detail.

Velocity of the vehicle is calculated from the test data (data were recorded every 0.02 sec). Live load is estimated from the LVDT and DCDT readings by multiplying them by the stiffness of the elastomeric bearing pads. For the test shown in Figure 2.24, velocity of the truck equals 75 ft/sec (51 mph), and the live load equals 19,000 lbs, which is 30% of an AASHTO HS20-44 truck. Three wheel loads spacing 14' and 30' with a velocity of 75 ft/sec are applied to the model for transient dynamic analysis. The damping ratio is assumed to be 3%. By trial and error, the analytical mid-span strains shown in Figure 2.29 were obtained with the following parameters: $I_1 = I_0/30$, $I_2 = I_0/600$, $I_3 = I_0/600$, $I_4 = I_0$, $I_5 = I_0$, and $I_6 = I_0/30$. It can be seen that the results match the test data very well.

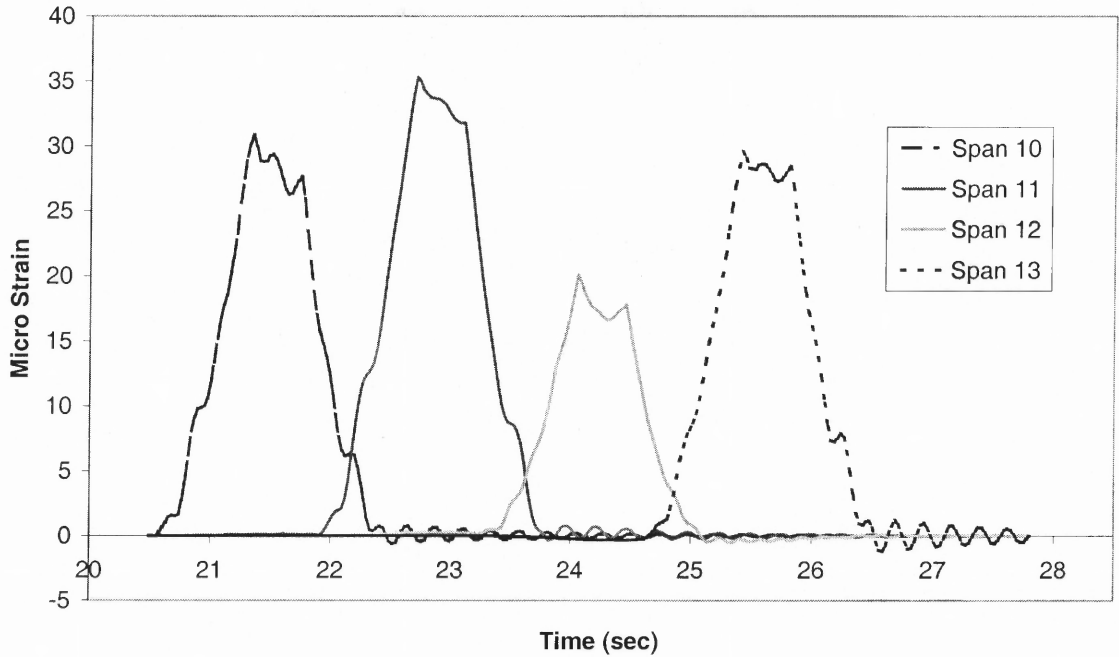


Figure 2.29 Analytical mid-span strains from model 2.

The 3rd model is simply to get the analytical responses assuming full continuity at all supports. The same parameters (load, speed, damping ratio etc.) as in model 2 are used, except that I_1 through I_6 are all equal to I_0 . The results are shown in Figure 2.30.

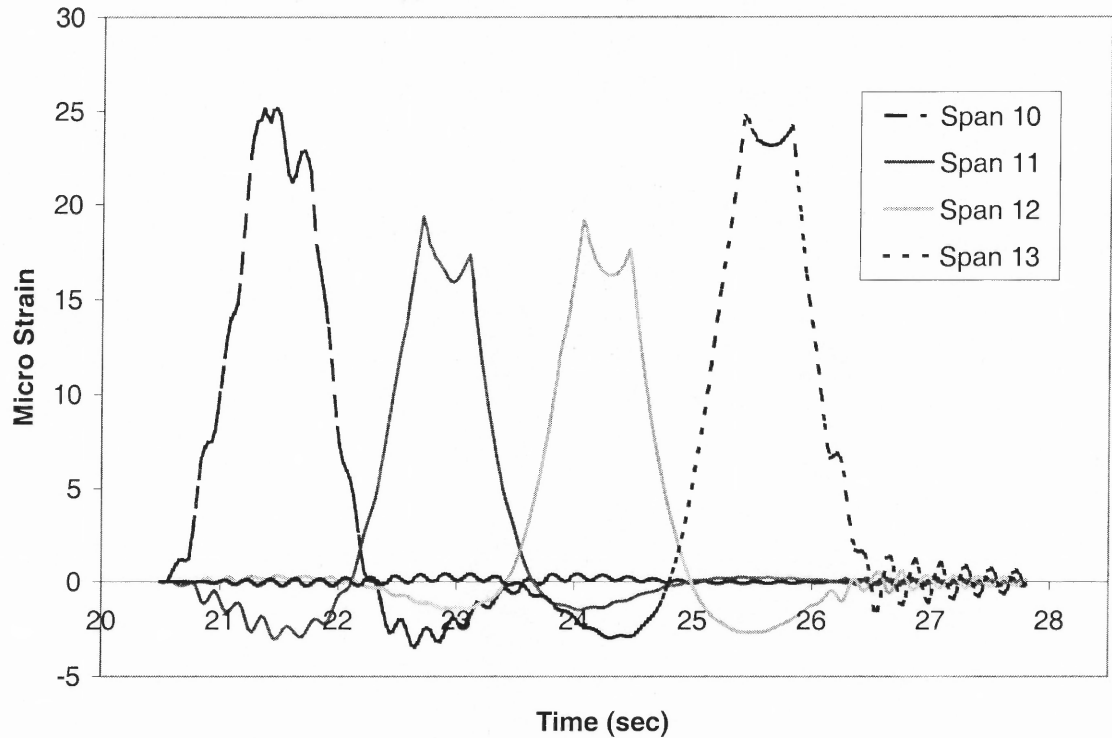


Figure 2.30 Analytical mid-span strains from model 3.

Following Mirmiran's definition^[11], the continuity indices for spans 10, 11, 12 and 13 at mid-span would be 1.25, 1.85, 1.07 and 1.25, respectively. The closer the continuity index is to one, the higher is the degree of continuity. Thus, span 12 is the most continuous while span 11 is the least continuous. Spans 10 and 13 have the same continuity.

It is more natural to define degree of continuity as 0% for simple spans and 100% for fully continuous spans. *Degree of continuity* is defined as:

$$D.O.C. = (\varepsilon_s - \varepsilon_t) / (\varepsilon_s - \varepsilon_c)$$

where *D.O.C.* – degree of continuity.

ε_s – midspan strain for simple spans.

ε_t – midspan strain from test.

ε_c – midspan strain assuming full continuity.

The degrees of continuity thus calculated for four spans are 57%, 17%, 95% and 65%, respectively. It can be seen that span 12 has the highest D.O.C. (95%), span 11 has the lowest (17%) and spans 10, 13 are around 60%, which agree with the results using Mirmiran's definition. The average degree of continuity for this bridge is 59%.

2.5 Analysis of Support Details

From the above field tests, it is clear that the support details (having two bearings at each pier and providing anchor bolts in the continuity diaphragm) make the bridges behave differently from analysis assuming idealized “pin” or “roller” supports. This section presents an analytical study on the support details using 2-D finite element models.

A two-span continuous bridge with equal spans of 80' is taken as an example. The girders are 54" deep and the deck is 6" in thickness. The continuity diaphragm between the two girder ends is 12" and the distance between the center line of the two bearings at each pier is 20". A concentrated load of 72 kips is applied at the midspan of span 1.

The girder, deck, part of pier and bearings are all modeled with 2-D plain stress elements. The modulus of elasticity is 4.5×10^6 psi for girder concrete and 0.2×10^6 psi for bearing. Since the bearings only take compression and the load is applied to the left span, only the left bearing is modeled. The composite girder is divided into five elements in the vertical direction and 41 elements in the horizontal direction for each span. The continuity diaphragm is divided into four elements in the horizontal direction.

Three support details are studied: 1) without anchor bolts, 2) with one row of anchor bolts placed in the middle of the diaphragm, and 3) with two rows of anchor bolts spaced 12" apart (6" each side from the diaphragm center). Each row has two anchor bolts of 2" diameter put in the transverse direction. Figure 2.31 shows the model without anchor bolts. The top figure shows the whole model. The bottom is a close-up of the support area.

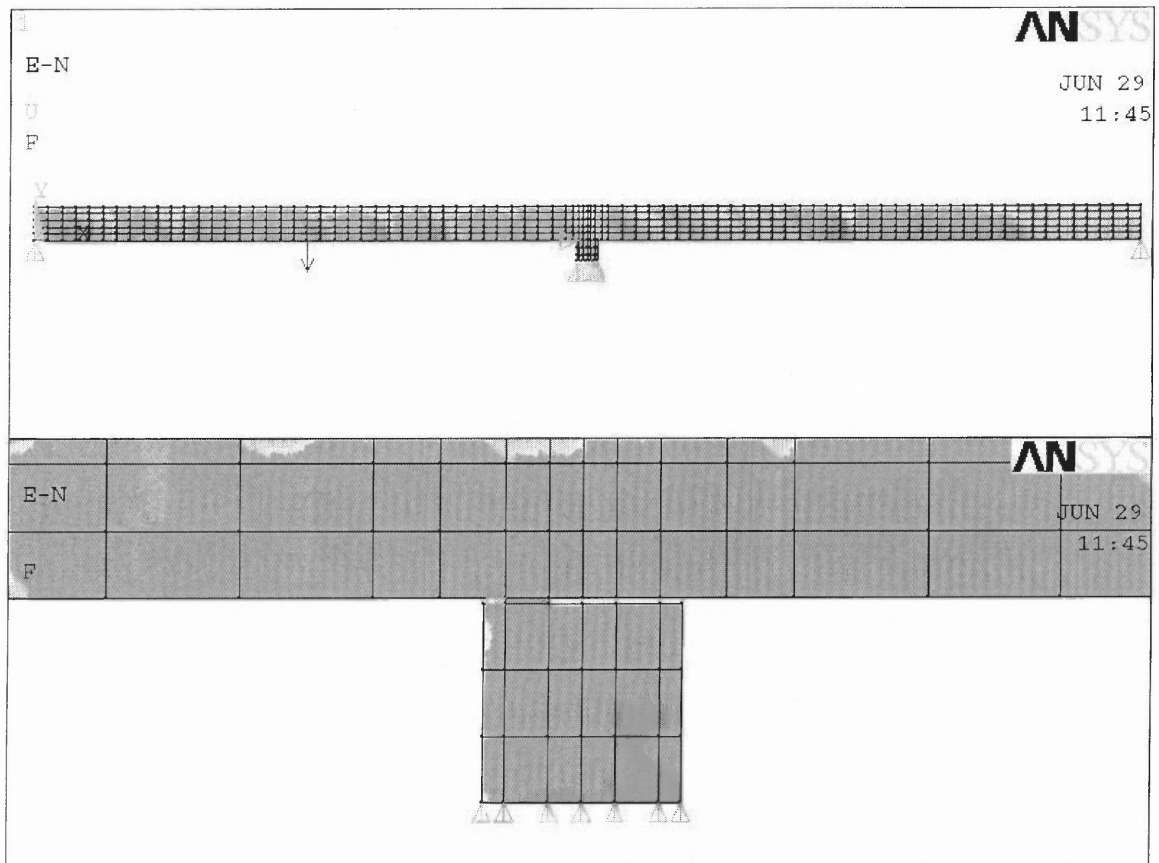


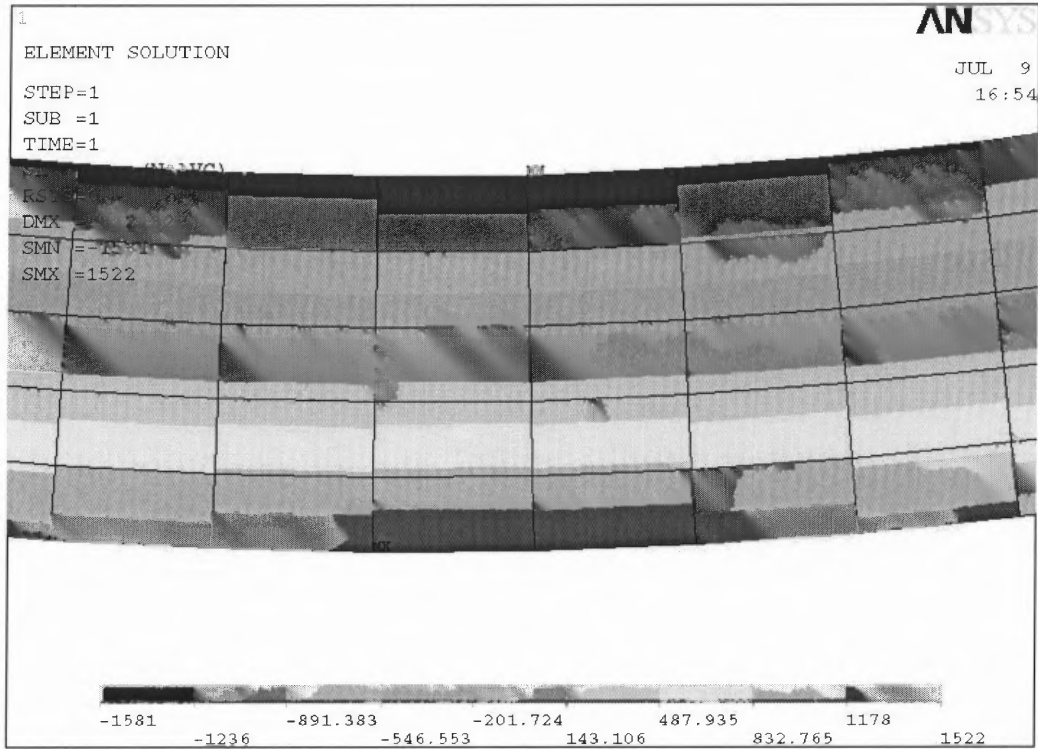
Figure 2.31 2-D finite element model of a 2-span bridge.

Analytical results are listed in Table 2.2. The second column lists the horizontal stress at midspan. It can be seen that the values are close to one another. The stress at midspan with one row of bolts is 3% less than that without bolts and the stress with two rows of bolts is 7% less than that without bolts. For the stresses in the diaphragm, the three

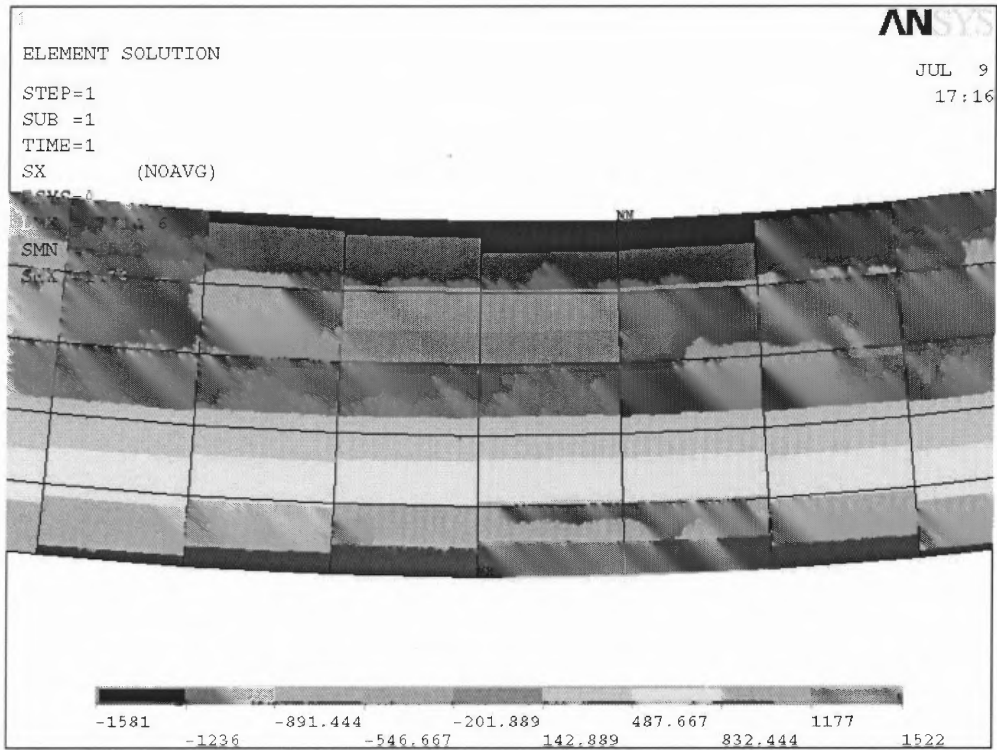
models differ considerably from one another. For horizontal stress, the value changes from -648 psi (compression) to -62 psi for one row of bolts case and to 80 psi (tension) for two rows of bolts case. For vertical stress, the value increases from 230 psi to 1,164 psi for one row of bolts case and to 1,485 psi for two row of bolts case, which is 6.5 times higher than the case without bolts. These tension stresses - combined with the positive restraint moment caused by time dependent effects - make the diaphragm prone to cracking. Therefore, it is desirable not to use anchor bolts in the continuity diaphragm. If anchor bolts have to be provided, they should be placed in the diaphragm off the girder lines and be sheathed. Figures 2.32 to 2.34 show comparisons of stresses at the midspan and at the support.

Table 2.2 Comparison of Midspan and Diaphragm Stresses

	Horizontal Stress At Midspan (psi)	Horizontal Stress In the Diaphragm (psi)	Vertical Stress In the Diaphragm (psi)
Without Bolts	1,522	-648	230
With 1 Row of Bolts	1,473	-62	1,164
With 2 Row of Bolts	1,422	80	1,485

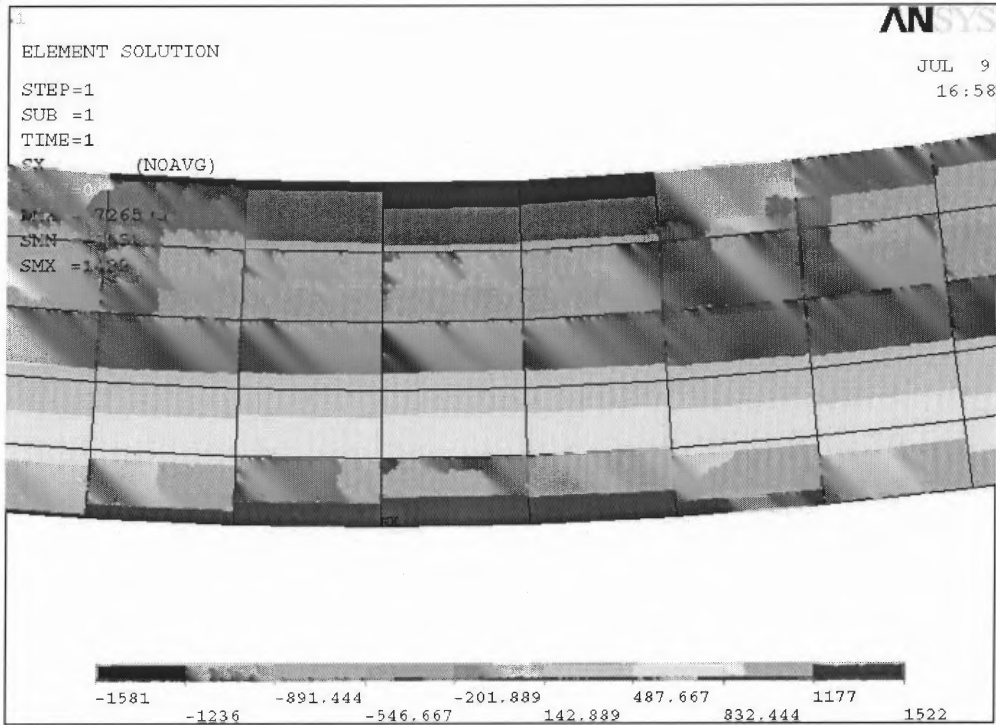


(a) Without anchor bolts.



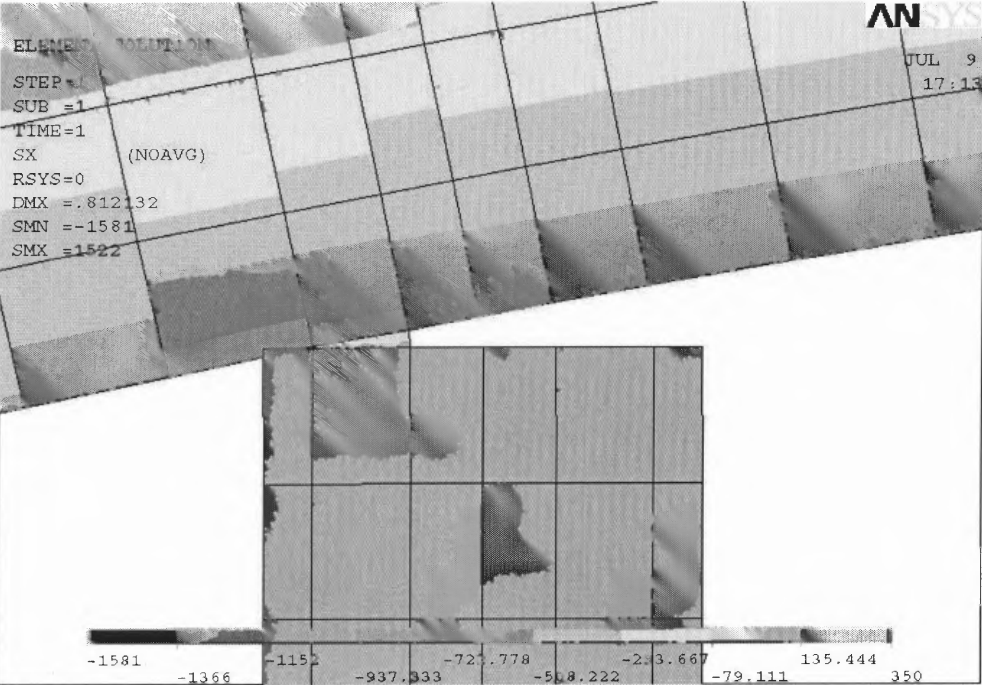
(b) With 1 row of anchor bolts.

Figure 2.32 Comparison of horizontal stresses at midspan.



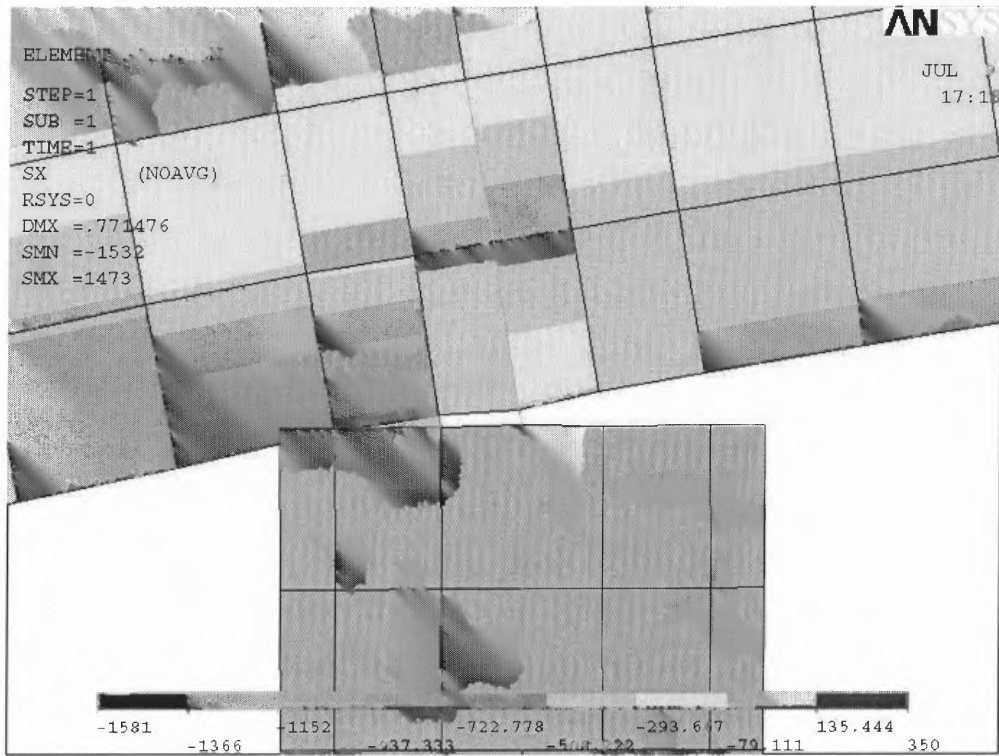
(c) With 2 row of anchor bolts.

Figure 2.32 Comparison of horizontal stresses at midspan (continued).

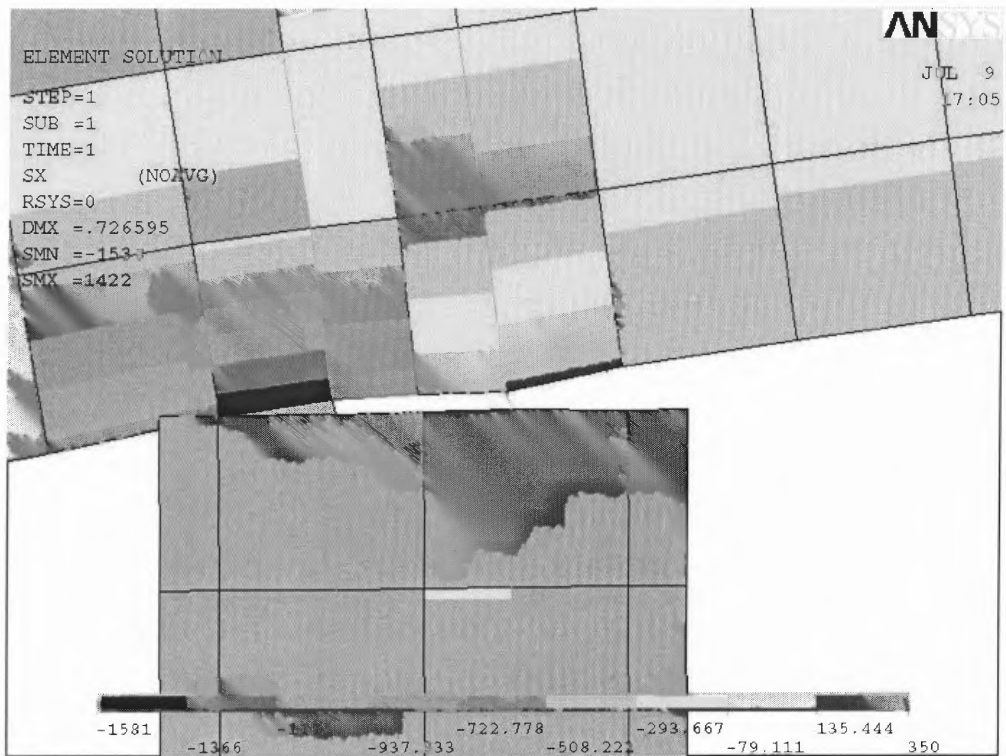


(a) Without anchor bolts.

Figure 2.33 Comparison of horizontal stresses at the support.

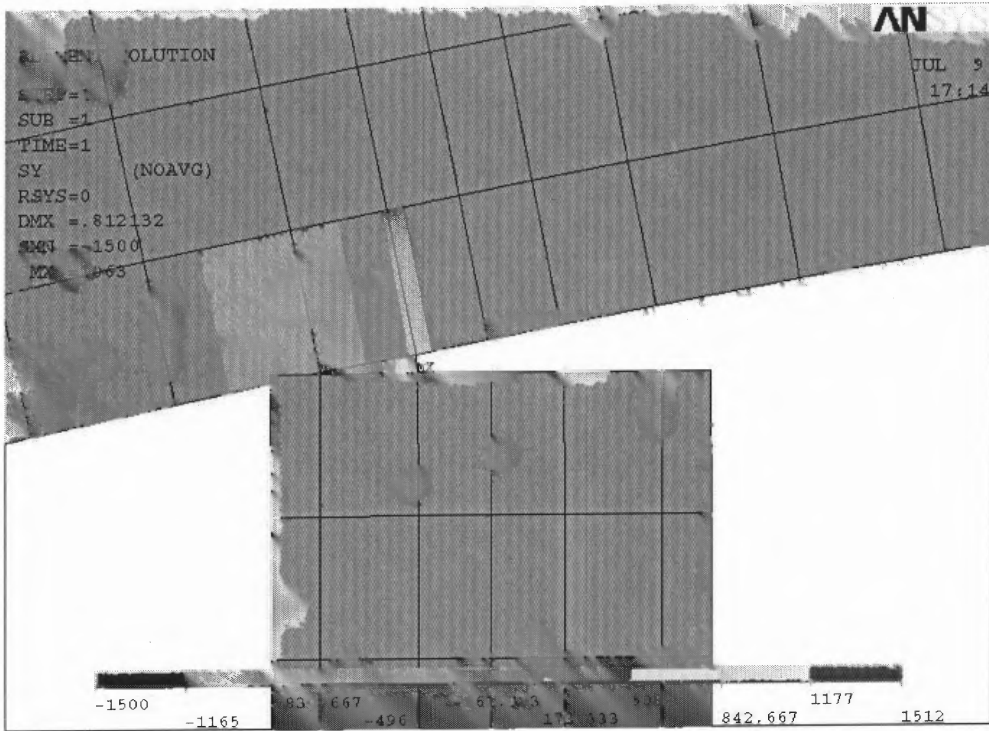


(b) With 1 row of anchor bolts.

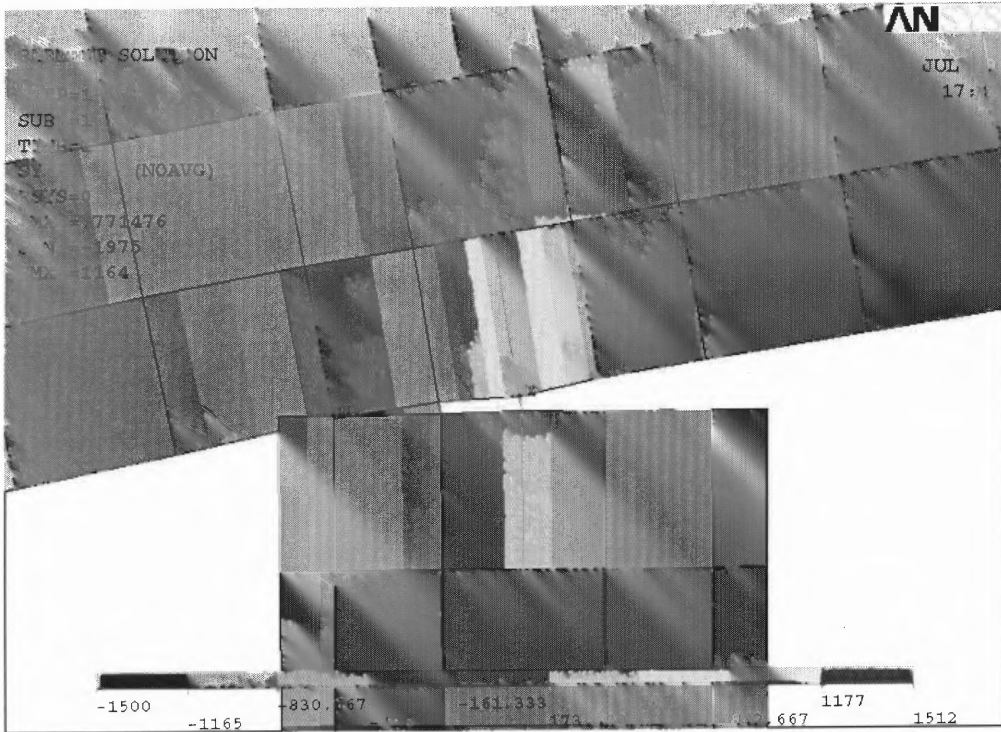


(c) With 2 row of anchor bolts.

Figure 2.33 Comparison of horizontal stresses at the support (continued).

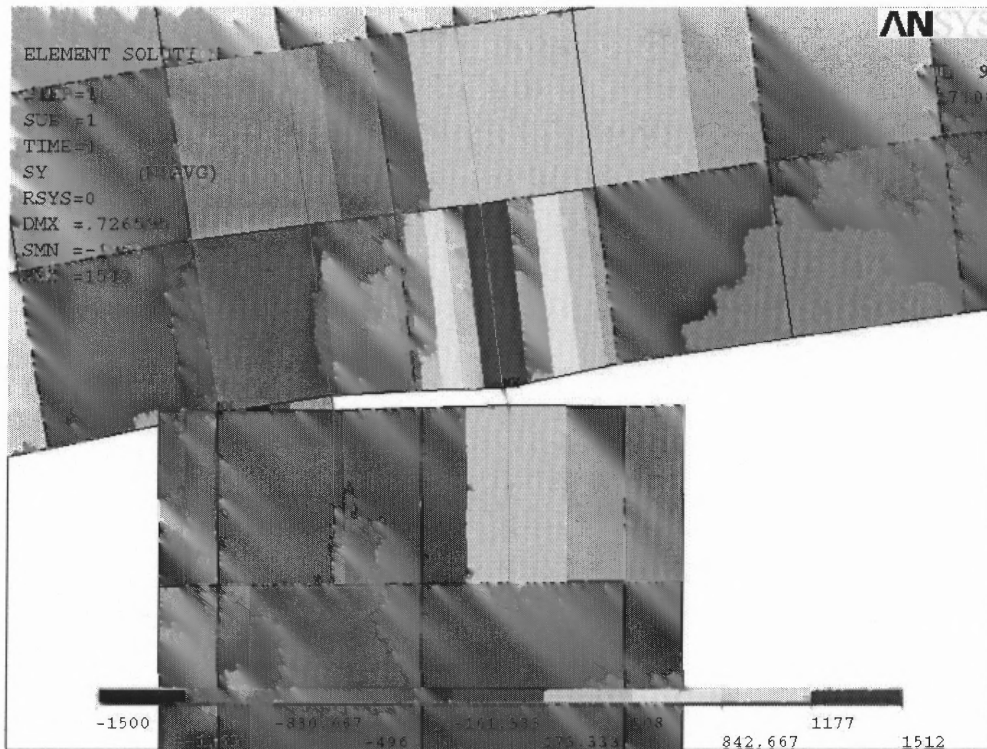


(a) Without anchor bolts.



(b) With 1 row of anchor bolts.

Figure 2.34 Comparison of vertical stresses at the support.



(c) With 2 row of anchor bolts.

Figure 2.34 Comparison of vertical stresses at the support (continued).

2.6 Conclusions And Recommendations

Based on the above experimental and analytical studies, the following conclusions are made:

1. The degree of continuity under service load ranges from 0% to 90% for the bridges tested. The bridge on I-287NB over Darlington Avenue has 90% continuity, the bridge on Rt. 1&9SB in Newark has 59% continuity and the bridge on I-287NB over Skyline Drive has 0% continuity.
2. The difference in continuity is caused by many factors, among which time dependent effects (mainly creep) play an important role. A thorough comparison of the three bridges suggests that girder age at continuity might be the most important factor. The girder age data are difficult to get. Visual inspection shows that the Skyline Overpass has more of a creep effect, because one can clearly see its upward camber after 10 years of service. This supports the fact that its diaphragms crack and no continuity was measured.

3. Embedding the girders in the diaphragm, using thin elastomeric pads that has little lateral deformation capacity and providing anchor bolts in girder lines make the supports more like “fixed”. The fixity restrains the girders from sliding and rotating, and causes cracking in the diaphragm and even in the top flange of the girders. Skyline overpass has one 1.25” diameter anchor rod; Rt. 1&9 bridge has four 2.5” diameter anchor rods; Darlington bridge doesn’t have anchor bolts in girder lines, instead 6” diameter posts are put in the diaphragm between the stringers. These posts are separated from the diaphragm by compressible pads. Darlington bridge turns out to have the highest degree of continuity. Possible improvements for the current design include: a) de-bonding the girder ends or not embedding them at all; b) avoid using anchor bolts in girder lines; if they have to be used, try to put them in the diaphragm between stringers and sheath them to allow for free rotation of the girders; c) it is preferable to design only one “pin” support (fixed both vertically and horizontally) for continuous spans to allow for longitudinal deformation. If more than one pin is provided, design shall account for all the longitudinal forces including temperature changes, axial creep of the prestressed girders, shrinkage of the concrete, wind on live load and wind on structures, etc.

4. U-shaped positive moment connections don’t perform as well as expected, especially when the horizontal development length is inadequate. Per PCA test results, it is recommended that welded connections be used for the positive moment reinforcement. Or more effectively, make the girders continuous for slab dead load and avoid providing the positive moment reinforcement in the diaphragm.

CHAPTER 3

FINITE ELEMENT ANALYSES

As mentioned in the literature review, much work has been done, and computer programs have been developed to calculate the time dependent effects of simple span girders made continuous since 1960s, but all these efforts were based on beam theory and usually employed two-dimensional models. With the rapid development of digital computing, there are many comprehensive engineering software packages available (such as ANSYS, ADINA, and ABAQUS) to solve these problems. All of these packages have mature nonlinear equation solvers, and convergence control techniques. There are also 3-D solid elements suitable to model reinforced concrete structures. Finite element analysis can give more insight into the problem in question, especially for the connection area (girder ends and diaphragms including negative and positive moment reinforcement).

This chapter presents the finite element analysis of simple span girders made continuous. Material properties including the creep and shrinkage of concrete and the relaxation of prestressing strands are programmed and linked to ANSYS. The finite element model using these materials is then verified with PCA tests. Two important factors affecting the performance of simple span girders made continuous, namely the girder age at continuity and the amount of the positive moment reinforcement, are studied using the verified finite element model.

3.1 The Finite Element Model

3.1.1 Material Models

Concrete creep and shrinkage and strand relaxation are the driving factors for the restraint moment that will develop in bridges composed of simple span girders made continuous. ACI-209R (92) concrete creep and shrinkage models and PCI strand relaxation model are used in this study. These material models are not readily available in the existing software packages. They were programmed and linked into ANSYS under this study through “User Supplied Material Model” option.

ACI Committee 209 – Concrete Creep Model

Creep is defined as the time-dependent increase of strain in hardened concrete subjected to sustained stress. It includes drying creep, where no moisture movement to or from the environment, and drying creep which is caused by drying of the concrete. Creep coefficient is the ratio of creep strain to initial elastic strain. The creep prediction recommended by ACI-209 applies to normal weight and all lightweight concrete using both moist and steam curing and Type I and III cement. According to ACI-209, the creep coefficient at any time “t” is:

$$C_t = \frac{t^{0.6}}{10 + t^{0.6}} C_u$$

where C_t = Creep coefficient at time “t”.

C_u = Ultimate creep coefficient, usually 2.35, should be modified by factors determined from concrete age at loading, ambient temperature and humidity, minimum size of specimen, volume surface ratio, etc.

t = Time after loading (days).

Creep strain

$$\varepsilon_{cr} = \varepsilon_i \cdot C_t = \frac{\sigma_i}{E_{ci}} \cdot \frac{t^{0.6}}{10 + t^{0.6}} C_u$$

where ε_{cr} = Creep strain at time “t”

ε_i = Initial strain

σ_i = Initial stress

E_{ci} = Initial Modulus of Elasticity

Rate of creep

$$\dot{\varepsilon}_{cr} = \frac{6 \cdot \sigma_i \cdot C_u}{E_{ci}} \left[\frac{t^{-0.4}}{(10 + t^{0.6})^2} \right]$$

An incremental solution scheme is carried out. The time steps used in this model as well as the following models should not be very large, especially at the beginning, in order to get accurate results.

ACI Committee 209 – Concrete Shrinkage Model

Shrinkage is the decrease with time of concrete volume due to changes in the moisture content of the concrete and physico-chemical changes. Shrinkage includes drying shrinkage, autogenous shrinkage and carbonation shrinkage. Drying shrinkage is due to moisture loss in the concrete; autogenous shrinkage is caused by cement hydration; and carbonation shrinkage results as the cement hydration products are carbonated in the presence of CO₂. The ACI-209 shrinkage model applies to normal weight and all lightweight concrete using both moist and steam curing and Type I and III cement. For seven-day moist cured concrete, shrinkage is:

$$(\varepsilon_{sh})_t = \frac{t}{35+t} \cdot (\varepsilon_{sh})_u$$

For 1~3 days steam cured concrete, shrinkage is:

$$(\varepsilon_{sh})_t = \frac{t}{55+t} \cdot (\varepsilon_{sh})_u$$

where $(\varepsilon_{sh})_t$ = Shrinkage at time “t” after curing.

$(\varepsilon_{sh})_u$ = Ultimate shrinkage of concrete, usually 780×10^{-6} in/in, should be modified by factors determined from days of curing, ambient temperature and humidity, minimum size of specimen, volume surface ratio, etc.

t = Time in days after curing.

Concrete shrinkage is modeled as thermal loads:

$$(\varepsilon_{sh})_t = \alpha \cdot \Delta T$$

$$\Delta T = (\varepsilon_{sh})_t / \alpha$$

where ΔT = Equivalent temperature drop

α = Coefficient of thermal expansion of concrete

PCI Model - Relaxation of Prestressing Strands

Relaxation is the stress reduction in the strands with time when they are stressed to some initial value and held at a constant strain. This phenomenon only becomes significant at high stress levels. Elevated temperature (above 100°F) may greatly increase the relaxation. PCI^[32] models are used in the finite element analysis.

For stress relieved strands,

$$f_{sr} = f_{si} \cdot \frac{\log_{10}(24t)}{10} \left(\frac{f_{si}}{f_y} - 0.55 \right)$$

For low relaxation strands,

$$f_{sr} = f_{si} \cdot \frac{\log_{10}(24t)}{45} \left(\frac{f_{si}}{f_y} - 0.55 \right)$$

where f_{sr} = Relaxation of pre-strands at time “t” (psi).

f_{si} = Initial stress of pre-strands (psi).

f_y = Yield strength of pre-strands (psi).

t = Time in days after pre-stress application.

Rate of relaxation,

$$\dot{f}_{sr} = \frac{f_{si}}{45 \ln_{10}} \left(\frac{f_{si}}{f_y} - 0.55 \right) \cdot \frac{1}{t}$$

Equivalent rate of creep,

$$\dot{\epsilon}_{sr} = \frac{f_{si}}{45 \ln_{10} \cdot E_s} \left(\frac{f_{si}}{f_y} - 0.55 \right) \cdot \frac{1}{t}$$

where E_s = Modulus of elasticity of pre-strands.

3.1.2 Finite Element Model

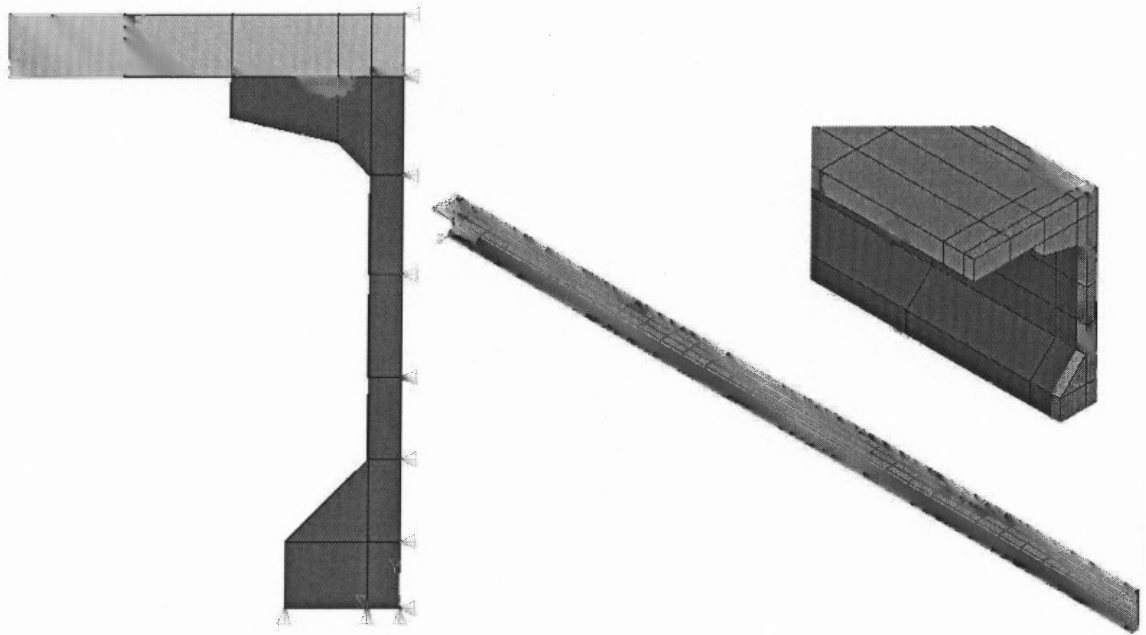
The girder, deck and diaphragm concretes are modeled with 3-D solid elements (Solid65 in ANSYS) with creep, cracking and crushing capabilities. Reinforcement and prestressing strands are modeled with 3-D spar elements (Link8 in ANSYS) with bilinear material properties.

For a two-span continuous bridge with equal spans, only a quarter of a stringer is modeled because of symmetry. Boundary conditions are applied accordingly. At a cross section, the girder (half) is modeled with ten Solid65 elements, the deck slab (half) is modeled with five Solid65 elements. Meshing in the longitudinal direction varies

according to the problems. Figure 3.2 shows the finite element model.

Element birth and death features were used to model staged construction. Initially, the girder is simply supported and the gravity load of the girder is applied. The girder then experiences time dependent effects (creep and shrinkage of concrete and relaxation of prestressing strands) up to the age when deck and diaphragm concrete are poured. At this stage, the deck, diaphragm concrete and the reinforcement are born stress-free. The whole structure then experiences the time dependent effects until the application of the live load.

Time step is small at the beginning of the solution and gets larger towards the end. During the first 100 days, time increment is set to one day. From 101 days up to a year time step is increased to five days, and thereafter time step is set to ten days. In addition, automatic time stepping is turned on, which means whenever the solution is not converged at certain time step, the program will automatically cut the time step in half, then in quarter ..., until the solution converges. Convergence criteria is set to 0.001, i.e. when the square root sum of squares (SRSS) of the imbalanced forces is less than one thousandth of the SRSS of the applied forces, the solution at that time step is converged.



(a) Cross section

(b) Isotropic view

Figure 3.1 Finite element model.

3.2 Comparison with PCA Tests and Other Analytical Methods

To verify the finite element model, the analytical results using this model were compared to PCA test results and those of other analytical methods.

3.2.1 PCA Test Outline

The PCA tests were carried out on two half-scale specimens of a real two-span bridge. Each span of the test structure was 33' long. The girders were simply supported at first and then made continuous through cast-in-place deck slabs. Beam1/2 (composed of simple girders 1 and 2) and Beam3/4 (composed of simple girders 3 and 4) were virtually identical except that Beam3/4 had positive moment reinforcement (4 #3) at the interior support while Beam1/2 didn't have any positive moment reinforcement.

The girders were I-shaped in cross section. Each girder was prestressed with 28

seven-wire stress relieved strands of $\frac{1}{4}$ inch diameter. The prestressing force was 175 kips. The strands were released at the girder age of 8 days. After the prestress release, each pair of girders was positioned on top of three columns that served as supports. Thirteen days after positioning, 800 lb concrete blocks were hung every 3' along the girders to compensate for the dead weight of the half-scale model. The negative and positive moment reinforcements (if any) were then installed and deck/diaphragm concrete was cast at a girder age of 28 days. The deck formwork was removed 7 days later.

After removal of the deck formwork, service live load tests were carried out at different intervals. The central support reaction, mid-span deflection and strains in the negative moment reinforcement were measured during each test. The structures were finally tested to destruction at a girder age of 680~690 days.

The cross section of the specimen is illustrated in Figure 3.1 and the material properties are listed in Table 3.1.

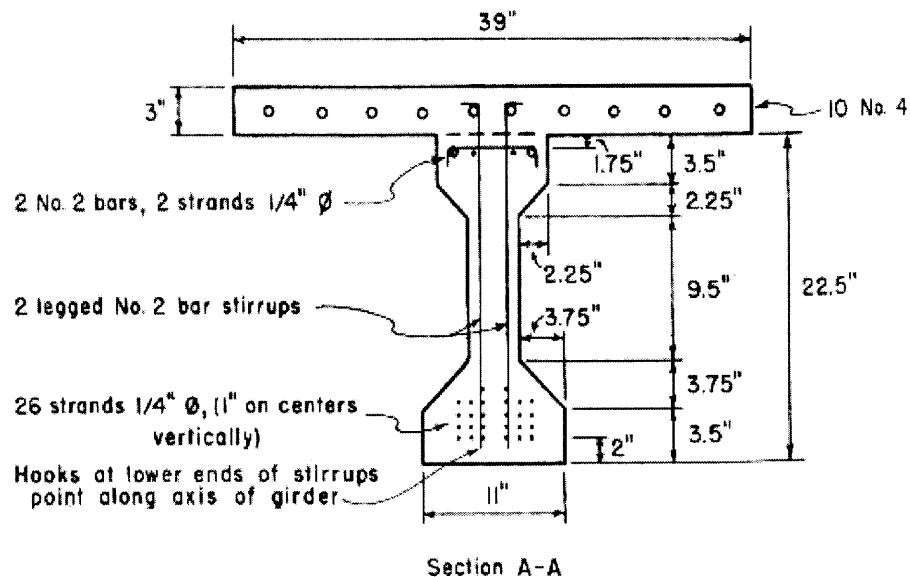


Figure 3.2 Cross section of PCA specimens.

Table 3.1 Material Properties of PCA Specimens

Item	Properties
Prestressing Strands	$f_u = 280 \text{ksi}$ $f_y = 254 \text{ksi}$ $E_s = 28,700 \text{ksi}$
Negative Steel over piers	$f_y = 48.5 \text{ksi}$ $E_s = 29,500 \text{ksi}$
Positive Steel in Diaphragm	$f_y = 50 \text{ksi}$ $E_s = 29,500 \text{ksi}$
Girder Concrete	3-day moist cure, type III cement, 70°C, 50% humidity $f_c' = 5,450 \text{psi}$
Deck and Diaphragm Concrete	3-day moist cure, type III cement, 70°C, 50% humidity $f_c' = 4,820 \text{psi}$

3.2.2 Comparison of Results

The finite element model described in Section 3.1 was used to do the analysis. A total of 1055 elements were used to model a quarter of each PCA specimen, among which 345 were Solid65 8-node block elements and 710 were Link8 2-node bar elements. The solution time for each run was approximately four to five hours.

A comparison of the central support reaction of Beam3/4 is plotted in Figure 3.3. The results of PBEAM^[9] and REATRAINT^[11] are also plotted. It can be seen that the finite element results agree well with the PCA test data. At the beginning, differential shrinkage dominates, causing the central support reaction to increase. Then the creep effect catches up as time passes causing the central support reaction to decrease. Both the FEA and PBEAM results underestimate the decrease of central support reaction. The

reason could be that the ACI model underestimates the concrete creep in this case. The ACI model assumes seven days moisture cure or one to three days steam cure of concrete, but the specimens were moisture cured for three days in PCA tests and ACI doesn't give any modification factor to account for this case. The FEA results also underestimate the differential shrinkage a bit. Results from RESTRAINT agree well with the decrease of the central support reaction, but overestimates the increase by about 20%.

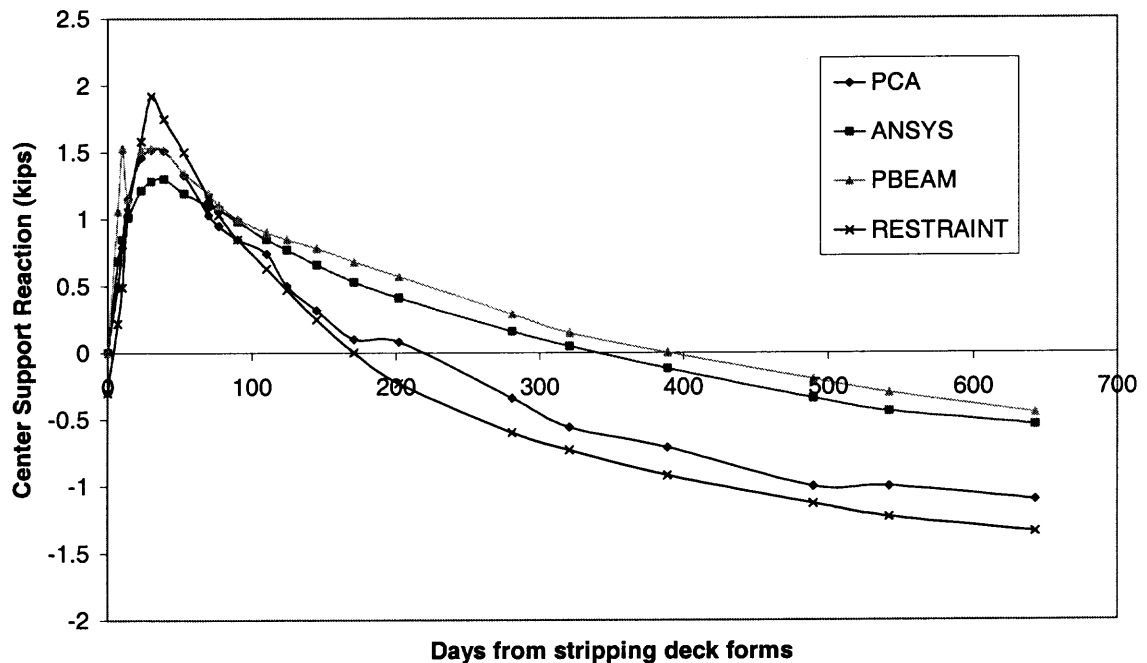


Figure 3.3 Comparison of central support reaction of Beam3/4.

A comparison of the central support reaction of Beam1/2 is plotted in Figure 3.4. Results of RESTRAINT are also plotted. No data are available from PBEAM or CTL for this beam. RESTRAINT in this case overestimates the increase of the reaction. For some reason, the decrease is not complete, but it can be seen that the data underestimate the decrease of central support reaction. The FEA results agree well with the ascending branch, but again underestimate the descending branch.

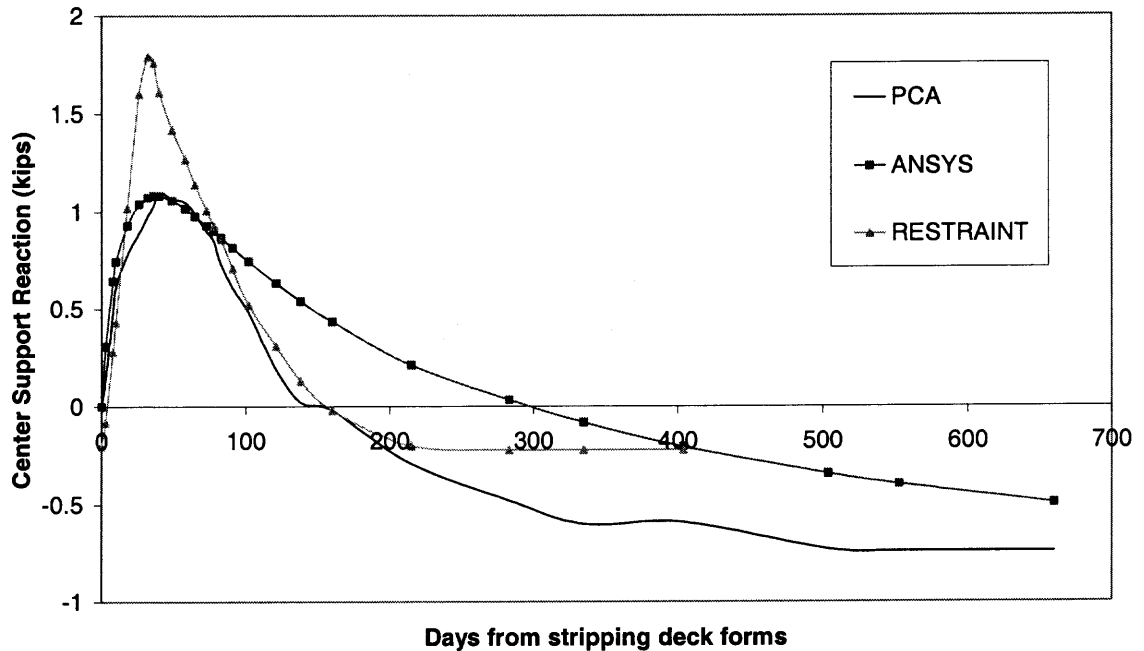
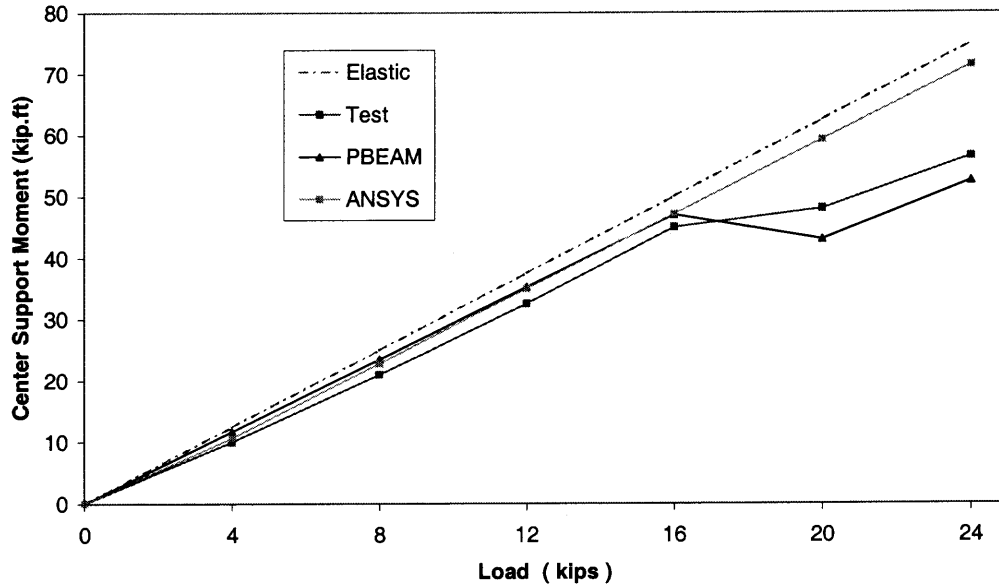
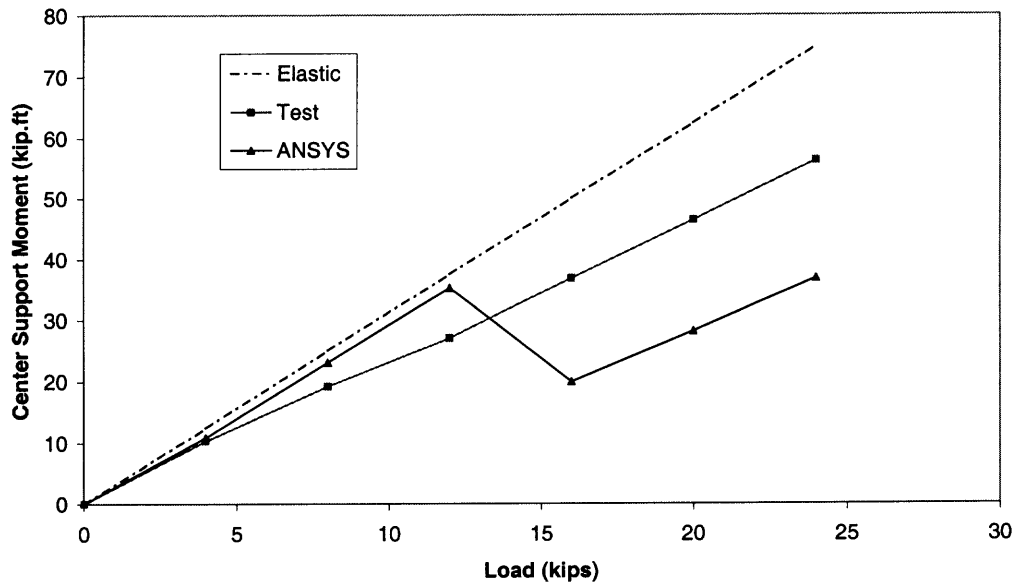


Figure 3.4 Comparison of central support reaction of Beam1/2.

Figure 3.5 shows the variation of Beam3/4 central support moment due to live load at different stages. The finite element model predicts cracking of deck slab at a girder age of 55 days instead of 45 days, meaning that the FE model slightly underestimates the differential shrinkage.

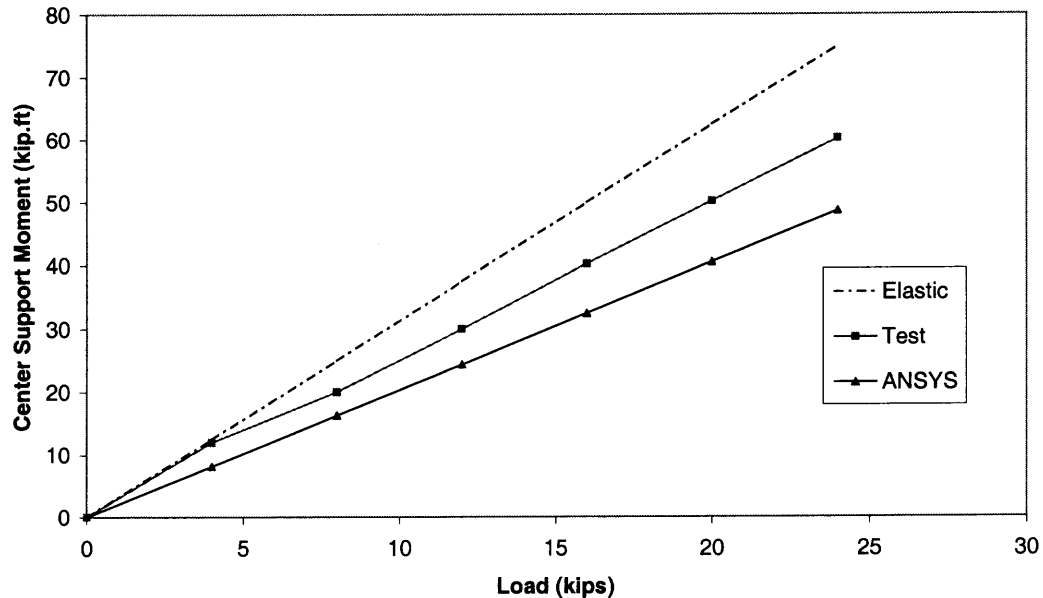


(a) Girder age of 45 days.



(b) Girder age of 55 days.

Figure 3.5 Variation of central support moment with load at different girder ages.



(c) Girder age of 684 days.

Figure 3.5 Variation of central support moment with load at different girder ages (continued).

For Beam1/2, the central support moment is still linear with regard to live load instead of bi-linear which would indicate the closing of the cracks. This means that the FE model overestimates the positive moment resistance. The reasons could be that: 1) the creep coefficient used in the FE model was lower than the real value, thus the positive restraint moment was not large enough to crack the diaphragm; 2) the negative moment reinforcement was placed in two layers (top and bottom) while in reality it was in one layer in the middle of the deck slab. If the crack propagated into the deck slab, the bottom reinforcement could resist some moment; and 3) to help convergence, a small amount of positive moment reinforcement was provided in the diaphragm.

From the comparison of results, it is concluded that the FE model is capable of analyzing the time dependent effects of bridges composed of precast, prestressed concrete

girders made continuous with acceptable accuracy. This model is used to study two most important factors affecting degree of continuity.

3.3 Parametric Study

The support restraint moment depends on many factors such as creep and shrinkage properties of the girder and deck concrete, relaxation of the prestressing strands, girder age at deck casting, girder age at application of live load, construction sequence of the deck and the diaphragm, the amount of positive moment reinforcement, and structural features like span length, number of spans, girder spacing, etc. Two important factors, namely the girder age at deck casting and the amount of positive moment reinforcement, were studied using the finite element model described in section 3.1. A total of 1,822 elements were used to model a quarter of each stringer, of which 495 were Solid65 8-node block elements and 1,327 were Link8 2-node bar elements. The solution time for each run was approximately 8 hours.

3.3.1 Girder Age at Deck Casting

The girder age at deck casting is an important factor for time dependent effects, specially for differential shrinkage. When girders are made continuous at an early age only a small amount of differential shrinkage develops between the girder concrete and deck concrete. Therefore, creep dominates. If live loads are applied at late ages, creep of the girder concrete can cause a large positive moment at inner supports resulting in severe cracks in the diaphragm. On the other hand, when the girders are made continuous at late ages differential shrinkage will dominate. If live loads are applied early, large negative moments develop at the piers, which will cause severe transverse deck cracking over the piers.

A parametric study was carried out to investigate this effect. A two-span continuous stringer was taken out from the bridge on I-287 over Darlington Ave for analysis. The girders are AASHTO Type VI girders. The deck is 7.5" thick. The first span is 120' long and the second is 118', with an 8" diaphragm between the two girders. Positive moment reinforcement equals $2.4M_{cr}$ (8 pre-strands are provided at the diaphragm bottom). To create a scenario that can cause maximum positive moment over the pier, the ultimate creep coefficient for both girder and deck concrete is set at 3.25. Ultimate shrinkage is set to be 600×10^{-6} in./in. Girder age at deck casting is chosen to be 10, 28, 60 and 90 days, respectively. Live load is applied 2 years after continuity is established.

Figure 3.6 shows the variation of mid-span moment with girder age at deck casting. It should be noted that the live load application is elongated for clarity. In the analyses, the live load was applied within one day, so time dependent effects are negligible during live load application. The same notion applies to all following figures in this chapter containing live load applications.

For the 10-day case, little differential shrinkage develops and creep dominates. The mid-span moment increases with time because a positive restraint moment develops at the inner support. The diaphragm section fails at the girder age of 138 days when the positive moment reinforcement yields. Creep also dominates the 28-day case. For the 60-day and 90-day cases, differential shrinkage develops and causes the mid-span moment to drop first and then pick up when creep strain accumulates.

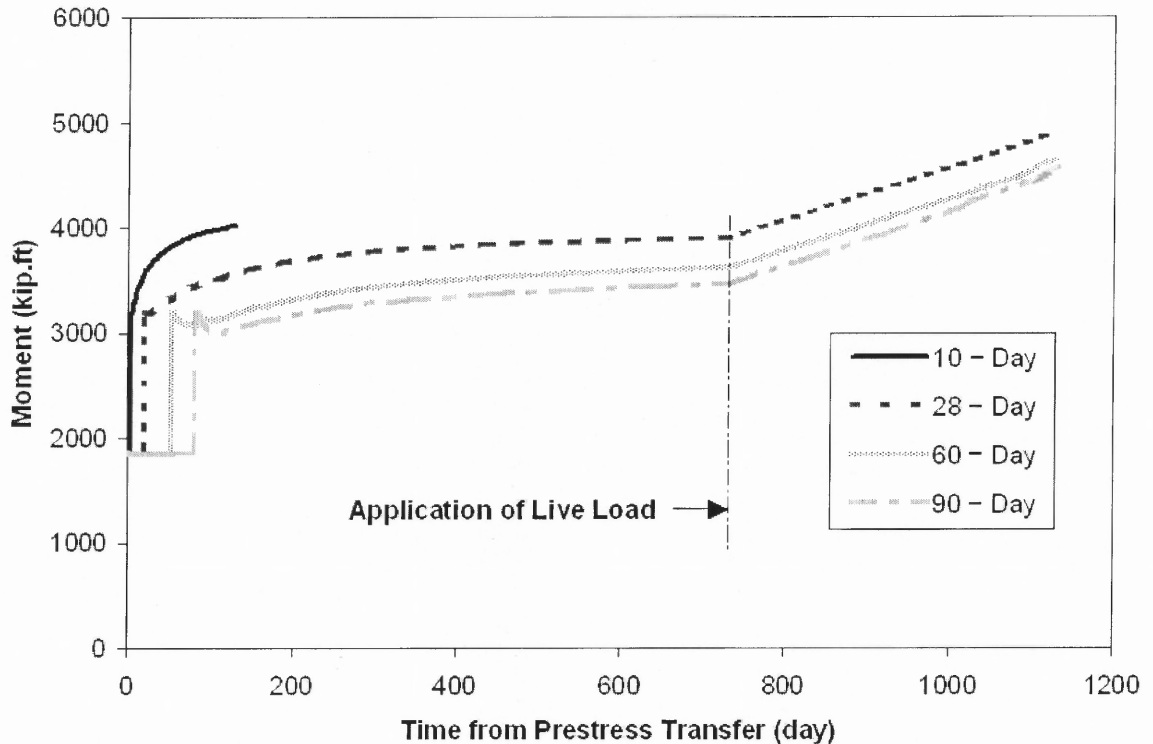


Figure 3.6 Variation of mid-span moment with girder age at deck casting.

The curves go parallel to one another after the peak of differential shrinkage. At service load, they're still parallel except that the 60-day and 90-day curves jump up a little bit because of cracking of the deck over the central support. The younger the girder at deck casting, the bigger the mid-span moment. The difference in the mid-span moment between 28-days and 90-days is 11% before the application of live load, and this value drops to 7% at the service load level.

Figure 3.7 shows the variation of the central support moment with girder age at deck casting. Again, for 10-day and 28-day cases, no or little differential shrinkage develops and creep dominates. Large positive moment develops over the central support. While in the case of 60-day and 90-day casting, differential shrinkage develops at the beginning, causing negative moment at the central support. As the differential shrinkage

reaches its peak, some minor cracks occur in the deck over the pier. Then creep catches up and the curves go parallel to the 28-day one. At the live load level, the curves are also parallel to one another except that the 60-day and 90-day curves have slope changes because of cracking of the deck slab. The difference in the central support moment between the 28-day and 90-day cases is 875 kip-ft before the application of live load, and the difference changes to 640 kip-ft at the service load level.

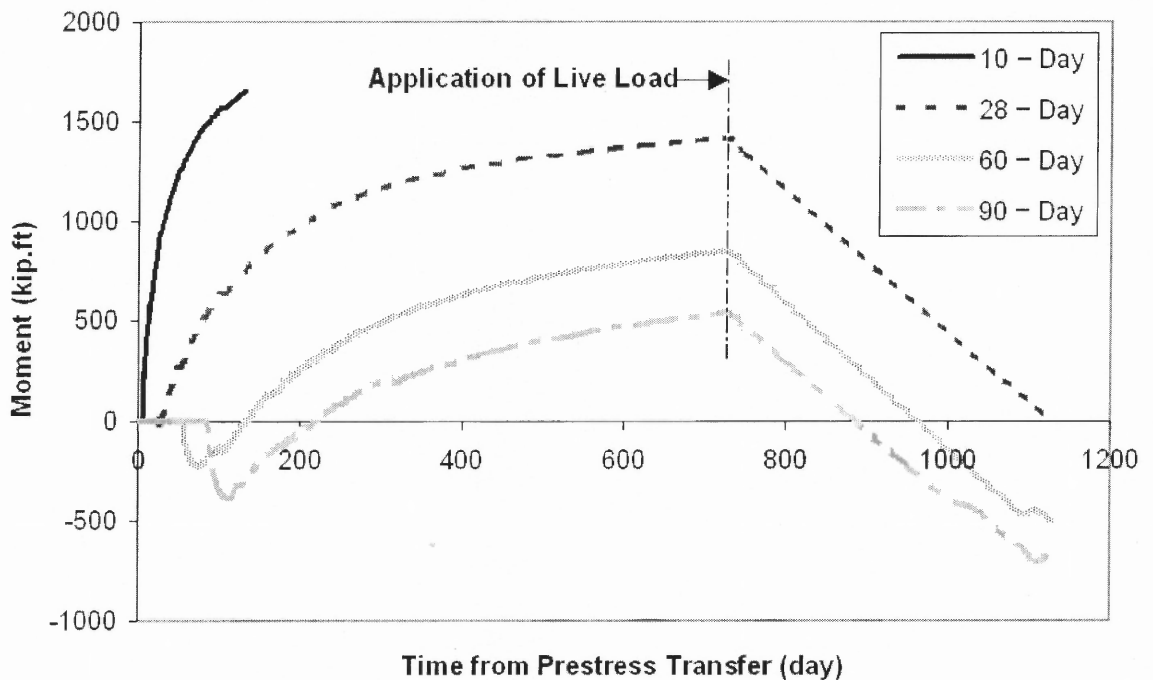


Figure 3.7 Variation of central support moment with girder age at deck casting.

When a small creep coefficient of 1.625 is specified, differential shrinkage will dominate, specially when the girders are older at deck casting.

From the above discussion, it is concluded that girder age at deck casting plays a major role in developing the time dependent effects. There is a remarkable difference in the design moments, especially over the piers (up to 62% in this case). Conventional design without considering girder age can be un-conservative.

Some states like Tennessee specifies a minimum girder age of 90 days before pouring the deck and diaphragm concrete. Continuity at later age can cause large differential shrinkage between the girder and deck concrete. As a result, the deck concrete might crack severely due to live load and additional negative moment caused by differential shrinkage. Many factors affecting concrete creep and shrinkage, such as the components of the concrete mix, properties of the concrete components, ambient temperature and relative humidity, are beyond designer's control. It might not be appropriate to specify a specific girder age at continuity, but pouring the deck concrete at an early girder age (less than 28 days) is not recommended based on this study.

3.3.2 Amount of Positive Moment Reinforcement

To study the effect of the amount of positive moment reinforcement on the behavior of this type of bridge, the same example is used. The ultimate creep coefficient for both girder and deck concrete is 3.25 and the ultimate shrinkage is 600×10^{-6} in./in. Deck and diaphragm concrete is cast at a girder age of 28 days. The positive moment reinforcement is chosen to be $0.48M_{cr}$, $1.2M_{cr}$, $2.4M_{cr}$, and $4.8M_{cr}$, respectively, where M_{cr} is the positive cracking moment of the continuity diaphragm.

Figure 3.8 shows the variation of central support moment with the amount of positive moment reinforcement. Observe that a larger central support moment develops with more positive moment reinforcement, but the differences are relatively small. The maximum difference before live load application is 212 kip-ft (17%) between amounts of reinforcement equivalent to $0.48M_{cr}$ and $4.8M_{cr}$. The difference drops to 45 kip-ft under live load. The small amount of reinforcement for $0.48M_{cr}$ should develop a moment of M_{cr} (1,137 kip-ft). The model predicts a positive restraint moment of 1,250 kip-ft, which

is 10% larger than expected. This additional resistance comes partly from the small amount of reinforcement ($0.48M_{cr}$) and partly from the two 1' long elastomeric bearings at the support. It must be stressed again the two bearings at the support never act like a single idealized pin.

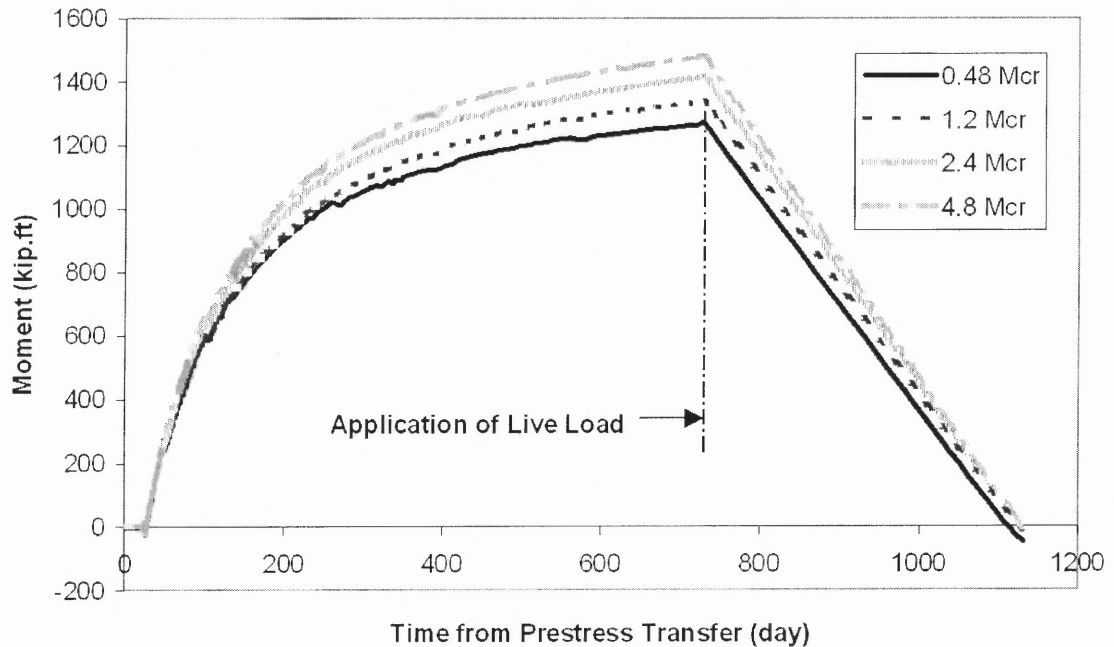


Figure 3.8 Variation of support moment with amount of +M reinforcement.

The variation of mid-span moment with the amount of positive moment reinforcement is illustrated in Figure 3.9. It can be seen that the moments are very close to one another, with a maximum difference of 106 kip-ft (only 3%) between cases of $0.48M_{cr}$ and $4.8M_{cr}$ just before live load application. The difference drops to 22 kip-ft (0.5%) under live load. Although more positive moment reinforcement can reduce the midspan live load moment, a larger positive restraint moment also develops at the inner support. This positive restraint moment will in turn increase the mid-span moment, canceling the reduction in midspan live load moment because of more continuity. As a result, the mid-span moment is practically independent of the amount of positive moment

reinforcement provided. The above statement also holds for cases with other creep and differential shrinkage combinations. It is concluded that the amount of positive moment reinforcement in the diaphragm has a negligible effect on the resultant mid-span moment. This confirms the analytical studies conducted by CTL^[10] and Mirmiran (et al.)^[11].

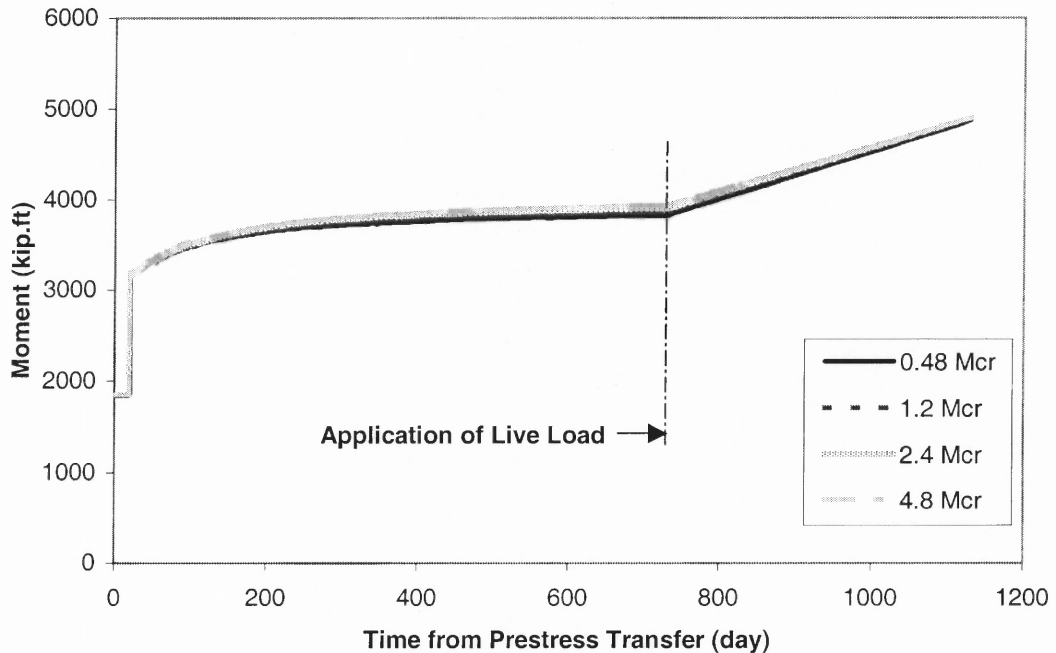


Figure 3.9 Variation of mid-span moment with amount of +M reinforcement.

Although the finite element analysis described in this chapter can give more accurate results than simplified computer programs utilizing a beam theory, the analysis requires expertise in Finite Element Methods. Because of its high nonlinearity and large number of elements, each run takes about 8 hours. This is not suitable for design engineers to use on a day-to-day basis. A simple yet effective analytical tool is needed to solve the time dependent restraint moments and to determine the degree of continuity of this kind of bridge. The next chapter introduces a computer program called CONTINUITY developed under this study.

CHAPTER 4

THE COMPUTER PROGRAM – CONTINUITY

4.1 Introduction

As stated in the literature review, there are several computer programs available to analyze simple span girders made continuous: PBEAM by Suttikan^[9], BRIDGERM by CTL^[10] and RESTRAINT by Kulkarni^[11]. The program PBEAM uses discrete elements and can account for the time dependent effects, but the “use of PBEAM is very cumbersome” and “time consuming”^[10]. The program BRIDGERM is based on elastic analysis and it uses simplified models (single span plus diaphragm) for exterior and interior spans rather than a whole continuous structure. The program RESTRAINT takes into account cracking of the sections but it is only good for two equal spans. Besides, based on the survey and the field tests, utilizing two bearings at each support and providing anchor bolts in the diaphragm make the bridges perform differently from analyses using idealized pins or rollers. Therefore, it is necessary to develop a simple yet effective tool for engineers to check the restraint moments and the degree of continuity, with special consideration to the support details.

The program CONTINUITY is developed based on RMCalc, a Visual Basic version of BRIDGERM, with the following major modifications:

1. Program capacity expands from equal spans to unequal spans.
2. Inelastic analysis is incorporated. Reduced moment of inertia of the diaphragm and girder sections due to concrete cracking is taken into account.
3. Besides ACI-209, more concrete creep and shrinkage models (CEB-FIP and HPC) are incorporated.

4. Degree of continuity analysis.
5. Two supports at each inner pier with capability to model nonlinear boundary condition (modeling uplift at supports).

The program is able to determine the design moments at mid-spans and supports due to time dependent effects, live loads (plus impact) and superimposed dead loads for two to four-span continuous bridges with varying span lengths. Non-linear material properties like concrete cracking, concrete creep and shrinkage and relaxation of the prestressing strands are all considered. Based on the live load moments and restraint moments calculated, the program can further determine the degree of continuity of the bridge.

Both I-shaped and box girders are included in this program. Three concrete creep and shrinkage models are incorporated: ACI-209 (American Concrete Institute), CEB-FIP (European) and HPC (High Performance Concrete). Both US and SI units can be used. The program supports both GUI (graphic user interface) and file input.

4.2 Concrete Creep and Shrinkage Models

4.2.1 ACI-209 Model

Readers are referred to Section 3.1 for detailed information on ACI-209 concrete creep and shrinkage model. This is the default model used by the program.

4.2.2 CEB-FIP Model

The current ACI-209 prediction models for concrete creep and shrinkage have been developed for more than 30 years. Over the years, new prediction models taking into account the effects of the more and more popular admixtures have been proposed by engineers and researchers. CEB-FIP model code 1990 took the first step to predict the

creep and shrinkage of concrete on the basis of a computerized data bank. It takes into account some of the important factors affecting creep and shrinkage such as the type of cement, the type of aggregate and the compressive strength of the concrete, which are not considered in ACI-209. The CEB-FIP model is described below ^[26].

Creep

The creep coefficient at time t , $\phi(t, t_0)$, when concrete is loaded at time $t_0 \leq t$, may be estimated from the following general relation:

$$\phi(t, t_0) = \phi_{RH} \cdot \beta(f_{cm}) \cdot \beta(t_0) \cdot \beta_c(t, t_0) \quad (4.1)$$

$$\text{where } \phi_{RH} = 1 + (1 - RH/RH_0) / (0.46 (h/h_0))^{1/3} \quad (4.2)$$

$$\beta(f_{cm}) = 5.3 / (f_{cm} / f_{cm0})^{0.5} \quad (4.3)$$

$$\beta(t_0) = 1 / (0.1 + (t_0 / t_1))^{0.2} \quad (4.4)$$

$$\beta_c(t, t_0) = [(t - t_0) / t_1 / (\beta_H + (t - t_0) / t_1)]^{0.3} \quad (4.5)$$

$$\text{with } \beta_H = 150 [1 + (1.2 RH/RH_0)^{18}] h / h_0 + 250 \leq 1,500 \quad (4.6)$$

where RH = relative humidity of the ambient environment in [%];

$h = 2A_c/u$; A_c = cross-sectional area of the structural member in [mm²];

u = perimeter of the structural member in contact with the atmosphere in [mm];

f_{cm} = mean compressive strength of concrete in [N/mm²] at the age of 28 days;

t = age of concrete in [days] at the moment considered;

t_0 = age of concrete at loading in [days];

and $RH_0 = 100\%$, $h_0 = 100\text{mm}$, $f_{cm0} = 10 \text{ N/mm}^2$, $t_1 = 1 \text{ day}$.

Effect of Type of Cement

The effect of type of cement on the creep coefficient of concrete may be taken into account by modifying the age at loading t_0 according to Eq. 4.7:

$$t_0 = t_{0,T} [9 / (2 + (t_{0,T} / t_{1,T})^{1.2} + 1)]^\alpha \geq 0.5 \text{ days} \quad (4.7)$$

where $t_{0,T}$ = age of concrete at loading in days according to Eq. 4.9;

$$t_{1,T} = 1 \text{ day};$$

α = coefficient which depends on type of cement;
 = -1 for slowly hardening cement,
 = 0 for normal or rapid hardening cement,
 = 1 for rapid hardening high strength cement.

The value for t_0 according to Eq. 4.7 to be used in Eq. 4.4; the duration of loading $t-t_0$ to be used in Eq. 4.5 is the actual time under load in days.

Effect of Elevated Temperatures

The creep coefficient at elevated temperatures may be roughly estimated from Eq. 4.8:

$$\phi_T(t, t_0) = \phi_{T,st}(t, t_0) + \Delta\phi_{T,trans} \quad (4.8)$$

where $\phi_{T,st}$ = steady state creep coefficient, which may be calculated using Eq. 4.1 ($\phi_{T,st}(t, t_0) = \phi(t, t_0)$) and Eqs. 4.2 to 4.7, considering the modifications given in Eqs. 4.9 to 4.12;

$\Delta\phi_{T,trans}$ = transient creep coefficient which may be estimated from Eq. 4.13.

Effect of Elevated Temperatures – Steady State Creep

The effect of an elevated temperature T to which concrete is exposed prior to or during – the load being applied after temperature rise – may be taken into account employing Eqs. 4.9 to 4.12:

$$t_T = \sum_{i=1}^n \Delta t_i \cdot \exp[13.65 - 4000 / (273 + T(\Delta t_i) / T_0)] \quad (4.9)$$

where t_T = modified age of concrete at loading in [days], which has to be used in Eq. 4.7;

$T(\Delta t_i)$ = temperature in [°C] during the time period Δt_i ;

Δt_i = number of days prior to loading , where the temperature T prevails;

$T_0 = 1^\circ\text{C}$.

$$\beta_{H, T} = \beta_H \cdot \exp[1500 / (273 + T/T_0 - 5.12)] \quad (4.10)$$

where $\beta_{H, T}$ = temperature dependent coefficient replacing β_H in Eq. 4.5;

β_H = coefficient according to Eq. 4.6.

$$\phi_{RH, T} = \phi_T + [\phi_{RH} - 1] \cdot \phi_T^{1.2} \quad (4.11)$$

$$\text{with } \phi_T = \exp[0.015 \cdot (T/T_0 - 20)] \quad (4.12)$$

where $\phi_{RH, T}$ = temperature dependent coefficient which replaces ϕ_{RH} in Eq. 4.1;

ϕ_{RH} = coefficient according to Eq. 4.2.

In Eqs. 4.10 to 4.12, T is a constant temperature while concrete is under load, and $T_0 = 1^\circ\text{C}$.

Effect of Elevated Temperatures – Transient Creep

Transient temperature conditions, i.e. the increase of temperature while the structural member is under load, leads to an additional creep $\Delta\phi_{T, \text{trans}}$, which may be calculated from Eq. 4.13:

$$\Delta\phi_{T, \text{trans}} = 0.0004 \cdot (T/T_0 - 20)^2 \quad (4.13)$$

where T is the temperature in [$^\circ\text{C}$] to which the structural member under load is heated and $T_0 = 1^\circ\text{C}$.

Effect of High Constant Stresses

For stresses in the range of $0.4f_c(t_0) < \sigma_C \leq 0.6f_c(t_0)$, where $f_c(t_0)$ is the mean compressive strength of concrete at the age t_0 , the increased creep due to stress level dependent nonlinearity may be taken into account using Eq. 4.14:

$$\begin{aligned} \phi\sigma(t, t_0) &= \phi(t, t_0) \cdot \exp[\alpha_\sigma(\sigma - 0.4)] & \text{for } 0.4 < \sigma \leq 0.6 \\ &= \phi(t, t_0) & \text{for } \sigma \leq 0.4 \end{aligned} \quad (4.14)$$

where $\phi(t, t_0)$ = creep coefficient according to Eq. 4.1;

σ = stress – strength ratio $\sigma/f_c(t_0)$

$\alpha_\sigma = 1.5$, for mass concrete and for creep at very high relative humidity, the coefficient α_σ may be as low as 0.5.

Shrinkage

The strain due to shrinkage or swelling at normal temperatures may be calculated from

Eq. 4.15:

$$\epsilon_{cs}(t, t_s) = \epsilon_{cso} \cdot \beta_s(t - t_s) \quad (4.15)$$

where ϵ_{cso} = nominal shrinkage coefficient according to Eq. 4.16;

β_s = coefficient to describe the development of shrink age with time according to Eq. 4.20;

t = age of concrete in [days];

t_s = age of concrete in [days] at the beginning of shrinkage or swelling.

The nominal shrinkage coefficient may be obtained from Eq. 4.16:

$$\epsilon_{cso} = \epsilon_s(f_{cm}) \cdot \beta_{RH} \quad (4.16)$$

$$\text{with } \epsilon_s(f_{cm}) = [160 + 10 \cdot \beta_{sc} \cdot (9 - f_{cm}/f_{cmo})] \cdot 10^{-6} \quad (4.17)$$

where β_{sc} = coefficient which depends on type of cement;
 = 4 for slowly hardening cement,
 = 5 for normal or rapid hardening cement,
 = 8 for rapid hardening high strength cement,

$$\beta_{RH} = \begin{cases} -1.55 \cdot \beta_{SRH} & \text{for } 40\% \leq RH < 99\% \\ +0.25 & \text{for } RH \geq 99\% \end{cases} \quad (4.18)$$

$$\text{where } \beta_{SRH} = 1 - (RH / RH_0)^3 \quad (4.19)$$

In Eqs. 4.17 and 4.19, f_{cm} is the mean compressive strength of concrete in [N/mm²], and RH is the mean relative humidity of the ambient atmosphere in [%], respectively; $f_{cmo} = 10$ N/mm² and $RH_0 = 100\%$.

The development of shrinkage with time is given by:

$$\beta_S(t - t_s) = [(t - t_s) / t_s / (\beta_{SH} + (t-t_s)/t_s)]^{0.5} \quad (4.20)$$

$$\text{with } \beta_{SH} = 350 \cdot (h / h_0)^2 \quad (4.21)$$

where $t-t_s$ = duration of drying or swelling in [days], $h = 2A_c/u$ (A_c = cross – sectional area of structural member in [mm²]; u = perimeter of the structural member in contact with the atmosphere in [mm]), $h_0 = 100$ mm and $t_1 = 1$ day.

Effect of Elevated Temperatures

The effect of elevated temperatures T on shrinkage of concrete may be taken into account using Eqs. 4.22 to 4.24:

$$\beta_{SHT} = \beta_{SH} \cdot \exp[-0.06 (T/T_0) - 20]) \quad (4.22)$$

where β_{SHT} = temperature dependent coefficient replacing β_{SH} in Eq. 4.20;

β_{SH} = coefficient according to Eq. 4.21.

$$\beta_{RH, T} = \beta_{RH} \cdot \beta_{ST} \quad (4.23)$$

$$\text{with } \beta_{ST} = 1 + [8 / (103 - 100 RH/RH_0)] \cdot [(T/T_0 - 20) / 40] \quad (4.24)$$

where $\beta_{RH, T}$ = temperature dependent coefficient which replaces β_{RH} in Eq. 4.16;

β_{RH} = coefficient according to Eq. 4.18.

In Eqs. 4.22 and 4.24, T is a constant temperature, $T_0 = 1^\circ\text{C}$ and $RH_0 = 100\%$.

4.2.3 Creep and Shrinkage Models for High Performance Concrete

High Performance Concrete (HPC) becomes more and more popular in bridge engineering. Because of its low water to cementitious materials ratio and the use of admixtures, the creep and shrinkage characteristics of HPC are substantially different from those of Normal Strength Concrete (NSC). The total creep of HPC is significantly lower than that of NSC. According to Dilger (et al.)^[27] the ultimate creep coefficient of

silica fume HPC can be as low as 30% of that of NSC, and the specific creep (creep strain per unit stress) is as low as 15% of that of NSC. The basic (autogenous) shrinkage of HPC develops very fast and stabilizes after a few weeks. Drying shrinkage of HPC is much lower than that of NSC. Among a number of prediction models, Dilger's (et al.)^[27] model was selected because it had been verified with extensive experimental data and had good agreements. Dilger's model is described below^[27].

Creep

Total Creep

The total creep coefficient is the sum of the basic creep coefficient and the drying creep coefficient.

$$\phi_c(t, t_0) = \phi_{bc}(t, t_0) + \phi_{dc}(t, t_0) \quad (4.38)$$

Basic Creep

$$\phi_{bc}(t, t_0) = \phi_{bso} \cdot \beta_{bc}(t, t_0) \quad (4.39)$$

$$\phi_{bso} = 0.74 (1 + t_0^{-0.4}) \quad (4.40)$$

The time function for basic creep is given by

$$\beta_{bc}(t, t_0) = (t - t_0)^{0.5} / (\gamma_{bc} + (t - t_0)^{0.5}) \quad (4.41)$$

$$\text{with } \gamma_{bc} = 0.29 + 0.5 t_0^{0.7} \quad (4.42)$$

Drying Creep

$$\phi_{dc}(t, t_0) = \phi_{dco} \cdot \beta_{RH} \cdot \beta_{dc}(t, t_0) \quad (4.43)$$

$$\phi_{dco} = 0.62 + 0.1 t_0^{-0.8} \quad (4.44)$$

The effect of the relative humidity (RH in %) on basic creep is

$$\beta_{RH} = 1.22 - 1.75(RH/100)^3 \quad (4.45)$$

and the development of drying creep follows Eq. 4.46.

$$\beta_{dc}(t, t_0) = (t - t_0)^{0.5} / (0.04 \gamma_{dc} (V/S) + (t - t_0)^{0.5}) \quad (4.46)$$

where V/S is the volume to surface ratio and γ_{dc} is defined as

$$\gamma_{dc} = -3.2 + 8.5 t_0^{0.3} \quad (4.47)$$

Shrinkage

Basic Shrinkage

The basic shrinkage developing between ages t and t_s is

$$\epsilon_{bs}(t, t_s) = \epsilon_{bs}(t) - \epsilon_{bs}(t_s) \quad (4.25)$$

where:

t = time of observation in days

t_s = age of concrete where shrinkage starts in days

$$\epsilon_{bs}(t) = \epsilon_{bso} \cdot \beta_{bs}(t) \quad (4.26)$$

$$\epsilon_{bso} = 700 \cdot \exp(-3.5 \cdot w/cm) + 120 \quad \text{for silica fume concrete} \quad (4.27)$$

$$\epsilon_{bso} = 700 \cdot \exp(-3.5 \cdot w/cm) \quad \text{for non-silica fume concrete} \quad (4.28)$$

The time function for basic shrinkage is expressed by

$$\beta_{bs}(t) = t^{0.7} / (\gamma_{bs} + \alpha_{bs} \cdot t^{0.7}) \quad (4.29)$$

$$\text{where } \alpha_{bs} = 1.04 - 1/3 \cdot w/cm \quad (0.15 \leq w/cm \leq 0.40) \quad (4.30)$$

$$\text{and } \gamma_{bs} = 16.7 (1 - \alpha_{bs}) \quad (4.31)$$

Drying Shrinkage

The drying shrinkage component, $\epsilon_{ds}(t, t_s)$ may be calculated from

$$\epsilon_{ds}(t, t_s) = \epsilon_{dso} \cdot \beta_{RH} \cdot \beta_{ds}(t, t_s) \quad (4.32)$$

$$\text{where } \epsilon_{dso} = [(100 \cdot w/c)^2 f_{c28}^{-0.23} + 200] 10^{-6} \quad (4.33)$$

The effect of the relative humidity (RH in %) is given by

$$\beta_{RH} = 1.22 - 1.75 (RH/100)^3 \quad (4.34)$$

and time function for drying shrinkage is expressed as follows

$$\beta_{ds}(t, t_s) = (t - t_s)^{0.6} / (16 (V/S/100)^2 \gamma_{ds} + (t - t_s)^{0.6}) \quad (4.35)$$

$$\text{where } \gamma_{ds} = 6.42 + 1.5 \ln(t_s) \quad (4.36)$$

Total Shrinkage

The total shrinkage is the sum of the basic shrinkage and the drying shrinkage:

$$\epsilon_s(t, t_s) = \epsilon_{bs}(t, t_s) + \epsilon_{ds}(t, t_s) \quad (4.37)$$

4.3 Algorithm

The program can be divided into the following steps.

1. Input data. Geometry of the girder, deck, and spans, number and location of the prestressing strands and reinforcement, live load, creep and shrinkage characteristics of the girder and deck concrete, girder age at prestress transfer, girder age at continuity and the solution time need to be input either from GUI or from an input file. GUI is introduced in Section 4.4. The input file format is included on the CD-ROM.
2. Determine time steps at which results will be output. Time steps are determined from input values of the girder age at continuity, the solution times and a predetermined time vector in the program. The time vector ranges from 1 to 50,000 days with increasing time intervals. The girder age at continuity and the time values of user's choice are inserted into the predetermined time vector. The user specified maximum time will cut off the rest of the time vector.
3. Calculate section properties. Area, moment of inertia and volume to surface ratio of the composite and non-composite sections are calculated for later use. For an I-girder composite section, the effective top flange width is the smallest of: a) girder spacing, b) 12 times deck thickness plus web width, and c) $\frac{1}{4}$ of span length.
4. Determine prestress losses up to prestress release following PCI recommendations. These include the pre-strand relaxation before transfer and the elastic shortening of the girders.

5. Calculate prestress losses up to age of continuity. Three concrete creep and shrinkage models to choose from: ACI-209, CEB-FIP and HPC (see Section 4.2 for details). At each time step between prestress transfer and age of continuity, losses due to creep and shrinkage of girder concrete and strand relaxation are calculated and subtracted from the existing prestress in the strands.
6. Calculate restraint moments at each time step after continuity. Three concrete creep and shrinkage models to choose from: ACI-209, CEB-FIP and HPC. Each time step is further divided into the following sub-steps:
 - 1) The creep coefficient, shrinkage of the girder and deck concrete, and strand relaxation are calculated for this time step. Prestress losses are subtracted from the strands.
 - 2) In the first iteration, the elastic restraint moment at that time step is calculated. Based on a PCA^[6] analysis, the elastic restraint moment over the support can be determined as:

$$M_{rm} = (M_p - M_d)(1 - e^{-\phi}) - M_s(1 - e^{-\phi}) / \phi$$

where M_{rm} is the restraint moment, M_p is the support moment caused by the prestress assuming the girder and slab were cast and prestressed monolithically as a continuous girder, M_d is the support moment caused by the dead load assuming the girder and slab were cast monolithically as a continuous girder, M_s is the support moment caused by differential shrinkage between the girder and deck concrete assuming a monolithic continuous girder, ϕ is the creep coefficient of that time step, and e is the base of natural logarithm.

The elastic analysis uses a 2-D finite element analysis program “Beam2” from Ref. 29. Each bearing is modeled as a pin support, so there are two supports over each inner pier. Each span is divided into 10 elements. The portion of beam between the two bearings over each support is model as a single element. Therefore, for a four-span continuous bridge, there are 43 elements.

After each analysis, the reaction at each support is checked. If the reaction is less than zero, that support is deleted and another analysis based on the revised boundary condition is carried out.

- 3) The elastic restrain moments calculated from 2) are added to those obtained from the last time step to get the total restraint moments. The effective moment of inertia of each element subjected to the total moment is then determined.
- 4) In the second iteration, analysis is carried out based on the changed moment of inertia of each element.

- 5) The reaction at each support is checked. If the reaction is less than zero, that support is deleted and another analysis based on the revised boundary condition is carried out.
7. Live load and degree of continuity analysis. The solution for the restraint moment stops at the maximum time specified by the user. After that, the live load and degree of continuity analysis follow.
- 1) Inelastic live load moments. The program assumes AASHTO lane load controls. Truck load is not considered at this time. Loads are applied in 20 sub-steps. For each sub-step the same convergence criterion as in the restraint moment analysis is employed. Both support and midspan moments are calculated. Per AASHTO specifications, one concentrated load and as many spans of lane load are used for midspan moments; two concentrated loads and as many spans of lane load are used for support moments to produce the maximum moment. Support uplift is checked at each sub-step as in the restraint moment analysis.
 - 2) Elastic live load moments. The same loading condition as in 1) is used. The moments of inertia and the support conditions are reset to their initial values. Solution is done in a single step.
 - 3) Degree of continuity is calculated in a similar way as in Section 2.4.5 except that midspan moments instead of strains are used for computational convenience.

$$D.O.C. = (M_s - M_r) / (M_s - M_c)$$

where $D.O.C.$ – degree of continuity.

M_s – midspan moment assuming simply supported.

M_r – real midspan moment considering time dependent effects and concrete cracking.

M_c – midspan moment assuming full continuity.

Thus, D.O.C. equals 100% for fully continuous bridges and 0% for simple spans.

8. Output data. Time histories of the restraint moments at midspans and supports are output to the “Results” tab of the GUI. The inelastic live load moments, elastic live load moments and the degree of continuity are listed below the restraint moments. A report can also be created using the menu command.

A flow chart of the program is illustrated in Figure 4.1.

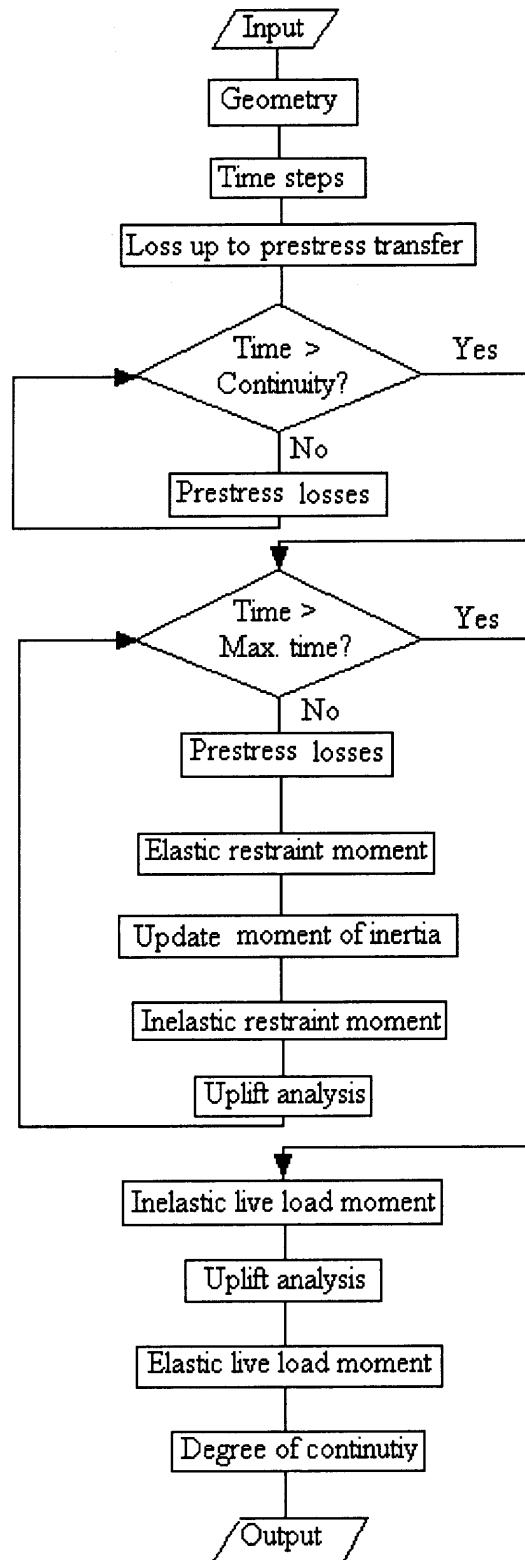


Figure 4.1 Flow chart of CONTINUITY.

4.4 Verification

PCA tests are also used to verify CONTINUITY. Readers are referred to Section 3.2.1 for details of the tests. Figure 4.2 illustrates a comparison of the center support reaction of Beam3/4. One can see that results from CONTINUITY agree well with the test data both for the ascending and descending branches of the curve.

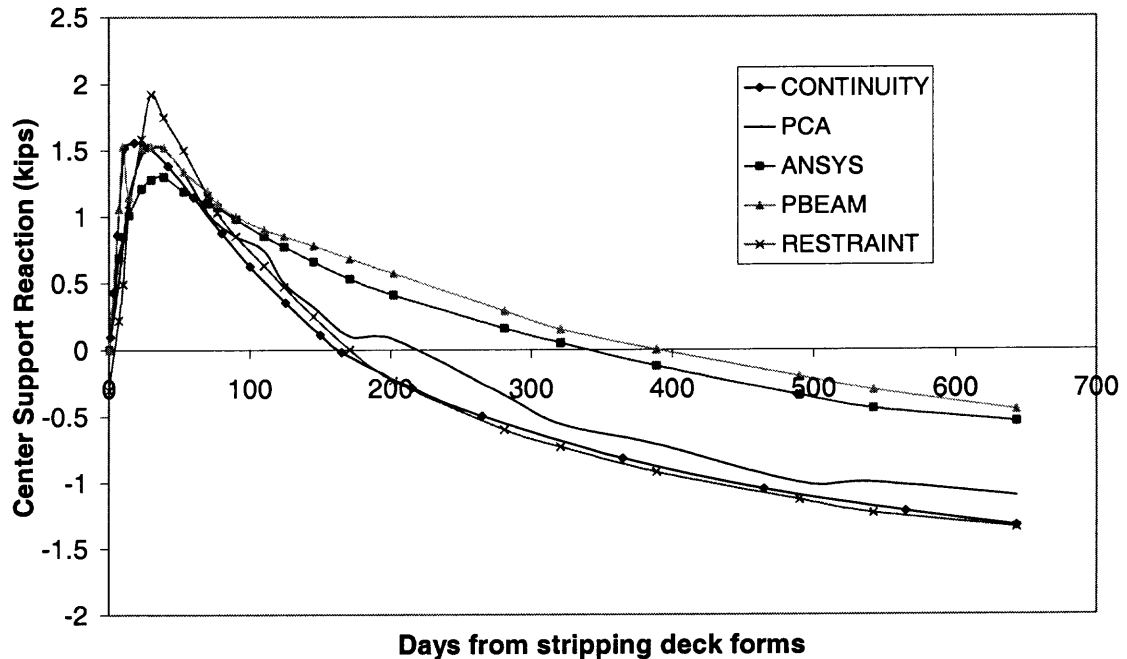


Figure 4.2 Verification with Beam3/4.

Figure 4.3 shows a comparison of the center support reaction of Beam1/2. The results from CONTINUITY agree well with the descending branch of the curve from test data and overestimate the ascending part. But in general, it is better than the prediction from RESTRAINT. It should be noted that the increase in center support reaction corresponds to negative support moment caused by the differential shrinkage between the deck and girder concrete. If Beam1/2 and Beam3/4 were identical except for the positive moment reinforcement, the negative moment over the support caused by differential

shrinkage should be the same. Therefore, the ascending branch of the center support reaction should also be the same, which is the case both for CONTINUITY and RESTRAINT. Most likely the conditions (concrete mix, creep and shrinkage, etc.) of Beam1/2 and Beam3/4 were different but not recorded in the PCA tests.

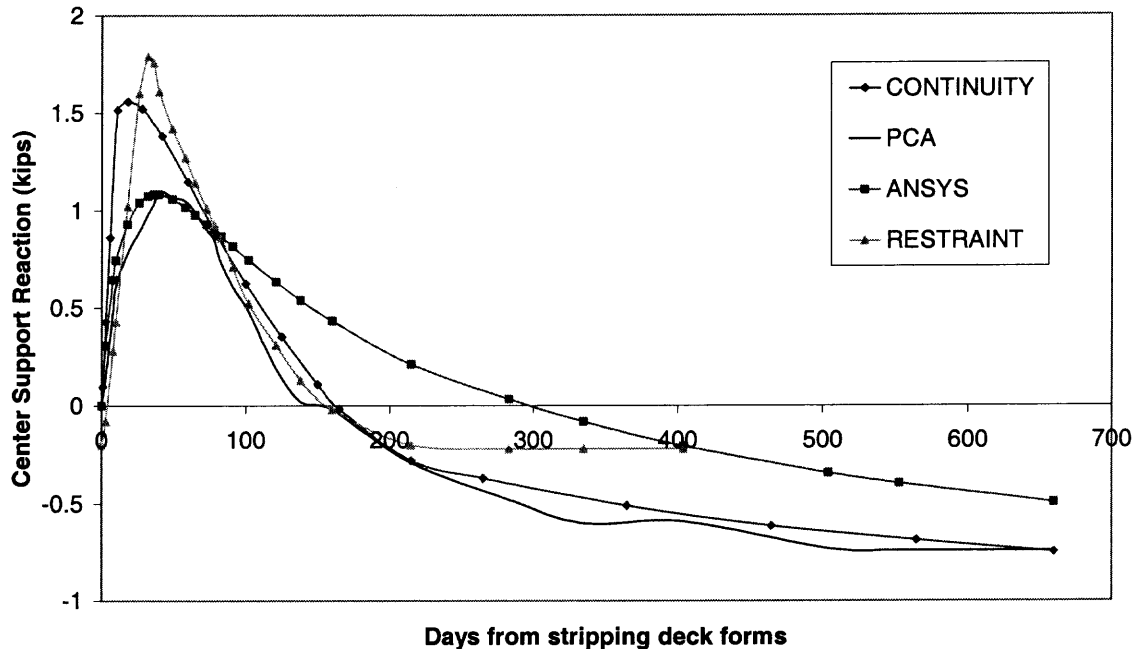


Figure 4.3 Verification with Beam1/2.

4.5 The Graphical User Interface

The GUI is user friendly and easy to use. Each input field is preceded with an explanation. Some fields even have tool tip helps (when the mouse is over that field, a text box appears and explains the content of that field). Units can be changed either by clicking the flag on the upper right corner of the application window or by selecting the menu “Units”.

The Dim's Tab

The Dim's tab let the users input girder dimensions. Both I-girders and Box girders are included.

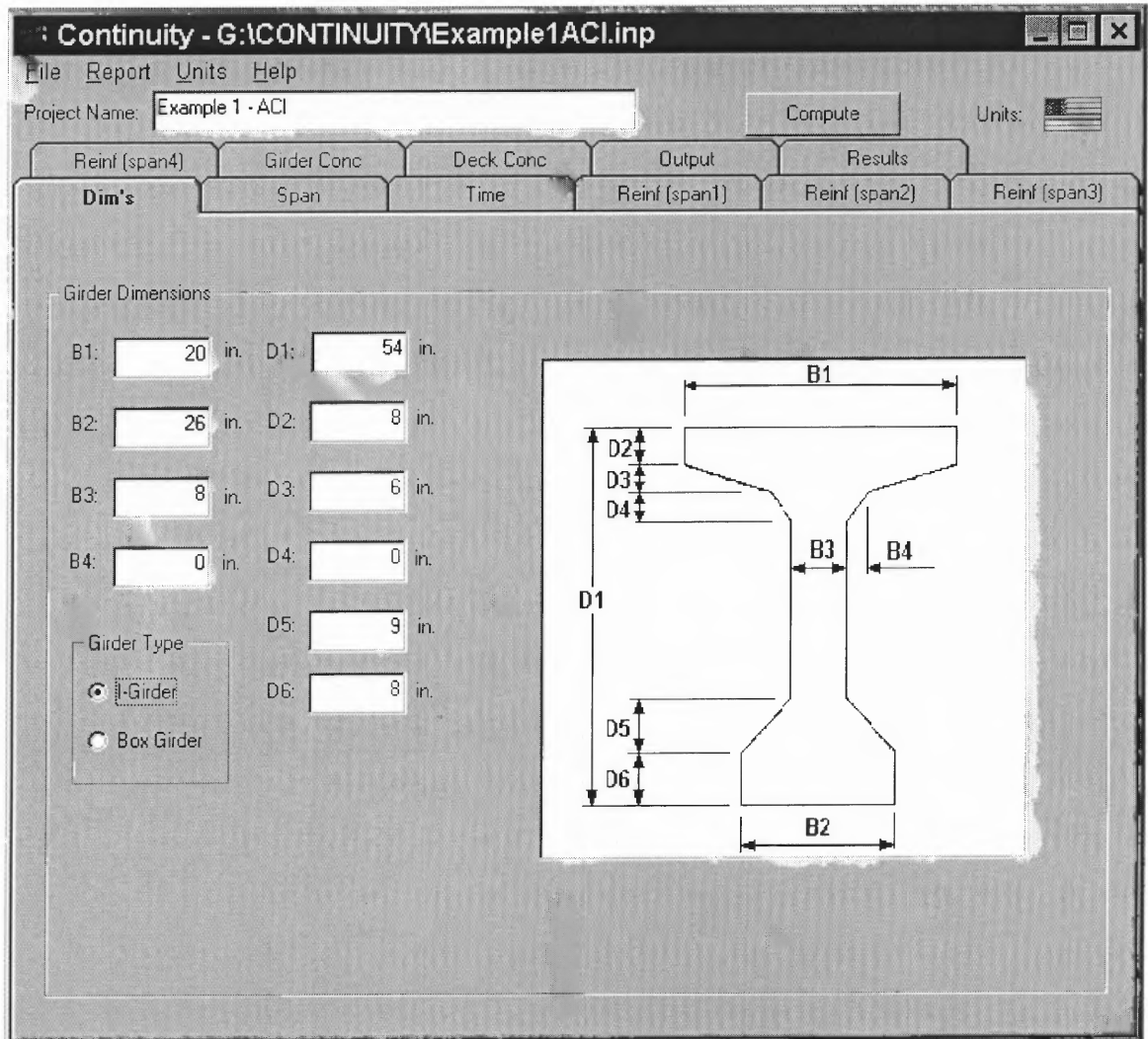
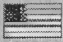


Figure 4.4 I-girder dimensions.

Continuity - G:\CONTINUITY\Example1ACI.inp

File Report Units Help

Project Name: Units: 

Reinf (span4) Girder Conc Deck Conc Output Results

Dim's Span Time Reinf (span1) Reinf (span2) Reinf (span3)

Girder Dimensions

B1: in. D1: in.

B2: in. D2: in.

B3: in. D3: in.

B4: in. D4: in.

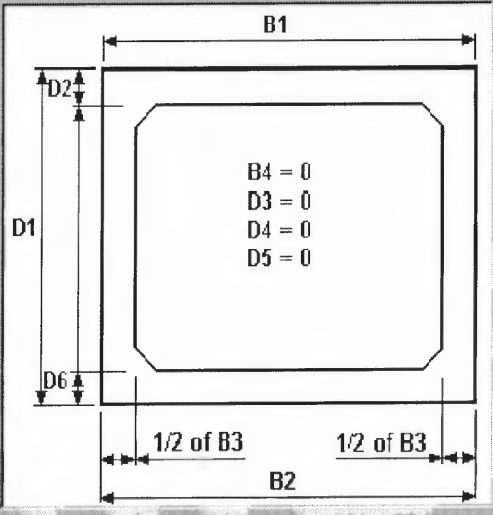
D5: in.

D6: in.

Girder Type

I-Girder

Box Girder



B4 = 0
D3 = 0
D4 = 0
D5 = 0

Figure 4.5 Box-girder dimensions.

The Span Tab

The Span tab allows the users to input number of spans, length of each span, diaphragm width, deck thickness, additional dead load and the live load factor.

Continuity - G:\CONTINUITY\Example1ACI.inp

File Report Units Help

Project Name: Example 1 - ACI Compute Units:

Reinf (span4) Girder Conc Deck Conc Output Results

Dim's **Span** Time Reinf (span1) Reinf (span2) Reinf (span3)

Span Data

Number of Spans(1-4):

Span Length: ft. ft. ft. ft.

Diaphragm Width: ft.

Girder Spacing: ft.

Deck Thickness: in.

Additional Dead Load: psf.

Live Load Factor: (enter 1.0 for HS20-44 loading)

Figure 4.6 The Span tab.

The Time Tab

The Time tab reads the girder age at prestress release, the girder age at continuity and the girder age when the deck concrete is poured.

Continuity - G:\CONTINUITY\Example1ACI.inp

File Report Units Help

Project Name: Example 1 - ACI Compute Units:

Reinf (span4) Girder Conc Deck Conc Output Results

Dim's Span **Time** Reinf (span1) Reinf (span2) Reinf (span3)

Construction Timing Data

Girder Age at Prestress Release: days

Girder Age at Continuity: days

Girder Age when Deck is Poured: days

Figure 4.7 The Time tab.

The Reinforcement Tabs

Each span has a reinforcement tab in which information about the prestressing strands and the positive and negative moment reinforcement can be input. If a span or support has the same reinforcement as a previous one, users can select so to avoid repetitive input.

Continuity - G:\CONTINUITY\Example1ACI.inp

File Report Units Help

Project Name: Units:

Reinf (span4) Girder Conc Deck Conc Output Results

Dim's Span Time **Reinf (span1)** Reinf (span2) Reinf (span3)

Prestressing Strands

Stress Relieved Strands Low Relaxation Strands

Cross-Sectional Area of a Single Strand: sq-in. Or choose strand area by diameter: ▾

Total Number of Strands: Number of Harped Strands:

Centroid of Straight Strands: in. from bottom of girder

Centroid of Harped Strands at Midspan: in. from bottom of girder

Centroid of Harped Strands at Girder Ends: in. from bottom of girder

Harp Length (as ratio of span length): Initial Strand Tension: ksi.

Positive(1~3) & Negative(4~6) Moment Reinforcement over 1st Inner Pier

Layer	Type	Area	Fy	Centroid from bot.	E	Strain @ rupture
+	1	<input type="text" value="2"/> sq-in.	<input type="text" value="240"/> ksi.	<input type="text" value="3.43"/> in.	<input type="text" value="29000"/> ksi.	<input type="text" value="0.4"/>
	2	<input type="text" value="0"/> sq-in.	<input type="text" value="0"/> ksi.	<input type="text" value="0"/> in.	<input type="text" value="0"/> ksi.	<input type="text" value="0"/>
	3	<input type="text" value="0"/> sq-in.	<input type="text" value="0"/> ksi.	<input type="text" value="0"/> in.	<input type="text" value="0"/> ksi.	<input type="text" value="0"/>
-	4	<input type="text" value="3"/> sq-in.	<input type="text" value="60"/> ksi.	<input type="text" value="56"/> in.	<input type="text" value="29000"/> ksi.	<input type="text" value="0.5"/>
	5	<input type="text" value="3"/> sq-in.	<input type="text" value="60"/> ksi.	<input type="text" value="60"/> in.	<input type="text" value="29000"/> ksi.	<input type="text" value="0.5"/>
	6	<input type="text" value="0"/> sq-in.	<input type="text" value="0"/> ksi.	<input type="text" value="0"/> in.	<input type="text" value="0"/> ksi.	<input type="text" value="0"/>

Figure 4.8 The Reinforcement tab (span 1).

Continuity - G:\CONTINUITY\Example1ACI.inp

File Report Units Help

Project Name: Example 1 - ACI Compute Units:

Reinf (span4) Girder Conc Deck Conc Output Results

Dim's Span Time Reinf (span1) Reinf (span2) **Reinf (span3)**

Prestressing Strands

Same as span 1. Same as span 2.

Number of Straight Strands: 22 Number of Harped Strands: 9

Centroid of Straight Strands: 3.43 in. from bottom of girder

Centroid of Harped Strands at Midspan: 4 in. from bottom of girder

Centroid of Harped Strands at Girder Ends: 50 in. from bottom of girder

Harp Length (as ratio of span length): 0.4 Initial Strand Tension: 189 ksi.

Positive(1~3) & Negative(4~6) Moment Reinforcement over 3rd Inner Pier

Same as inner pier 1. Same as inner pier 2.

Layer	Type	Area	Fy	Centroid from bot.	E	Strain @ rupture
+	1	1.2 sq-in.	240 ksi.	3.43 in.	29000 ksi.	0.4
	2	0 sq-in.	0 ksi.	0 in.	0 ksi.	0
	3	0 sq-in.	0 ksi.	0 in.	0 ksi.	0
-	4	4.8 sq-in.	60 ksi.	56 in.	29000 ksi.	0.5
	5	4.8 sq-in.	60 ksi.	60 in.	29000 ksi.	0.5
	6	0 sq-in.	0 ksi.	0 in.	0 ksi.	0

Figure 4.9 The Reinforcement tab (span 3).

The Girder Concrete and Deck Concrete Tabs

The strength at prestress transfer, strength at 28 days, unit weight, creep and shrinkage properties of the girder concrete are read from this tab. Users can choose from ACI-209, CEB-FIP and HPC models. Whenever a creep and shrinkage model is selected, the fields related to that particular model are enabled and those related to other models are disabled. When ACI model is selected, users can either give an ultimate creep coefficient and an ultimate shrinkage value or fill out the details below and let the program determine the

creep and shrinkage values. Once the details are filled out, click the “Calculate” button to get the ultimate creep and shrinkage values. The deck concrete tab works similarly.

Continuity - G:\CONTINUITY\Example1ACI.inp

File Report Units Help

Project Name: Units:

Reinf (span4) **Girder Conc** Deck Conc Output Results

Girder Concrete Data

Strength at Transfer (f'ci): ksi Strength at 28 Days (f'c): ksi Unit Weight: pcf.

Creep and Shrinkage

ACI-209 CEB-FIP (European) High Performance Concrete

Ultimate Creep Coeff: Ultimate Shrinkage: x 10⁻⁶ in./in. or optionally fill out details below.

Relative Humidity (%): Fine Aggregate %: Age at Loading: days.

Curing: day Cement Content: lb/yd³ Water/Cement:

Ambient Temp: F. Air Content (%):

Slump: in.

Aggregate Type

Basalt/Dense Limestone

Quartzite

Limestone

Sandstone

Silica Fume: With Without

Cement Type

Slowly Hardening

Normal or Rapid Hardening

Rapid Hardening High Strength

Figure 4.10 The Girder Concrete tab.

The Output Tab

The Output tab contains the output times of user's choice, or users can give a maximum solution time and let the program determine the time steps.

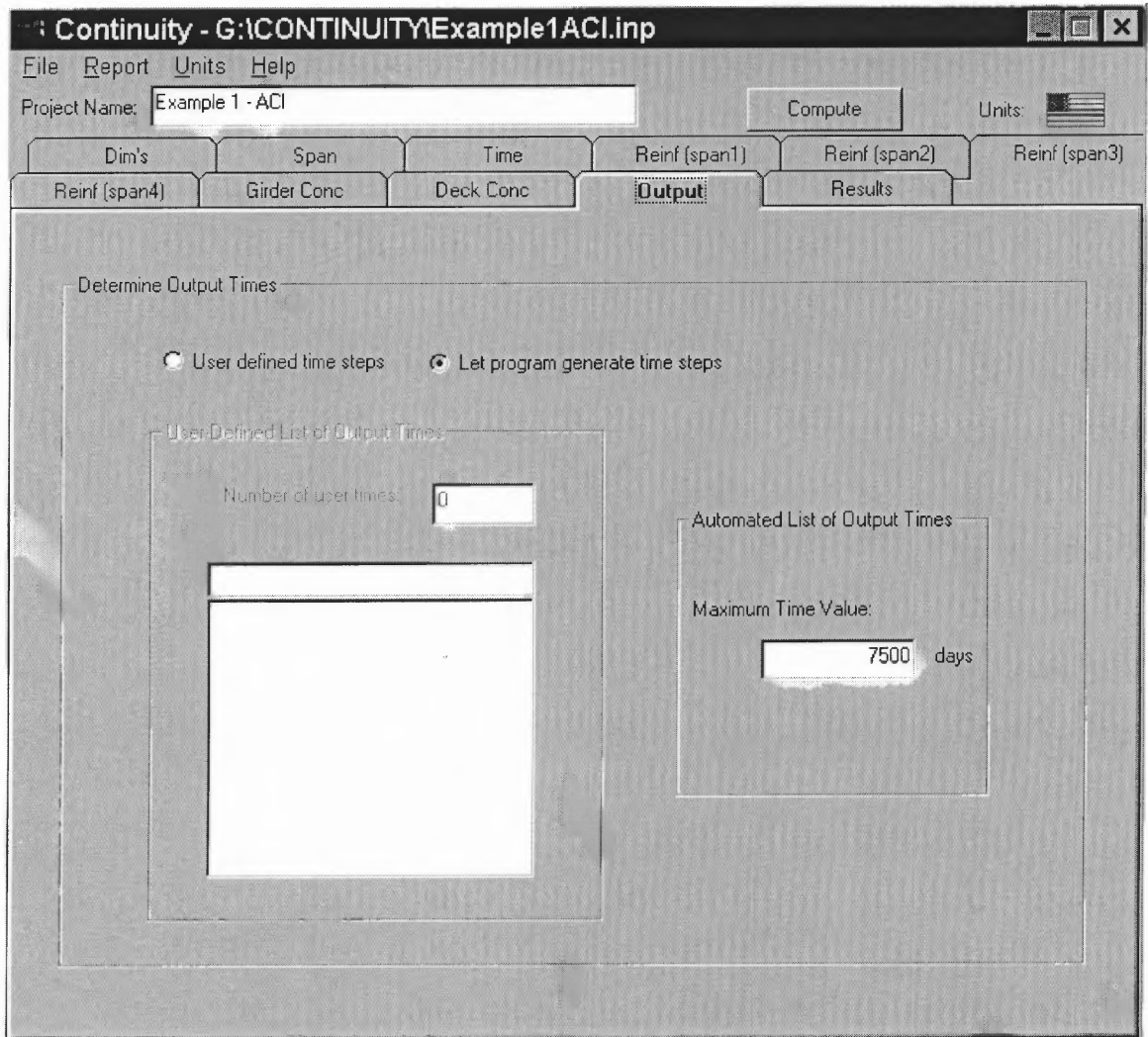


Figure 4.11 The Output tab.

The Results Tab

Once all the data are input, users can press the “Compute” button to start the analysis. The Results tab will automatically come up when the solution is done. The Results tab contains all the results of the current project including a time history of the restraint moments, the inelastic live load moments, the elastic live load moments and the degree of continuity of each span. Click the “Clear Results” button will delete all the results in this tab.

The screenshot shows the 'Results' tab in the Continuity software. The window title is 'Continuity - G:\CONTINUITYExample1ACI.inp'. The Project Name is 'Example 1 - ACI'. The 'Results' tab is selected, showing a table of moment values over time for various spans and restraints. The table has 7 columns: Time (Days), Moment MM1 (ft-kips), Moment MM2 (ft-kips), Moment MM3 (ft-kips), Moment MM4 (ft-kips), Moment RM1 (ft-kips), and Mc (ft-kips). The data shows a general increase in moment values over time, with some fluctuations.

Time (Days)	Moment MM1 (ft-kips)	Moment MM2 (ft-kips)	Moment MM3 (ft-kips)	Moment MM4 (ft-kips)	Moment RM1 (ft-kips)	Mc (ft-kips)
35	0.0	0.0	0.0	0.0	0.0	0.0
36	-5.4	-7.3	-7.3	-5.4	-10.8	-7.3
38	-22.4	-30.2	-30.2	-22.4	-44.8	-29.4
41	-40.0	-54.0	-54.0	-40.0	-80.1	-53.0
46	-65.7	-88.6	-88.6	-65.7	-131.3	-87.0
53	-58.2	-78.4	-78.4	-58.2	-116.3	-77.0
63	-44.7	-60.3	-60.3	-44.7	-89.5	-59.0
77	-24.4	-32.9	-32.9	-24.4	-48.8	-32.0
95	0.7	0.9	0.9	0.7	1.4	0.9
115	17.3	23.4	23.4	17.3	34.6	23.0
135	33.0	44.5	44.5	33.0	66.0	44.0
160	50.5	68.1	68.1	50.5	101.0	67.0
185	65.8	88.7	88.7	65.8	131.5	87.0
200	73.9	99.8	99.8	74.0	147.9	98.0
250	96.7	130.4	130.4	96.7	193.3	129.0
300	114.4	154.3	154.4	114.4	228.7	155.0
400	139.9	188.8	188.9	140.0	279.8	188.0
500	157.6	212.8	212.9	157.8	315.3	211.0
600	170.8	230.5	230.6	170.9	341.5	227.0
800	188.8	255.0	255.1	189.0	377.7	255.0
1,000	200.9	271.4	271.5	201.2	401.9	267.0

Figure 4.12 The Results tab.

4.6 Menu Commands

File Like most Windows programs, the **File** menu allows the user to create a new file, save existing data, open existing data files, and to close the program.

Report The **Report** menu enables the user to create printable reports for documenting the calculations. At any time the user may select “Create, Save, and View Report...” to make a report. While saving a report, the report file extension may be saved as either .rpt (the default) or .htm. Regardless of the file extension selected, the report will be saved in HTML format, allowing future viewing through Internet Explorer, Netscape, or other web browsers. “View Report” only works to view an existing report, provided the information on the “Results” tab has not changed.

While viewing the report, you will see another File menu. This menu allows the user to print the reports, preview the print job, and change page printing settings. In order to use these menus, Microsoft Internet Explorer must be installed on the computer. Additionally, the Print Preview command requires Internet Explorer version 5.5 or higher. Users with versions of Internet Explorer older than 5.0 may experience other problems with the reports, so in that case it is recommended to upgrade to the latest version of Internet Explorer.

Units The **Units** menu allows the user to switch between U.S. Customary units (inch, foot, pound) and S.I. (System International) Metric units (millimeter, meter, kilogram). The indicator of the current units is the flag displayed in the upper right corner of the program window. The United States flag indicates U.S. Customary units, and the United Nations flag indicates S.I. Metric units. To change units, the user can also click on the flags.

Changing units will cause the input data to be converted to the new units. Any output that is currently displayed will be unaffected by the change. However, future output will be displayed in the new units. Output reports will be printed using the currently selected units, although the restraint moments will be printed in whatever units they are presently displayed in.

Help The Help menu provides access to the introduction of the program, the input file format, how to use the menu commands, interpretation of the results, and the “About” display.

4.7 Getting Results

Calculated results are displayed on the “Results” tab. Users can also create a report by selecting “Report > Create, Save and View Report” from the menu command. The program first displays the time history of the support and mid-span restraint moments. Then it displays the live load moments including the effects of restraint moments, support uplifting and concrete cracking. The next row displays the elastic moments assuming uncracked sections under the same live loads. The last row contains the Degree of Continuity (D.O.C.) for each span. The following is a list of symbols used in the results:

RM1, RM2 = Restraint moments at the 1st inner pier. RM1 is for the left support and RM2 is for the right.

RM3, RM4 = Restraint moments at the 2nd inner pier. RM3 is for the left support and RM4 is for the right.

RM5, RM6 = Restraint moments at the 3rd inner pier. RM5 is for the left support and RM6 is for the right.

MM1 = Restraint moment at the midspan of span 1.

MM2 = Restraint moment at the midspan of span 2.

MM3 = Restraint moment at the midspan of span 3.

MM4 = Restraint moment at the midspan of span 4.

CHAPTER 5

THE NEW CONTINUITY CONNECTION

5.1 Concept

As stated in the literature review, it is desirable to make the girders also continuous for the slab dead load. More continuity not only improves the efficiency of the bridge (less materials or longer spans), but also cuts the maintenance cost. The proposed new continuity connection using Carbon Fiber Reinforced Polymer (CFRP) is shown in Figure 5.1.

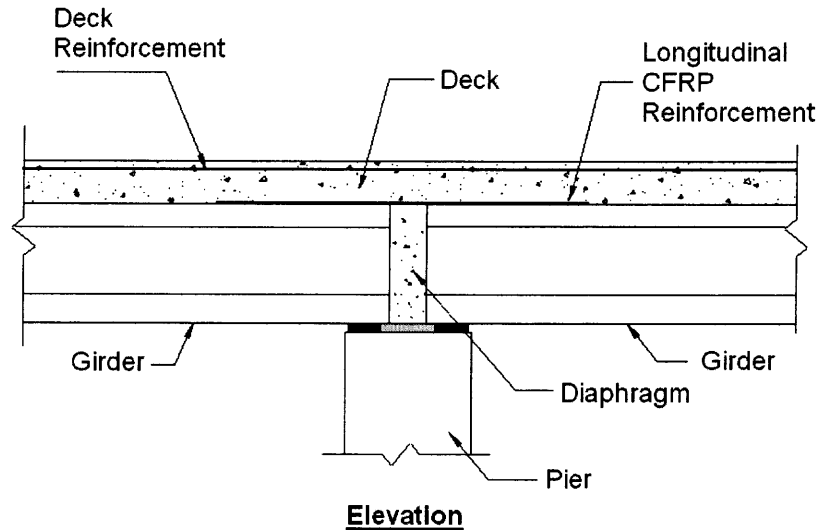


Figure 5.1 New connection.

Construction of the new connection will include the following steps:

1. Girders are erected and aligned in place.
2. Diaphragms are cast.
3. CFRP is attached to the girders to gain continuity. At the same time, deck forms and reinforcement are placed.
4. And finally, the slab concrete is cast.

Because the girders are connected before the deck slab is cast, the bridge is continuous not only for live load and superimposed dead load, but also for slab self-weight. As a result of more continuity, the slab self-weight will cause permanent negative moments over the inner piers. A calculation based on PCA test shows that the positive restraint moment caused by time dependent effects (17 kip-ft) is smaller than the negative moment caused by the weight of the deck slab (17.67 kip-ft). Thus, no positive moment reinforcement is needed in the diaphragm. If this is the case, the new method not only eliminates the costly and time-consuming positive moment connection, but also leads to a shortened gap of 3-4 inches between the girder ends, which further leads to narrowed diaphragms and smaller cap beams. Lightened superstructure also reduces column and foundation size.

5.2 Why CFRP?

Fiber Reinforced Polymer (FRP) products were first used to reinforce concrete structures in the 1950s. During the next two decades, the quality of the FRP materials improved considerably, manufacturing methods became more automated and material costs dropped. The use of these materials for external reinforcement of concrete bridge structure's started in the 1980s, first as a substitute to steel bonding plates and then as a substitute for steel confinement shells for bridge columns. The technology for external retrofitting was developed primarily in Japan (sheet wrapping) and Europe (lamine bonding). Today many concrete slab/steel girder bridges in Japan have been strengthened with sheet bonding to the slabs. Also, many thousands of bridge columns have been seismically upgraded with the same materials. In the US, FRP products are

also becoming more and more popular. Ongoing development of cost-effective production techniques for FRP composites has progressed to the level that they are ready for the construction industry. Reduced material cost coupled with labor savings inherent to its light weight and comparably simple installation, relatively unlimited material length availability, and immunity to corrosion make FRP materials an attractive solution for post-strengthening, repair, and seismic retrofit.

The FRP tendons and reinforcing bars have been used in new construction, but not FRP sheets and strips. Is the FRP material suitable for splicing the girders in new construction? From its lightweight, high strength and easy installation, it seems very attractive. Besides, the external bonded strips will alleviate the reinforcement congestion both in the girder end and in the diaphragm. To investigate this possibility, the new connection will utilize Carbon Fiber Reinforced Polymer (CFRP) because of its super high strength and good fatigue resistance. The tensile strength of CFRP can reach 400,000 psi, much higher than that of prestressing steel, which is 270,000 psi. Elongation at failure is 1~2%. The drawback of this material is that it has relatively low fire resistance. This can be improved if it is embedded in concrete, which is the case for its application in simple span girders made continuous.

5.3 Lab Tests

5.3.1 Introduction

The ACI Committee-440^[23, 24] presents summaries and design guidelines for FRP systems. Information includes material properties, design, installation, quality control, and maintenance. The recommended design procedure is similar to that of steel

reinforced concrete (cross-sections remain plane, strain compatibility, and force equilibrium) with additional reduction factors for the FRP material. The environmental-reduction factor accounts for the long-term durability and the bond-dependent reduction factor accounts for debonding of the FRP^[24].

The ACI Committee-440 guidelines focus on the use of FRP rebars/tendons and the strengthening of reinforced concrete structures. In the new connection design, the CFRP composites are directly applied to the diaphragm top, where there is no longitudinal steel reinforcement. The ACI Committee-440 does not provide any guide for this type of application, and even the literature on this topic is rare.

To investigate the feasibility of strengthening plain concrete with CFRP composites and validate the new continuity connection, 20 specimens were tested in the laboratory. They can be divided into two groups. The first group specimens are strengthened with CFRP strips (laminated by the manufacturer) and the second group specimens are strengthened with CFRP sheets (field laminated). All fibers are unidirectional.

The first group includes beams 1 through 5, beam1R and beam2D. Beams 1 through 4, beam1R and beam1D are 10' long. Beam 5 is two-span continuous with 8' span length. These beams are strengthened in the longitudinal direction with a 1.97" (50mm) wide, 0.0472" (1.2mm) thick CFRP strip except beam 1, which has no reinforcement over the support. Their cross section is the same – 6" wide and 12" high.

Beams 6 to 18 fall into the second group. Beams 6 to 11 are 22" long beams with a cross section of 6" by 4". Beams 12 to 14 are 30" long and beams 15 and 16 are 60" long. Beams 12 to 16 have the same cross section – 6" by 6". These beams are all

strengthened in the longitudinal direction with 2" wide CFRP sheets except beam 6, which is a control beam. Beams 17 and 18 are 10' long beams with a larger cross section – 6" by 12". They are strengthened longitudinally with two layers of 6" wide CFRP sheets. Some specimens are wrapped in the transverse direction with one layer of CFRP sheet. All beam geometries and concrete strengths are listed in Table 5.1.

Table 5.1 Summary of Beam Geometry and Materials

Group	Beam #	Length (in)	Width (in)	Height (in)	CFRP ¹	Bonded Length ² (in)	Wrap	f'c (psi)
I	1	120	6	12	-	-	-	5,250
	2	120	6	12	1	54	No	5,650
	1R	120	6	12	1	54	No	5,510
	2D	120	6	12	1	54	No	5,860
	3	120	6	12	1	54	No	6,630
	4	120	6	12	1	54	No	6,570
	5	192	6	12	1	36	No	5,500
II	6	22	6	4	-	-	-	5,920
	7	22	6	4	1	8	No	5,920
	8	22	6	4	2	8	No	5,920
	9	22	6	4	1	8	Yes	5,000
	10	22	6	4	2	8	Yes	5,000
	11	22	6	4	3	8	Yes	5,000
	12	30	6	6	2	6	Yes	6,050
	13	30	6	6	2	9	Yes	6,050
	14	30	6	6	2	12	Yes	6,050
	15	60	6	6	2	18	Yes	6,050
	16	60	6	6	2	24	Yes	6,050
	17	120	6	12	2	18	Yes	5,880
18	120	6	12	2	18	Yes	6,020	

1. For group I, numbers in column indicate number of CFRP strips. Each strip is 1.97" wide and 0.0472" thick. For group II, numbers in column indicate number of layers of CFRP sheets. Each layer is 2" wide and 0.02" thick except beams 17 & 18, in which each layer is 6" wide and 0.02" thick.

2. Bonded CFRP length on each side of the beam.

5.3.2 Properties of CFRP and Epoxy Resin

The CFRP and epoxy resin properties are listed in Table 5.2 through Table 5.5. Data are provided by the manufacturer ^[30].

Table 5.2 Properties of CFRP Strips

Thickness (in)	Width (in)	Modulus of Elasticity (psi)	Elongation at Break	Tensile Strength (psi)	Temperature Resistance
0.0472	1.97	23.9×10^6	1.69%	406,000	>300°F

Table 5.3 Properties of Epoxy Resin Used with CFRP Strips

Modulus of Elasticity (psi)	Elongation at Break	Tensile Strength (psi)	Shear Strength (psi)	Adhesive Strength on Concrete (psi)	Adhesive Strength on Steel (psi)
1.7×10^6	1%	3,600	3,600	>580 Concrete Failure	>3,770

Table 5.4 Properties of Cured CFRP Sheets

Thickness (in)	Modulus of Elasticity (psi)	Elongation at Break	Tensile Strength (psi)	Strength per Inch Width (lb)
0.02	8.2×10^6	1%	105,000	2,100

Table 5.5 Properties of Epoxy Resin Used with CFRP Sheets

Modulus of Elasticity (psi)	Elongation at Break	Tensile Strength (psi)
5.51×10^5	1.5%	4,350

5.3.3 Group I Tests

The CFRP strips are first selected for testing because of its high strength. Beam 1 has no reinforcement over the support (see Figure 5.2). Beam 2 is reinforced with a CFRP strip over the support. The two broken stubs from beam 1 are repaired with epoxy and then strengthened with CFRP on top. This repaired beam is numbered beam 1R. Similarly beam 2D is a repair of beam 2 stubs. Instead of gluing with epoxy, the stubs are connected by casting a concrete diaphragm in between and providing CFRP on top. Details of beams 2, 1R and 2D are shown in Figure 5.3. Test setup is shown in Figure 5.4 and Figure 5.5.

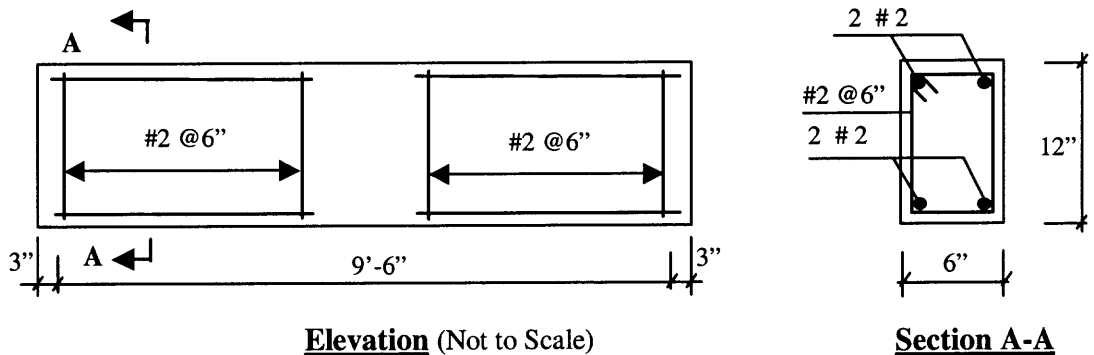


Figure 5.2 Beam 1 details.

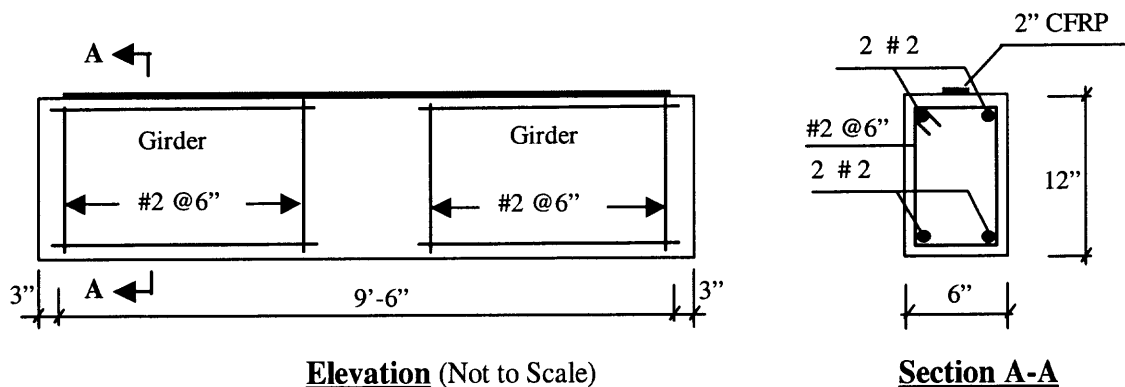


Figure 5.3 Details of beams 2, 1R and 2D.

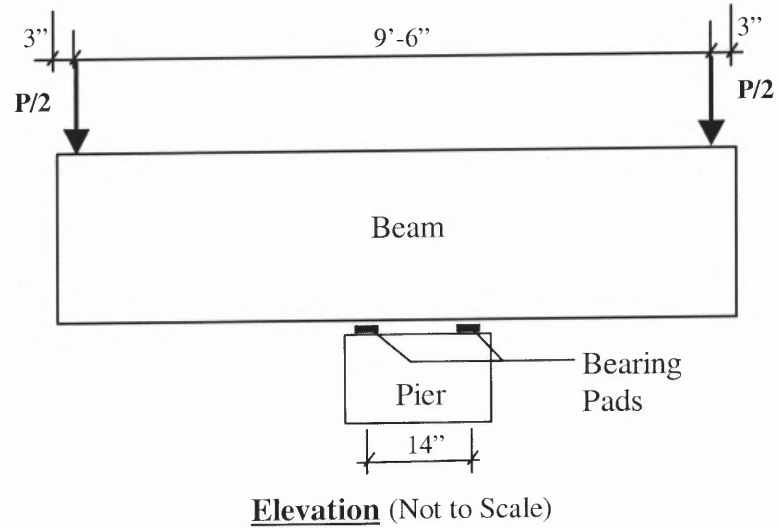


Figure 5.4 Test setup of beams 1, 2, 1R and 2D.



Figure 5.5 Testing of beam 2.

Load-deflection curves for beams 1, 2, 1R and 2D are illustrated in Figure 5.6. Beam 1 is linear elastic before cracking. After cracking the specimen fails because there is no reinforcement over the support. The maximum load for beam 1 is 2,073 lbs. Response for beams 2, 1R and 2D agrees well with the theoretical curve before the beams crack. After cracking, the load doesn't increase much. The ultimate loads for beams 2, 1R and 2D are only about 30% of the theoretical value assuming perfect bond.

The debonding failure mode of these beams can be seen from Figure 5.7. Unlike several distributed cracks in reinforced concrete beams, there is usually only one major crack over the support for beams strengthened with CFRP. Debonding starts right from the crack and travels towards the beam ends. Beams fail prematurely when debonding reaches either end of the CFRP.

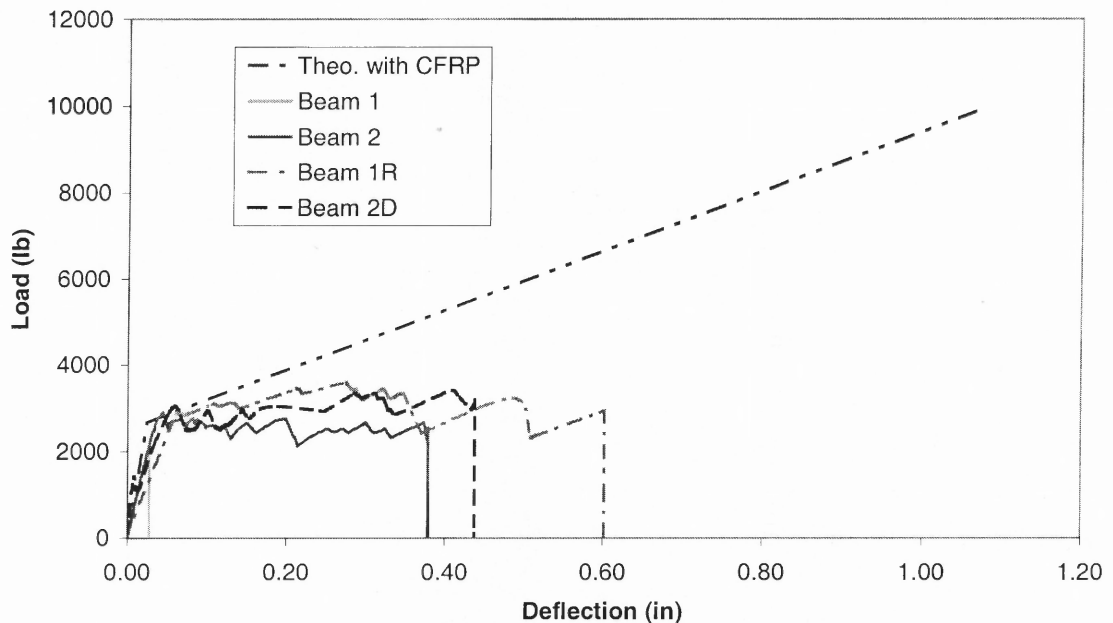


Figure 5.6 Test results of beams 1, 2, 1R and 2D.

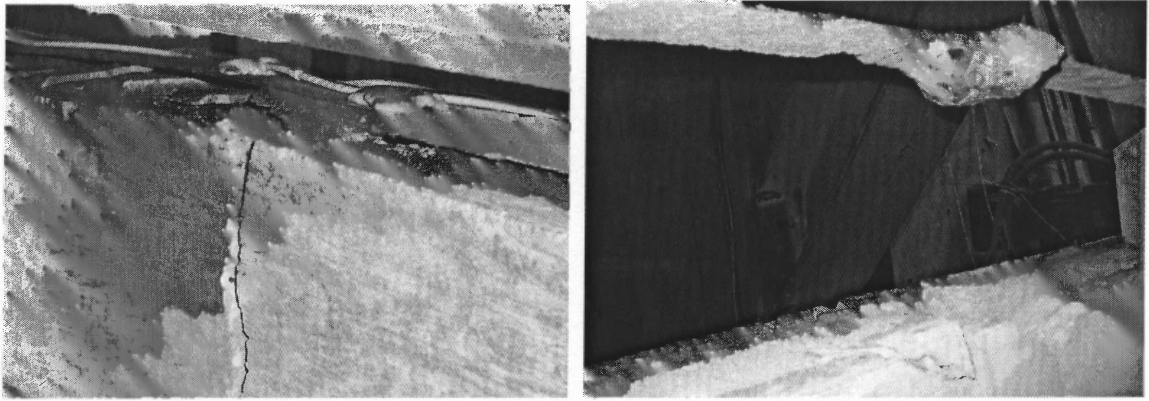


Figure 5.7 Failure mode of beam 2 (left) and beam 2D (right).

From the cracking pattern and the failure mode observed above, it is thought that two factors have played a role in the premature failure. One factor is shear. Theoretically there is no shear over the support because the setup produces pure bending between the two supports, but shear cracks develop at 45° . The distance between the supports is 14" while the beam depth is 12". Most likely the maximum moment region is under a combination of moment and shear. The shear force might have contributed to the debonding. The other factor is the presence of a single large crack. This causes a sharp slope change at the crack location. Because the CFRP strip is so rigid (modulus of elasticity equals 23.9×10^6 psi), it cannot follow this sharp slope change and debonding occurs. Based on these considerations, two changes are made to beams 3 and 4. The supports are moved out to 2' apart and the concrete is cut out $\frac{1}{2}$ " in the maximum moment region to form a void between the CFRP and the concrete. Thus if the concrete cracks, it won't initiate debonding of the CFRP. Test setup of beams 3 and 4 is shown in Figure 5.8 and Figure 5.9. Figure 5.9 also shows the failure mode of the two beams. Again one major crack forms in the maximum moment region and failure is caused by CFRP debonding.

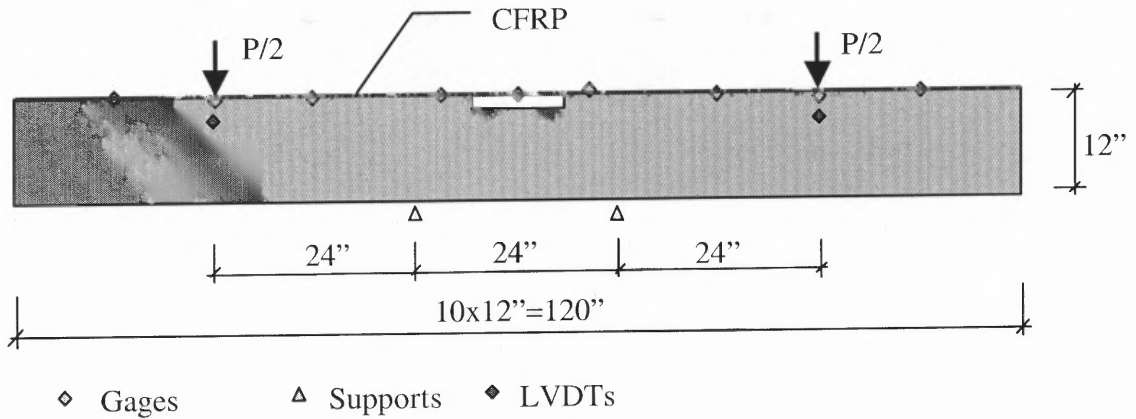


Figure 5.8 Test setup of beams 3 and 4.

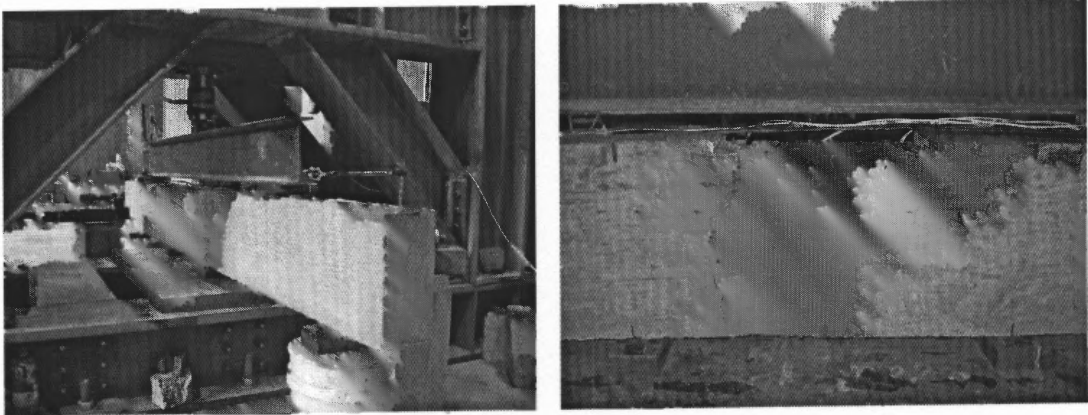
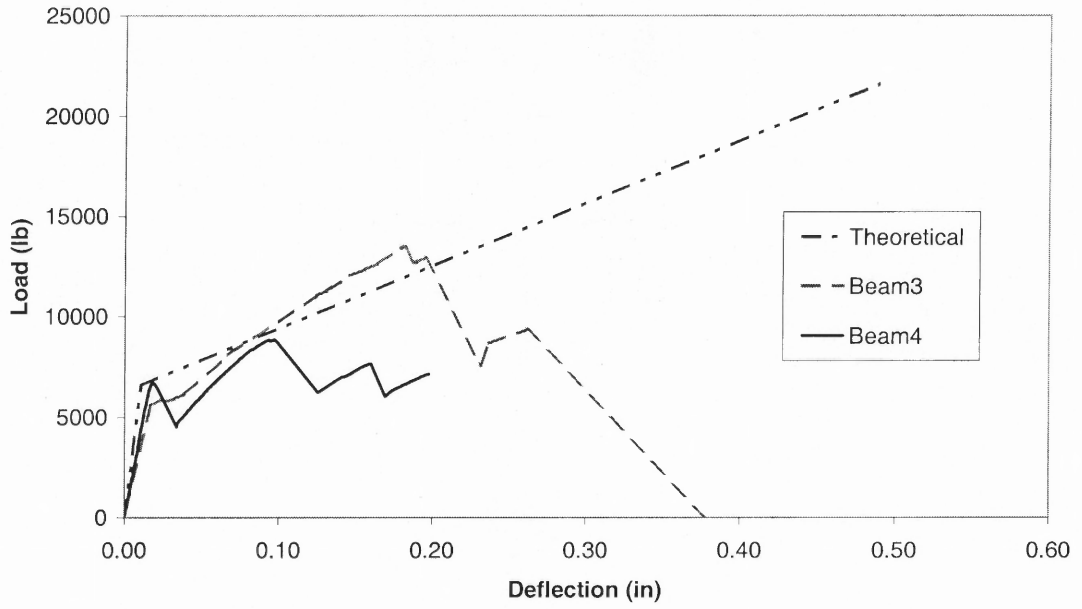
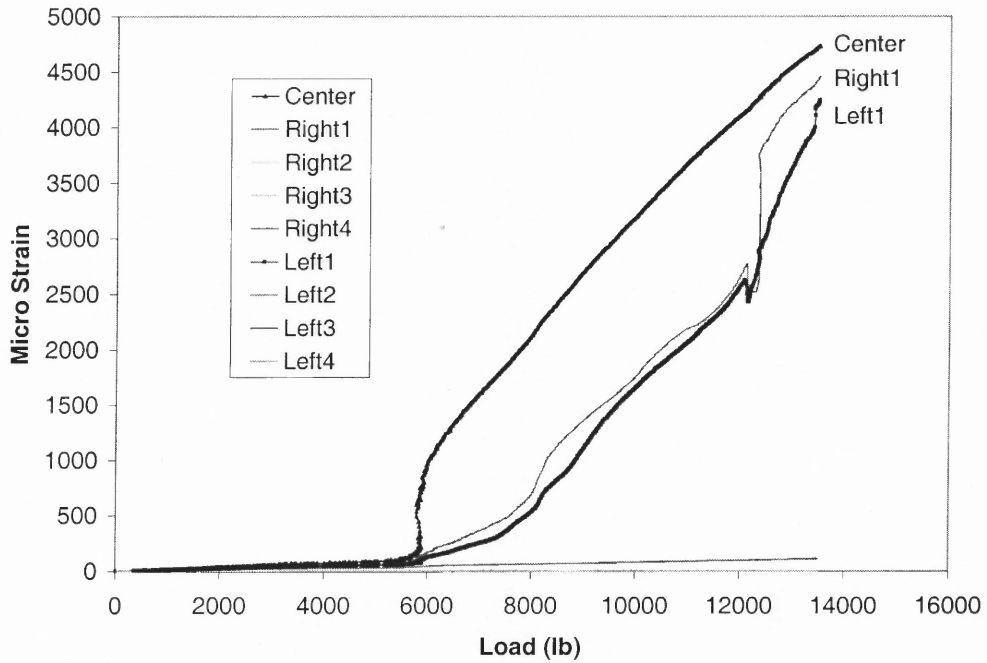


Figure 5.9 Test setup and failure mode of beams 3 and 4.

Test results are shown in Figure 5.10. There is a big improvement over beams 2, 1R and 2D. Beam 3 reaches 60% of its theoretical value assuming perfect bond while beam 4 reaches 40%. Figure 5.10(b) shows the strain gage readings of beam 3. All strains remain linear before the beam cracks. After beam cracking, the center 3 gages (center, left-1 and right-1) suddenly pick up strain while the others remain in low strain until the beam fails. Strain (or stress) is not linearly distributed in the CFRP. Instead, the CFRP suddenly picks up stress when debonding travels to that point.



a) Load-deflection curves



b) Strain in CFRP (beam 3)

Figure 5.10 Test results of beams 3 and 4.

Beams 1 to 4 were all supported in the middle and loaded at two ends. After the diaphragm cracked, the beam acted as two cantilevers which induced large deformations. A 16' long continuous beam was cast and tested in the thought that continuous beams have smaller deformations therefore would limit CFRP debonding.

The continuous beam setup (beam5) is shown in Figure 5.11. There is a 2" diaphragm cast after the two simple beams are cast. The distance between the central supports is 4". Each of the two simple beams is reinforced with five #4 rebar, two on top and three on bottom. Concrete cover is 1.5". The beam is cut out 1/2" over the central support as in beams 3 and 4. CFRP strip has 3' attachment on each side. Strain gages are mounted to the rebar at midspans and to the CFRP over the supports. LVDTs are installed at the loading points. Figure 5.12 shows beam 5 under testing.

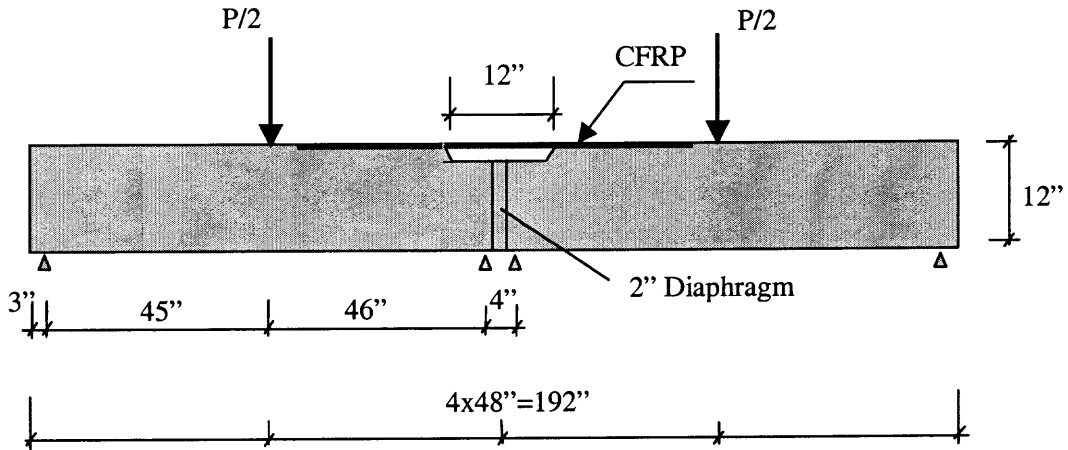


Figure 5.11 Beam 5 setup.

As seen in previous tests, the diaphragm cracks first. Then up to a load of 3,200 lbs, debonding starts from the middle of the diaphragm and travels to the ends. Figure 5.13 shows the test results of beam 5. Before debonding, the maximum strain in CFRP is $3,200 \times 10^{-6}$ in./in, which is only 32% of the possible maximum strain of $10,000 \times 10^{-6}$ in./in.

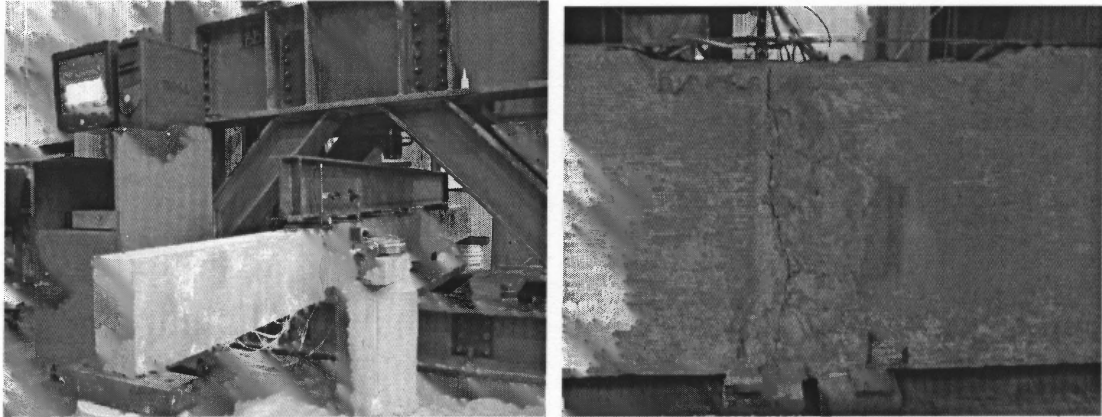
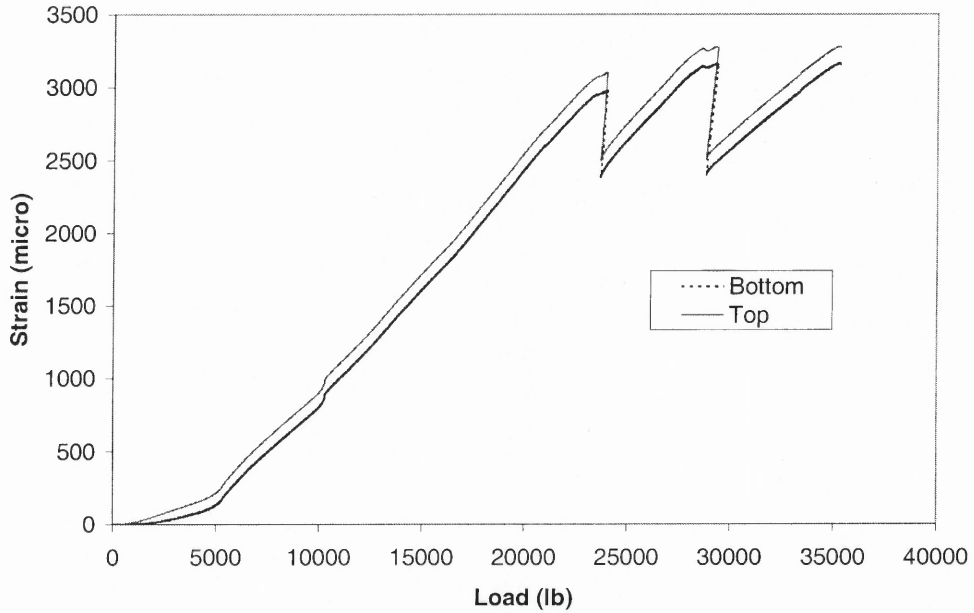
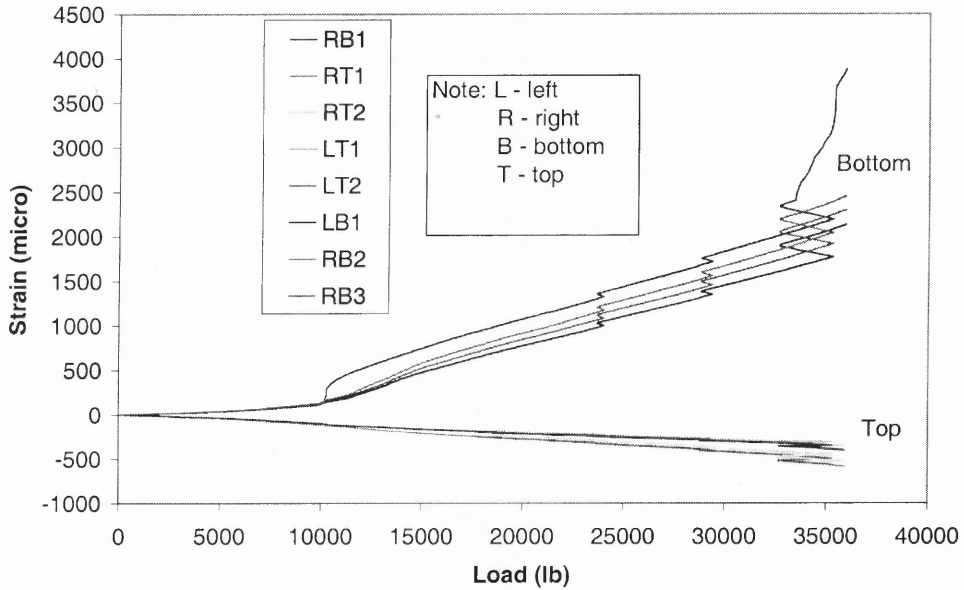


Figure 5.12 Beam 5 under test.



a) Strain in CFRP



b) Strain in rebars

Figure 5.13 Test results of beam 5.

Group I tests are summarized in Table 5.6. Although much effort has been made, the ultimate loads only get to 30% ~ 60% of their corresponding capacities. Failure is caused by debonding of the CFRP to the concrete. Previous studies (Lorenzis, Miller and Nanni)^[25] show that a reduction factor k_r should be applied to the ultimate strain of the CFRP to account for debonding and concrete cover de-lamination. Based on experimental study, this reduction factor is found to be:

$$k_r = \frac{6.75}{\sqrt{E \cdot t}}$$

where E is the modulus of elasticity and t is the thickness of the CFRP. For the CFRP used in Group I, $k_r=0.2$, which means only 20% of the CFRP strength can be used. To effectively utilize the strength, a more flexible material has to be used, either by reducing the modulus of elasticity or by reducing the thickness. This initiates the second group of tests.

Table 5.6 Summary of Group I Tests

Beam #	Conc. Surface	Height (in)	Bonded Length ¹ (in)	Max. Strain in CFRP ($\times 10^{-6}$)	Ult. Load (lb)	Theo. Load (lb)	Ratio ²
1	-	12	-	-	2,066	2,400	0.86
2	Sandblast	12	54	2,560	2,913	9,870	0.30
1R	Sandblast	12	54	2,700	3,574	9,870	0.36
2D	Sandblast	12	54	2,200	3,387	9,870	0.34
3	Sandblast	12	54	4,700	13,448	21,615	0.62
4	Sandblast	12	54	3,650	8,801	21,615	0.41
5	Sandblast	12	36	3,200	-	-	0.32

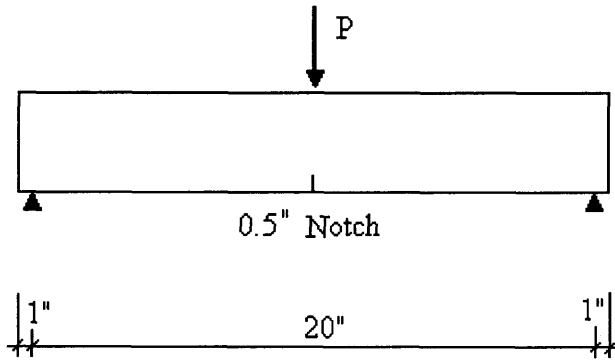
1. Bonded CFRP length on each side of the beam.

2. For beams 1 to 4, equals the ultimate test load divided by the theoretical load. For beam5, equals the maximum strain in CFRP divided by the maximum possible strain 0.01.

5.3.4 Group II Tests

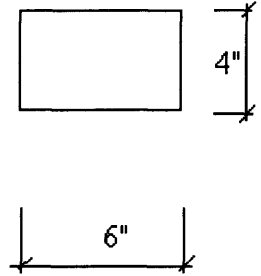
In group II a thinner CFRP is selected. Material properties are given in Section 5.3.2. The modulus of elasticity and thickness of CFRP sheets are much smaller than those of CFRP strips used for group I tests. Two techniques are used to improve bonding: one is wrapping, the other is cutting grooves on the top surface of the beams. Two parameters are studied: one is the number of CFRP layers, the other is the effective bonding length. Details follow.

Figure 5.14 shows the geometry and test setup of beams 6 to 11. Beam geometry and concrete compressive strength are described in Section 5.3.1. Beam 6 is a control beam, which is made of plain concrete. Beams 7 to 11 are all reinforced with 2" wide, 8" long CFRP sheets. Beam 7 has one layer of longitudinal CFRP reinforcement without wrap. Beam 8 has two layers of longitudinal CFRP reinforcement without wrap. Beam 9 has one layer of longitudinal CFRP reinforcement with one layer of transverse wrap. Beam 10 has two layers of longitudinal CFRP reinforcement with one layer of transverse wrap. Beam 11 has three layers of longitudinal CFRP reinforcement with one layer of transverse wrap. Wrap length is 6" each side beyond the surface of the longitudinal CFRP. All beams are saw-cut 1/2" at the midspan to control the crack location. The CFRP sheets are bonded 1" away from the cut to avoid debonding caused by the crack.

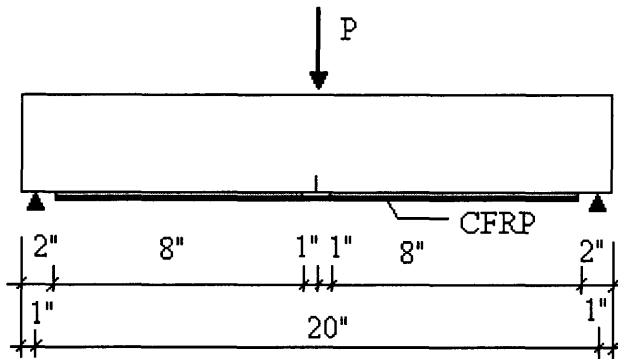


ELEVATION

(a) Beam 6

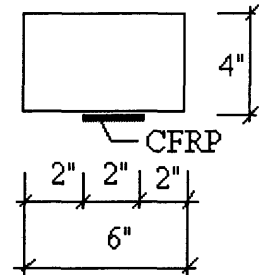


CROSS SECTION

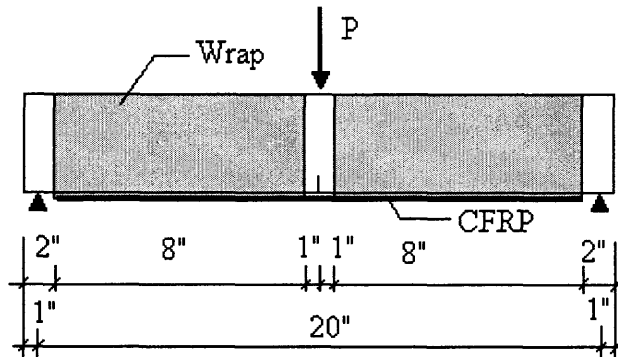


ELEVATION

(b) Beams 7 and 8

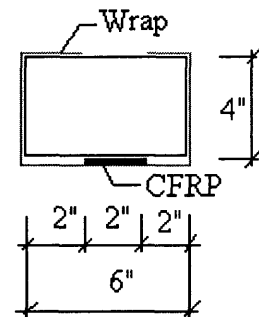


CROSS SECTION



ELEVATION

(c) Beams 9 to 11



CROSS SECTION

Figure 5.14 Details of beams 6 to 11.

Test results of beams 6 to 11 are shown in Figure 5.15. Beams 6 to 8 are from the same batch of concrete while beams 9 to 11 are from another batch. This explains the difference in the initial slopes. A comparison of the ultimate loads can be found in Table 5.7. Only beam 9 developed the full capacity of the material. All other specimens failed due to debonding with concrete substrate failure (see Figure 5.16 a and b).

Comparing beams 6-8 (without wrap) and 9-11 (with wrap), one can see that the ultimate load increases when more layers of CFRP are used, but the efficiency of the material (last column in Table 5.7) decreases. Another observation is that wrapping has a significant effect against debonding. By comparing beams 7 and 9 (or 8 and 10), it is clear that with the same amount of longitudinal CFRP reinforcement, wrapping increases the ultimate load by 36%. Wrapping also improves ductility of the beams. The deformation of beams 9 and 10 are 95% larger than that of beams 7 and 8.

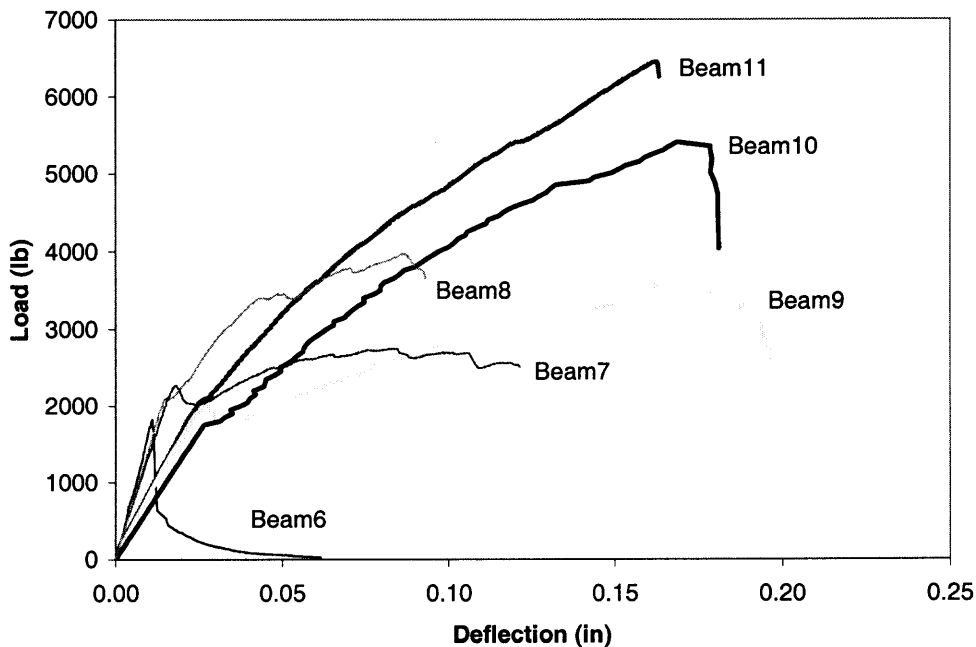
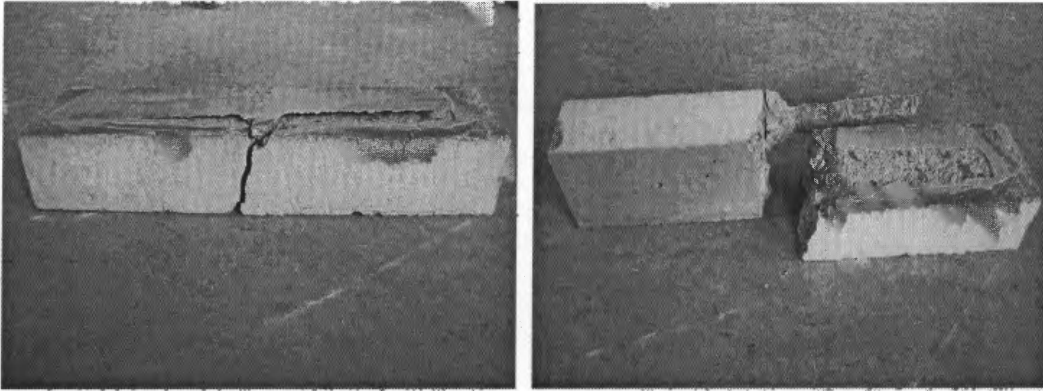
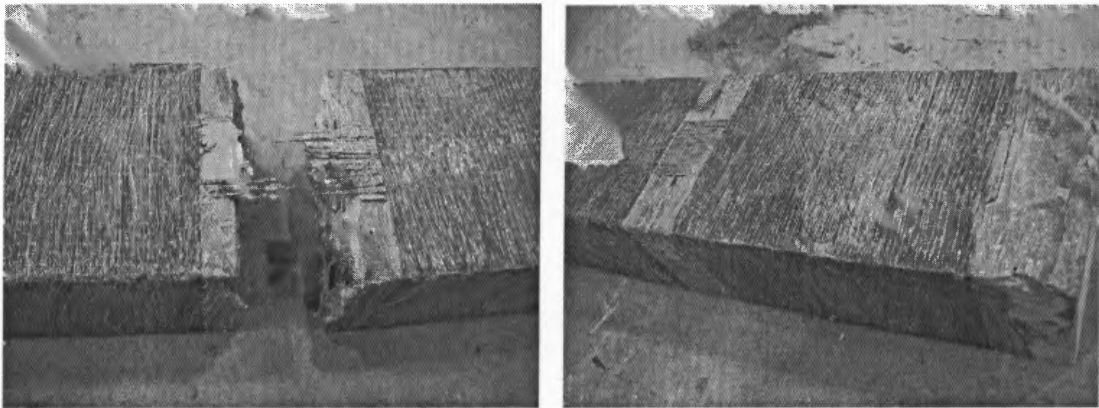


Figure 5.15 Load-deflection of beams 6 to 11.



(a) & (b) Debonding of CFRP without wrap (beam7).

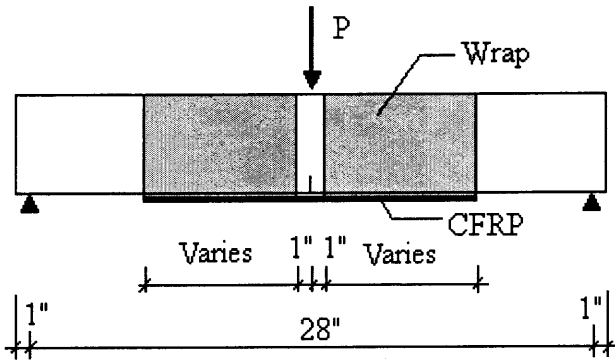


(c) CFRP rupture (beam9)

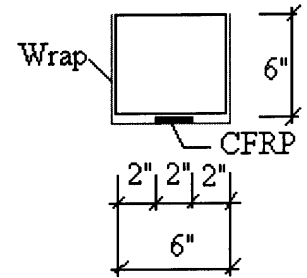
(d) Debonding of CFRP with wrap (beam10)

Figure 5.16 Failure modes of beams 7 to 11.

Calculation shows that one layer of CFRP sheet is not going to develop enough strength for real bridges. Therefore, the effective bonding length for two layers of CFRP with wrap needs to be determined. The cross section of the beams is increased to 6"×6" to accommodate the increased amount of CFRP reinforcement. Details of beams 12 to 16 are illustrated in Figure 5.17. Pictures of beams 12 to 16 are shown in Figure 5.18.

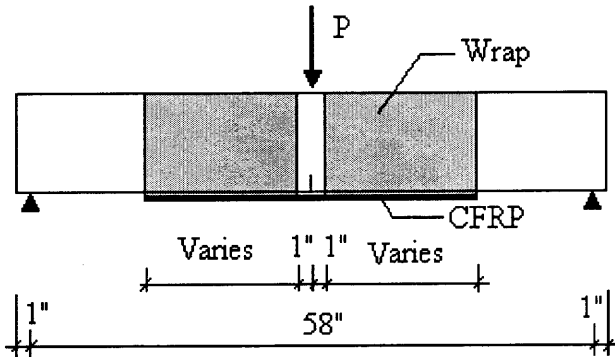


ELEVATION

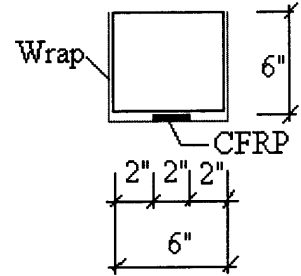


CROSS SECTION

(a) Beams 12 to 14 with bonding length of 6", 9" and 12", respectively.



ELEVATION



CROSS SECTION

(b) Beams 15 and 16 with bonding length of 18" and 24", respectively.

Figure 5.17 Details of beams 12 to 16.

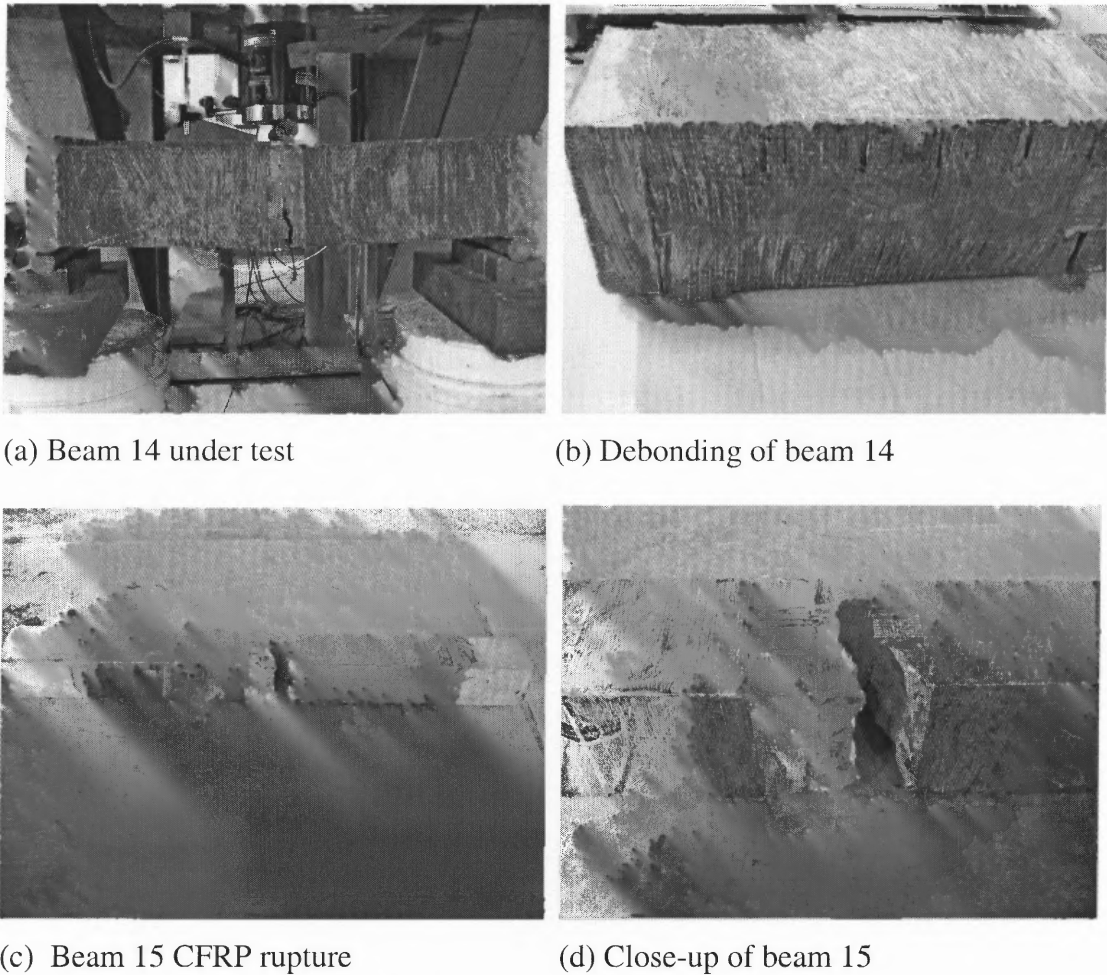


Figure 5.18 Test setup and failure modes of beams 12 to 16.

Table 5.7 contains a summary of beams 12 to 16. Based on the results for beams 12 to 14, one can see that the ultimate load increases when the bonding length increases. None of the beams from 12 to 14 develop the full capacity of the CFRP. Failure is caused by debonding. Span length is increased to 60" to allow for longer bonding length. In addition to sandblasting, 1/8" transverse grooves are made 3" apart along the bonding length. Beams 15 and 16 all developed 103% of the manufacturer recommended strength. Failure is caused by rupture of the CFRP sheets. With the help of grooves and wraps, 18" bonding length is needed for two layers of CFRP sheets used in this study.

Further increasing the bonding length cannot increase the ultimate load. Test results of beams 12 to 16 are illustrated in Figures 5.19 and 5.20.

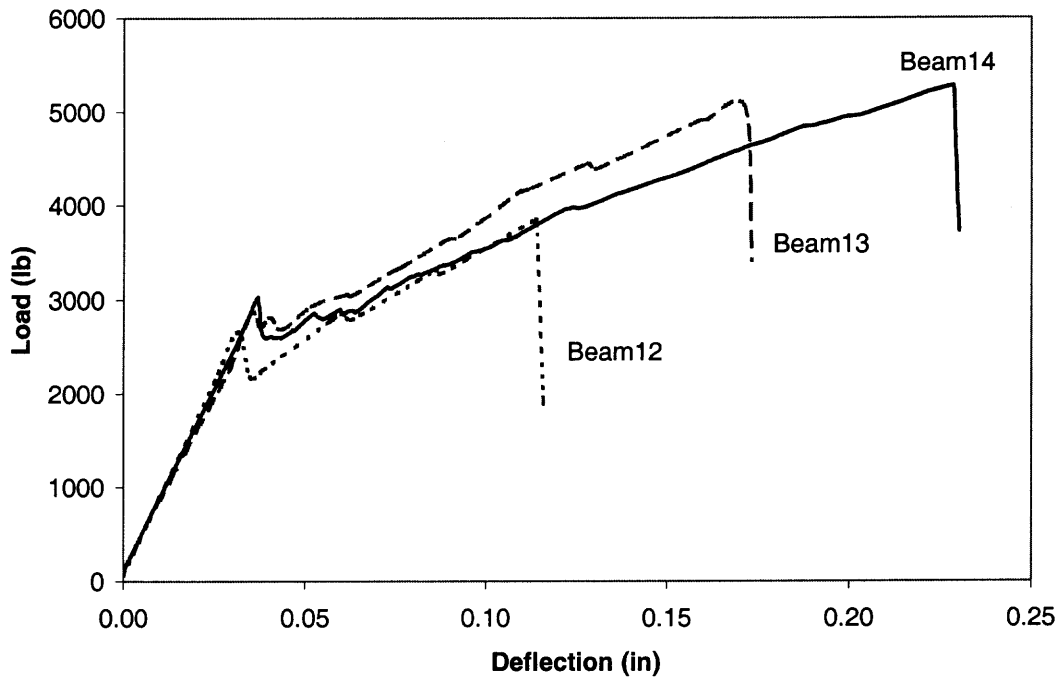


Figure 5.19 Load-deflection curves for beams 12 to 14 with different bonding length.

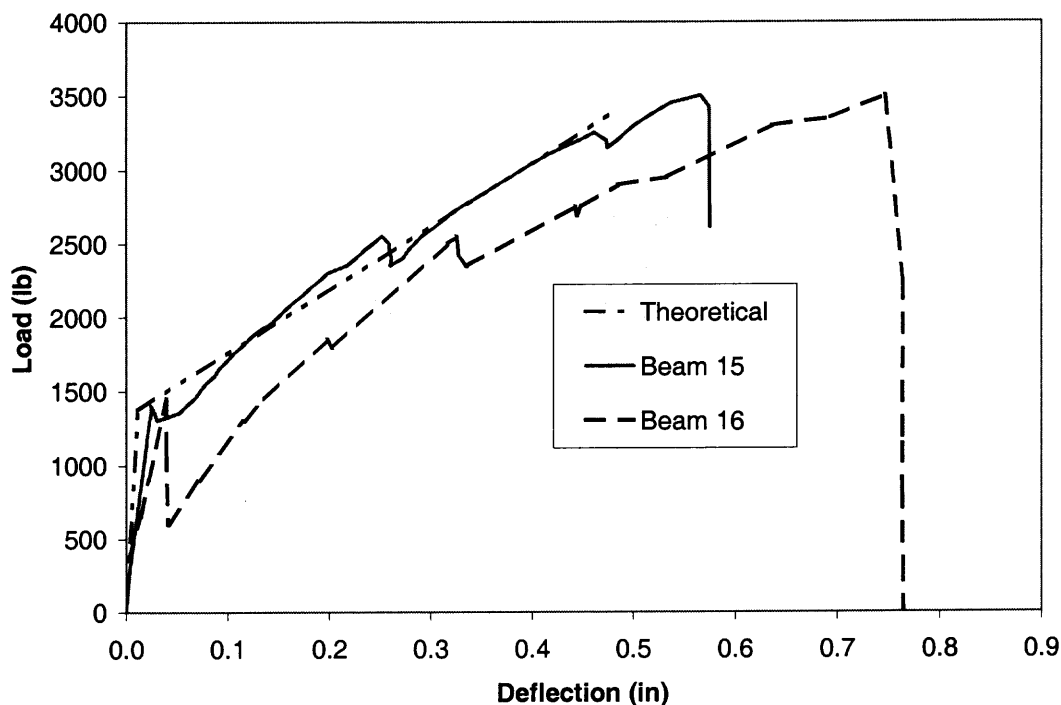


Figure 5.20 Load-deflection curves for beams 15 and 16 with different bonding length.

Based on group II tests described above, CFRP sheet is an ideal material to strengthen un-reinforced concrete members, but the specimens are relatively small. To further verify the effectiveness of this material, two 10' long beams with a cross section of 6" by 12" (same as in group I) have been tested. The beams are composed of two beam stubs connected with a 2" wide diaphragm. Each beam stub is reinforced with three #4 grade 60 rebars on top and two #4 rebars on bottom. The two beam stubs are connected with two layers 6" wide CFRP sheets on top. Similar to other specimens in group II, the longitudinal CFRP sheets are wrapped with a layer of transverse sheet. The bonding length on each beam stub is 18" for two layers of CFRP with wrap, as determined previously from small beams. Reinforcing details and test setup are shown in Figure 5.21. For clarity, the steel reinforcement in the beam stubs is not shown.

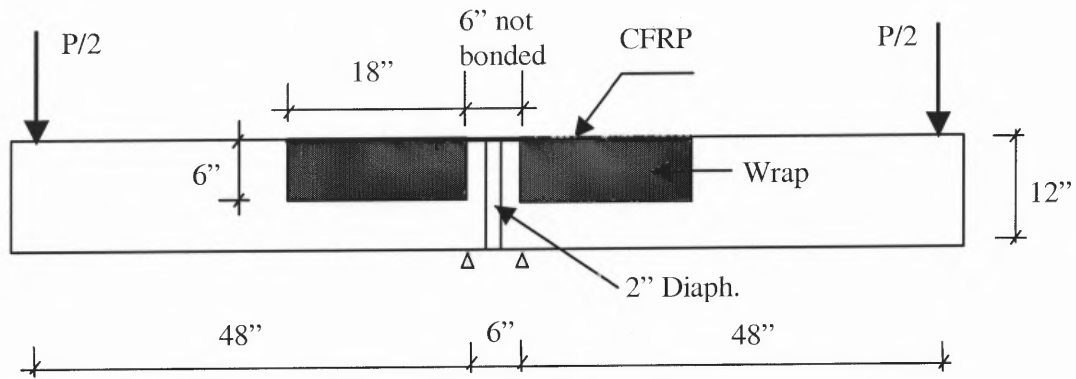


Figure 5.21 Detail of beams 17 and 18.

Because there is a cold joint between the diaphragm and the beam stubs, micro cracks form on their interface under the beam self weight. As the load increases, the cracks develop and additional cracks initiate in the beams. Failure is caused by CFRP rupture. No debonding is found either in the longitudinal or the transverse CFRP sheets. Figure 5.22 shows the failure mode of the specimens.

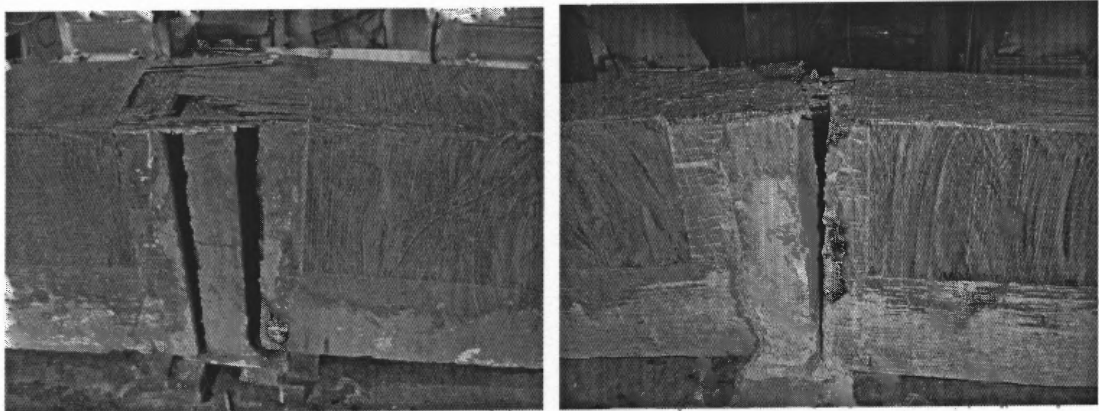


Figure 5.22 CFRP rupture of beams 17 (left) and 18 (right).

Figure 5.23 shows the load-deflection curves of the specimens. The analytical result using ANSYS is also shown. The ultimate test load is 85% of the analytical for beam 17, and 81% for beam 18. It should be noted that there is a discrepancy in the

material properties provided by the manufacturer. The analytical data presented in Figure 5.23 are based on the maximum load per inch width of CFRP, which is 2.1 kips. If the Young's modulus (8.2×10^6 psi) and the ultimate strain (0.01) are used, the maximum strength of CFRP would be 1.64 kips/in. The analytical load would then be 9.6 kips and the ultimate test loads would be 109% and 103% of the analytical for beam 17 and beam 18, respectively.

Group II tests are summarized in Table 5.7. These results support the viability of the proposed new continuity connection, which enhances bridge efficiency and live load performance.

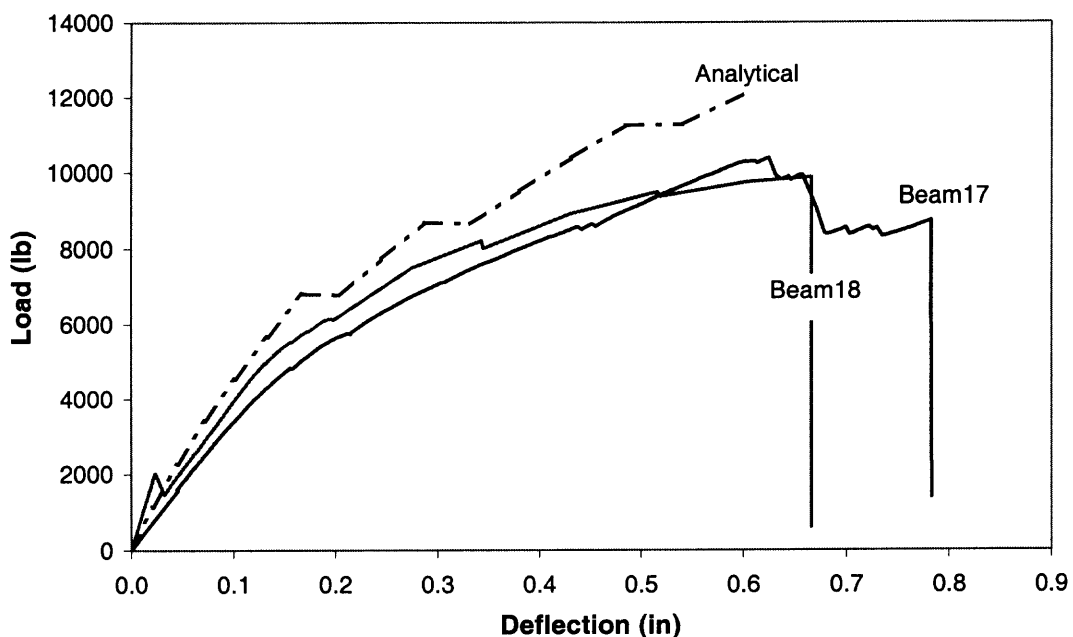


Figure 5.23 Analytical and test results of beams 17 and 18.

Table 5.7 Summary of Group II tests

Beam #	CFRP ¹	Bonded Length ² (in)	Wrap	Conc. Surface	Failure Mode	Test Load (lb)	Theo. Load (lb)	Ratio ³
6	-	-	-	-	Concrete cracking	1,822	1,846	0.99
7	1	8	No	Sandblast	Debonding	2,740	3,290	0.83
8	2	8	No	Sandblast	Debonding	3,969	6,443	0.62
9	1	8	Yes	Sandblast	CFRP rupture	3,733	3,290	1.13
10	2	8	Yes	Sandblast	Debonding	5,400	6,443	0.84
11	3	8	Yes	Sandblast	Debonding	6,451	9,457	0.68
12	30	6	Yes	Sandblast	Debonding	3,848	7,036	0.55
13	30	9	Yes	Sandblast	Debonding	5,050	7,036	0.72
14	30	12	Yes	Sandblast	Debonding	5,280	7,036	0.75
15	60	18	Yes	Sandblast +Grooves	CFRP rupture	3,503	3,397	1.03
16	60	24	Yes	Sandblast +Grooves	CFRP rupture	3,500	3,397	1.03
17	120	18	Yes	Sandblast +Grooves	CFRP rupture	10,289	12,158	0.85
18	120	18	Yes	Sandblast +Grooves	CFRP rupture	9,885	12,158	0.81

1. Numbers in column indicate number of layers of CFRP sheets used. Each layer is 2" wide and 0.02" thick except beams 17 & 18, in which each layer is 6" wide and 0.02" thick.

2. Bonded CFRP length on each side of the beam.

3. Ratio of the test load to the theoretical load assuming perfect bond.

5.3.5 Conclusions on Lab Tests

The following conclusions can be made based on the above laboratory tests:

1. For the external flexural strengthening of plain concrete members, the bond between the concrete and the reinforcement is the most critical element. Flexible FRP materials should be used. Rigid CFRP laminates can lead to premature failure because of debonding. Based on this study, CFRP sheets turn out to be an ideal material for the strengthening of un-reinforced concrete.
2. Wrapping and surface preparation (specially grooves) have a significant effect against debonding.
3. With other parameters staying the same, the ultimate load increases with the number of CFRP layers, although the efficiency of the material decreases.
4. With other parameters being the same, the ultimate load increases with the bonding length until it reaches the effective bonding length, beyond which there is no gain in strength.
5. For one layer of CFRP sheets considered in this study, 8" bonding length with wrap can develop the full capacity of the material.
6. For two layers of CFRP sheets used in this study, the effective bonding length with wrap is 18".

5.4 A Design Example

As mentioned in Section 5.1, a tentative calculation based on PCA test shows that the positive restraint moment caused by time dependent effects is smaller than the negative moment caused by the weight of the deck slab. Thus, no diaphragm cracking will occur in the newly proposed connection. To further clarify this issue, a design example based on the bridge on I-287 NB over Darlington Ave is presented below.

This is a three-span bridge with span 2 and span 3 made continuous via a continuity diaphragm and a deck. The deck slab is 7.5" thick and the girder spacing is 8'.

Per AASHTO Specification, the compressive strength of the diaphragm section can be taken as the same with that of the girders, which is 6,000 psi. For detailed geometry of the bridge please refer to Section 2.3.1.

The support moment caused by the slab dead load is 1,350 kip-ft. Assume that failure is caused by CFRP rupture. The maximum strain in the CFRP reinforcement is 0.01. Let the strain at the bottom of the girder be ϵ , the neutral axis is located at:

$$y = 72 \epsilon / (0.01 + \epsilon).$$

Assuming the concrete stress-strain relationship follows the equation proposed by Thorenfeldt, Tomaszewicz, and Jensen^[31],

$$f_c = f'_c \cdot n \cdot (\epsilon_{cf} / \epsilon'_c) / (n - 1 + (\epsilon_{cf} / \epsilon'_c)^{nk}) \quad \dots(5.1)$$

where f'_c = peak stress of concrete

$$n = 0.8 + f'_c / 2500 = 0.8 + 6000 / 2500 = 3.2$$

$$k = 0.67 + f'_c / 9000 = 0.67 + 6000 / 9000 = 1.337$$

$$E_c = \text{Initial Young's modulus of concrete} = w_c^{1.5} 33 (f'_c)^{1/2} = 4,696,000 \text{ psi}$$

$$\epsilon'_c = \text{strain at } f'_c = f'_c / E_c \cdot n / (n-1) = 0.00186$$

$$\text{Thus, } f_c = 6000 \cdot 3.2 \cdot (\epsilon_{cf} / 0.00186) / (2.2 + (\epsilon_{cf} / 0.00186)^{4.28}) \quad \dots(5.2)$$

Figure 5.24 shows the strain and force distribution of the diaphragm section. To get the moment, the compression zone is divided into 4 equal layers assuming the strain in each layer equal to the strain at the center of that layer. For each layer, stress is determined from strain based on Eq. 5.2. The moment contribution of each layer is simply a multiplication of the stress, area and distance to girder top of that layer. Summation of the moments should equal the applied moment of 1,350 kip-ft.

$$M = n f'_c A [7/8 \epsilon / 0.00186 / (2.2 + (\epsilon / 0.00186)^{4.28}) (72 - 72 \epsilon / 8 / (0.01 + \epsilon))$$

$$\begin{aligned}
 &+ 5/8 \epsilon / 0.00186 / (2.2 + (\epsilon / 0.00186)^{4.28}) (72 - 3 (72 \epsilon) / 8 / (0.01 + \epsilon)) \\
 &+ 3/8 \epsilon / 0.00186 / (2.2 + (\epsilon / 0.00186)^{4.28}) (72 - 5 (72 \epsilon) / 8 / (0.01 + \epsilon)) \\
 &+ 1/8 \epsilon / 0.00186 / (2.2 + (\epsilon / 0.00186)^{4.28}) (72 - 7 (72 \epsilon) / 8 / (0.01 + \epsilon))] / 12
 \end{aligned}$$

where $M = 1,350$ kip-ft

$$n = 3.2$$

$$A = \text{area of each layer} = 28 y / 4 = 7 (72 \epsilon) / (0.01 + \epsilon)$$

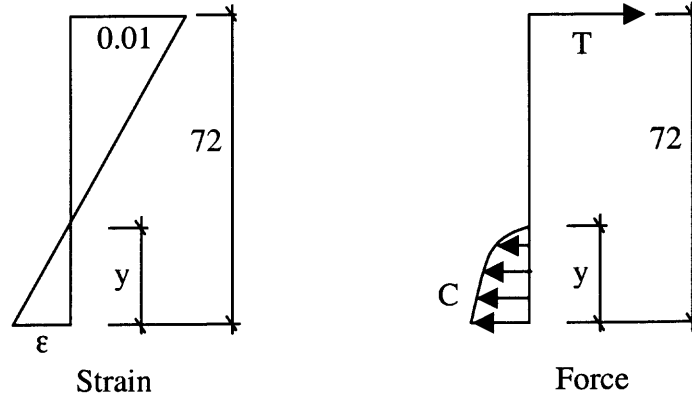


Figure 5.24 Cross sectional analysis.

By trial and error, ϵ is found to be 0.000723, y is 4.85”, and the tension force in CFRP is 230 kips. Table 5.8 lists the amount needed for different types of CFRP fabric. If the CFRP sheet listed in Table 5.4 is used, it requires a cross-sectional area of 2.2 in² (or 2-layer 54” wide CFRP). Assuming a safety factor of 2.0, 4.4 in² CFRP is provided on the top of the girders over the center support. The diaphragm should not be bonded to the CFRP reinforcement. The bonding length on each girder should not be less than 18”. Sandblast the concrete surface and make 1/8” deep transverse notches every 3” along the bonding length. The longitudinal CFRP should be wrapped with one layer transverse CFRP. The bonding length for the wrap should not be less than 6” beyond the top surface of the girders.

Table 5.8 Amount Needed for Different Types of CFRP Fabric Sheet

	Sikawrap 117C	Sikawrap 103C	Watson MBrace CF130	Watson MBrace CF160	Zoltek PX35FBUD0300
Thickness (in)	0.0200	0.0400	0.0065	0.0130	0.0228
Max. Strength per Unit Width (kip/in)	2.10	5.56	3.57	7.14	3.40
Number of Layers	2	2	2	2	2
Width Needed (in)	54	21	32	16	34

The finite element method described in Chapter 3 is used to analyze the midspan and support moments and the stress levels in the CFRP reinforcement. Results are compared to those of the conventional continuity connection.

First, an extreme case of large creep coefficient (3.25) and small ultimate shrinkage (600×10^{-6} in/in) is studied. The girder age at continuity is 28 days. Figure 5.25 shows a comparison of the midspan moments of the new connection method and the existing method. For clarity, the time period of the live load application is elongated.

The two curves go parallel to each other. The difference in the midspan moment before live load application is 190 kip-ft (5%). The reduction in midspan moment because of more continuity is not as significant as expected. This is because the reduction in midspan moment is canceled by the more positive restraint moment induced in the new continuity connection, half of which gets transferred to the midspan. In the

existing design, although the midspan moment caused by the slab dead load is larger, it also reduces the prestress level of girders. Therefore, less creep effects develop.

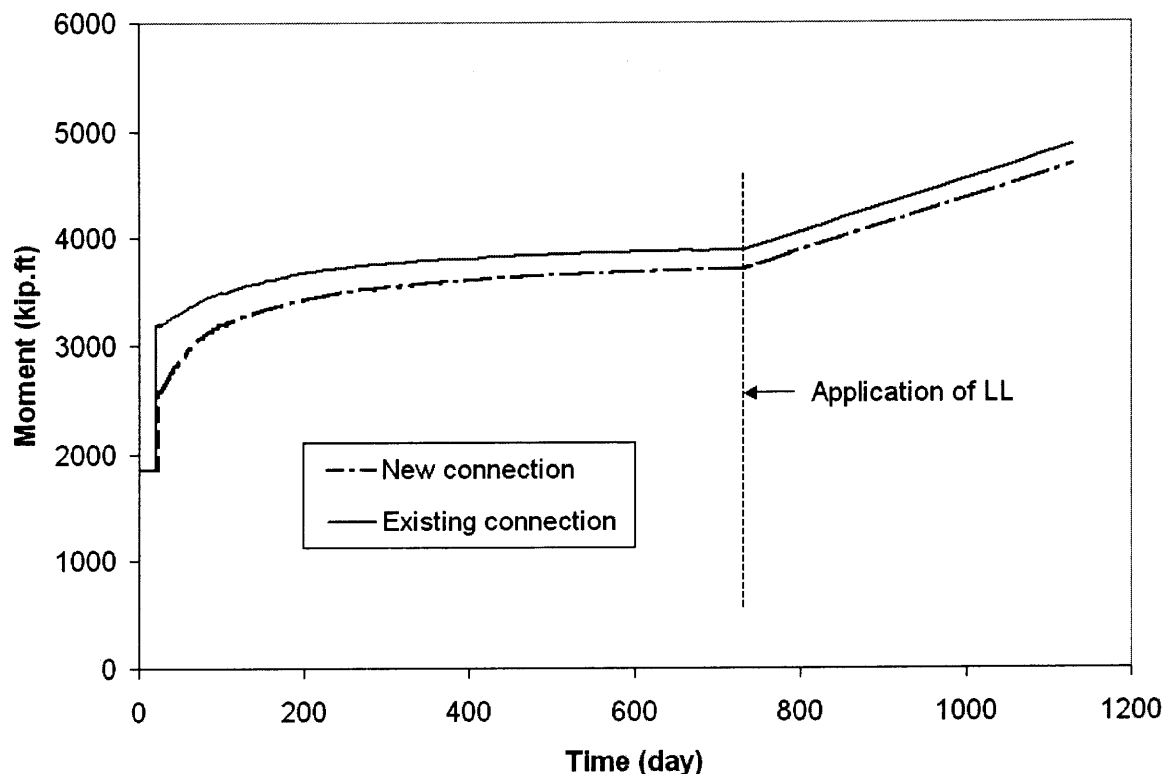


Figure 5.25 Comparison of midspan moments ($C=3.25$, $\epsilon=600\times 10^{-6}$ in/in).

Figure 5.26 shows a comparison of the support moment of the new construction and the existing one. These curves also go parallel to each other but the support moment drops from 1,415 kip-ft to 950 kip-ft. The reduction is significant (465 kip-ft, or 33%). Note that the cracking moment of the diaphragm section is 1,100 kip-ft, which means that by making the girders also continuous for slab dead load, the support moment drops from above the cracking moment to below the cracking moment.

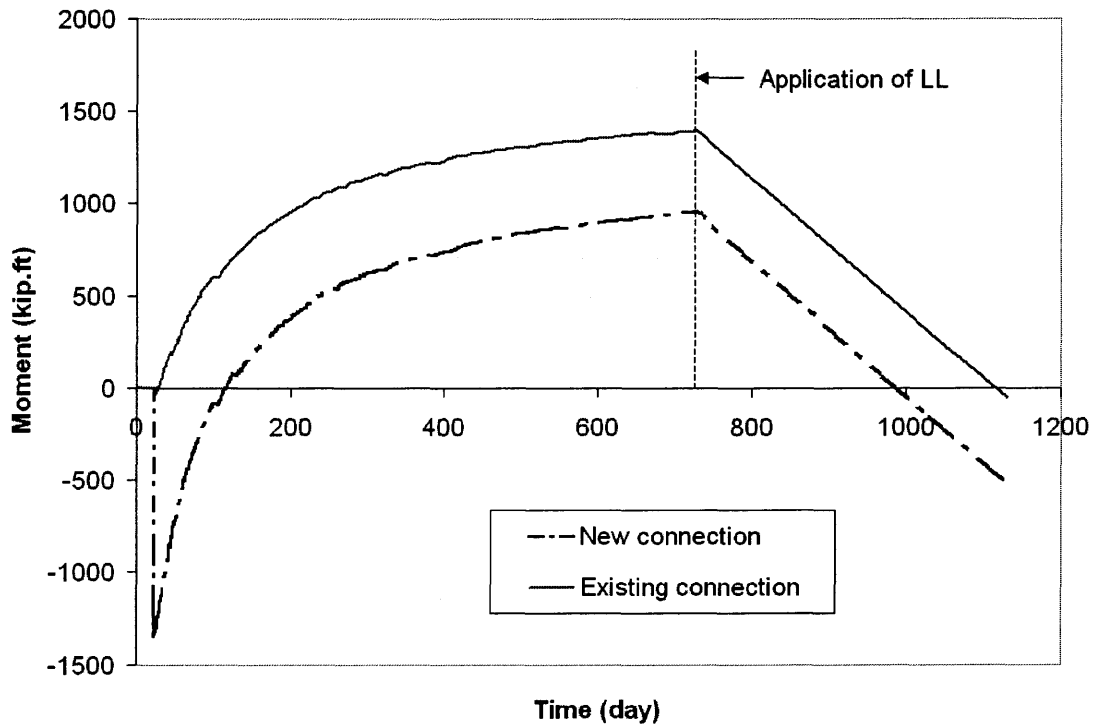


Figure 5.26 Comparison of support moments ($C=3.25$, $\epsilon=600\times 10^{-6}$ in/in).

For the second case, a more reasonable creep coefficient of 2.0 and ultimate shrinkage of 600×10^{-6} in/in are used to analyze the same bridge. Comparisons of midspan and support moments are shown in Figures 5.27 and 5.28, respectively. Before the application of live load, the midspan moment drops from 3,693 kip-ft to 3,405 kip-ft (8%) and the support moment drops from 1,004 kip-ft to 372 kip-ft (63%). Again, the reduction in support moment is significant.

The most critical stage for the CFRP reinforcement is when the deck concrete is poured. In this example, the stress in CFRP is 52,000 psi, half of its ultimate strength. The stress drops when time dependent effects cause positive restraint moment over the support. When the deck concrete hardens, a composite section forms and additional loads are mostly carried by the steel reinforcement in the deck because its modulus of elasticity (29×10^6 psi) is much higher than that of CFRP (8.2×10^6 psi). For the two cases

of this example, the stress in the CFRP reinforcement under live load is 238 psi and 400 psi respectively, far below its ultimate strength of 105,000 psi.

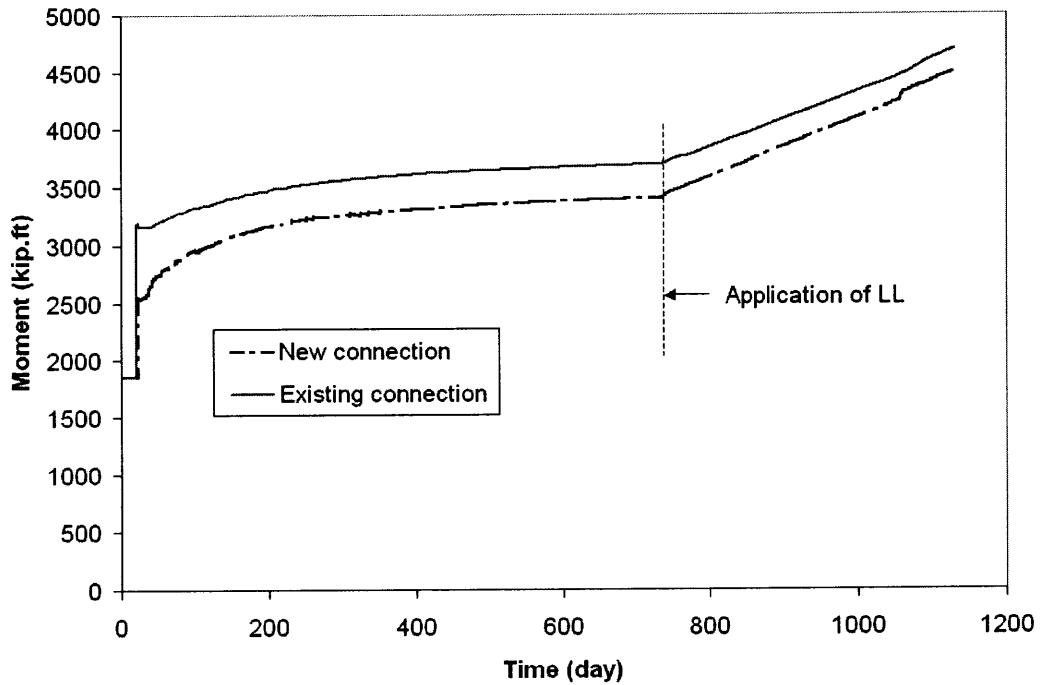


Figure 5.27 Comparison of midspan moments ($C=2.0$, $\epsilon=600 \times 10^{-6}$ in/in).

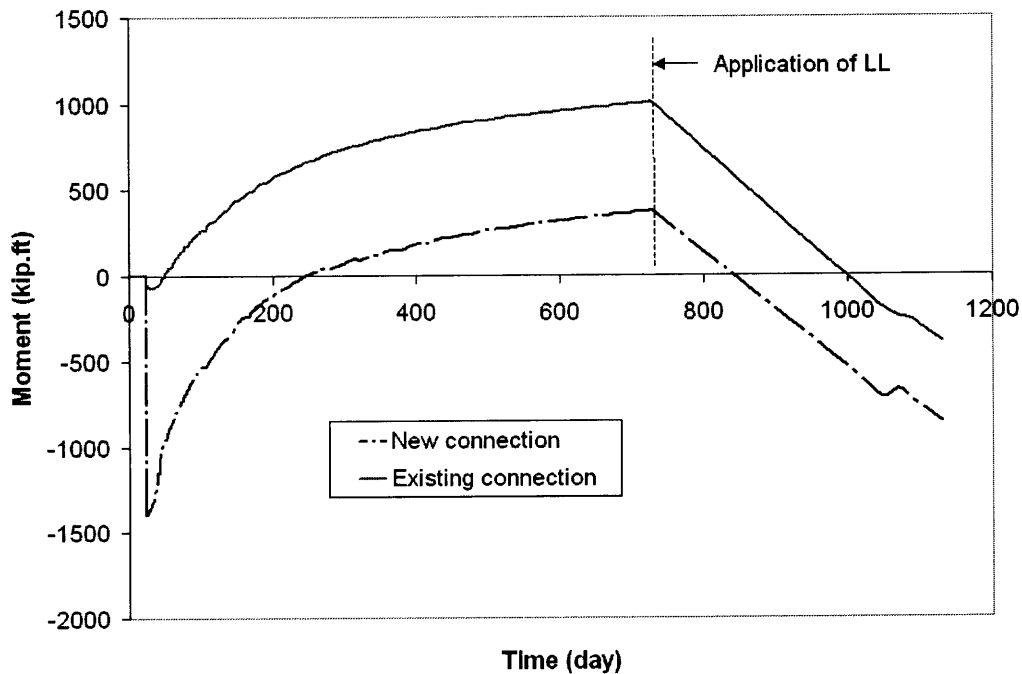


Figure 5.28 Comparison of support moments ($C=2.0$, $\epsilon=600 \times 10^{-6}$ in/in).

One concern about the new connection is the cost. CFRP is relatively expensive comparing to steel reinforcement, but the labor cost is much lower because of its lightweight and easy installation. The additional cost for the bridge on I-287 NB over Darlington Ave is estimated to be \$12,000 (\$2,000 per stringer). This is only a fraction of the total cost of a bridge like this, but the benefits are significant. The new connection increases the efficiency of the structure, leading to material savings or longer spans. It also improves the performance of the bridge. Since the slab introduces permanent moment over the support, the positive restraint moment is controlled below the cracking moment. Therefore no positive moment reinforcement is needed in the diaphragm and the connection is maintenance free. Once the deck is in place, the CFRP reinforcement is no longer needed. The presence of CFRP increases the integrity of the bridge and provide redundancy during extreme events.

From the experimental studies and the above analysis, it is concluded that the new continuity connection using CFRP can improve the structural efficiency and performance of bridges composed of simple-span prestressed concrete girders made continuous. Its application on this type of bridge is promising.

5.5 Standard Drawings and Construction Procedures

Based on the studies described in this chapter, standard drawings and construction sequence, consistent with the NJDOT format, is proposed as follow:

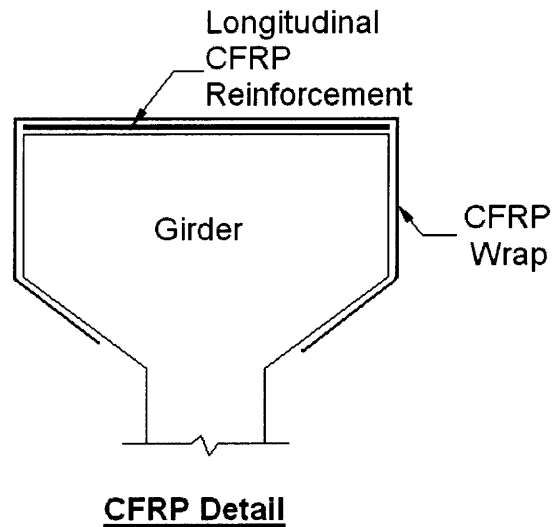
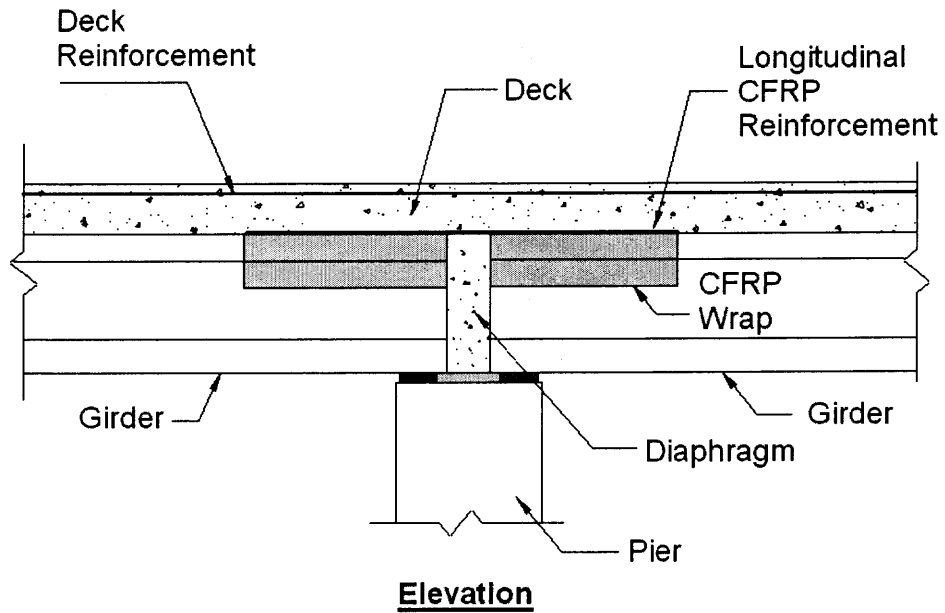


Figure 5.29 The proposed new continuity connection.

NOTES:

1. Construction includes the following steps:
 - Erect girders as simple spans.
 - Cast the diaphragm.

- Attach longitudinal CFRP reinforcement on the top of the girders and wrap in the transverse direction (see notes 2-6). Do not disturb for 24 hours.
 - Install forms and reinforcements for the deck slab.
 - Cast deck when the epoxy resin is at least seven days old.
2. Sandblast or use other approved mechanical means to prepare the concrete surface before CFRP application. The surface should be clean and even, free of water, dust, grease, curing compounds and other bond inhibiting materials. Uneven surfaces must be filled with an appropriate repair mortar.
 3. Provide 1/8" transverse grooves every 3" on the concrete surface over the length of the CFRP. This can be done during manufacturing of the girders.
 4. Flexible CFRP fabric should be used. Design to determine thickness, width and length of the fabric.
 5. The longitudinal CFRP reinforcement should be wrapped in the transverse direction by similar fabric.
 6. The diaphragm should not be bonded to the fabric.

CHAPTER 6

CONCLUSIONS

6.1 Summary

Based on a survey of the state departments of transportation in the U.S. and a literature review, the current practice concerning bridges composed of simple-span precast prestressed concrete girders made continuous is evaluated. Three bridges in New Jersey were instrumented and tested. Results show that the degree of continuity ranges from 0% to 90%. A comparison of the support details of these bridges suggests that anchor bolts be sheathed to allow for free rotation of the girders and prevent damage of the continuity diaphragm because of anchor bolt pull-out.

A computer program called "CONTINUITY" is developed to analyze the restraint moments and the degree of continuity of bridges up to four continuous spans with unequal span lengths. The program takes into account concrete creep and shrinkage and prestressing strand relaxation. For concrete creep and shrinkage, users can choose from three different models: ACI-209, CEB-FIP and HPC. Support details and cracking of the composite girder and diaphragm sections are also considered in the program.

Three-dimensional finite element analyses have been carried out to further study factors affecting restraint moments. The study confirms that the girder age at continuity plays a vital role in developing the restraint moments and that the amount of positive moment reinforcement at the support has a negligible effect on the resultant mid-span moment.

As part of this research a new continuity connection is developed using CFRP

composites. By making the girders continuous for slab self-weight as well, the additional negative moment over the continuity support can counteract the positive restraint moment and limit it below the cracking moment. Thus, cracks will not form in the diaphragm and positive moment reinforcement is not needed. Twenty laboratory tests were carried out to validate the new continuity connection. Results show that CFRP is effective for improving the continuity and performance of bridges of this type. Recommendations for the use of CFRP reinforcement and a design example are presented.

6.2 Conclusions

From the analytical and experimental studies discussed above, the following conclusions can be drawn:

1. The degree of continuity under service load varies dramatically for bridges composed of simple-span precast prestressed concrete girders made continuous. For the three bridges tested, it ranges from 0% to 90%.
2. Embedding the girders in the diaphragm, using thin elastomeric pads that has little lateral deformation capacity and providing anchor bolts at each girder line make the supports more like “fixed”. The fixity restrains the girders from sliding and rotating, and causes cracking in the diaphragm and even in the top flange of the girders.
3. Possible improvements for the current design include: a) debond the girder ends or not embed them at all; b) avoid using anchor bolts, or if needed put them in the diaphragm between stringers and sheath them to allow for free rotation of the girders and prevent damage to the diaphragm due to anchor bolt pull-out; c) it is preferable to design only one “pin” support (fixed both vertically and horizontally) for continuous spans to allow for longitudinal deformation. If more than one pin is provided, design shall account for all the longitudinal forces including temperature changes, axial creep of the prestressed girders, shrinkage of the concrete, wind on live load and wind on structures, etc.
4. U-shaped positive moment connections don't perform as well as expected, at least in a sense of serviceability, especially when the horizontal development length is inadequate. Per PCA test results, it is recommended that welded connections be used for the positive moment reinforcement. Another approach would be to make the

girders continuous for slab dead load and avoid providing the positive moment reinforcement in the diaphragm.

5. Finite element analyses confirm that the amount of positive moment reinforcement over the pier has negligible effect on the resultant mid-span moments.
6. Finite element analyses show that the girder age at continuity has a significant influence on restraint moment induced by time dependent effects.
7. The computer program CONTINUITY developed under this study is an effective tool for engineers to check the restraint moments caused by time dependent effects and to examine the degree of continuity of simple span girders made continuous.
8. For the external flexural strengthening of plain concrete members, the bond between the concrete and the reinforcement is the most critical element. Flexible CFRP materials should be used. Rigid CFRP laminates may lead to premature failure because of debonding. The CFRP fabric sheet is an ideal material based on this study.
9. Wrapping and surface preparation (specially grooves) have a significant effect against debonding.
10. The load carrying capacity increases with the number of CFRP layers used. However the efficiency of the CFRP reinforcement diminishes with the use of additional layers.
11. The load carrying capacity also increases with the CFRP bonding length until it reaches the effective bonding length, beyond which no more load can be gained.
12. By making the girders continuous for slab dead load as well, the additional negative moment over the support can counteract the positive restraint moment and limit it below the positive cracking moment of the section, therefore eliminate diaphragm cracking. Although more in-field tests are needed before its widespread application, the laboratory tests support the concept of making the girders continuous for slab dead load in addition to live load using CFRP composites.

6.3 Recommended Research

This research focuses on the flexural performance of bridges composed of simple-span precast prestressed concrete girders made continuous under static loads. The behavior of this kind of construction under earthquake and fatigue load still needs further study. The

program CONTINUITY assumes that the AASHTO lane loading controls for all cases. The AASHTO truck loading needs to be added to the program.

After the group I laboratory tests, efforts were focused on group II tests using CFRP fabric sheets. It is suggested that the bond-improving techniques used in group II tests, making transverse grooves on the concrete surface and wrapping, also be used for group I tests and further investigate the possibility of using CFRP strips.

The laboratory tests validated the concept of making the girders continuous for slab dead load using CFRP composites. In the group II tests, the small beams strengthened with 2" wide CFRP sheets developed 100% of their capacity while the larger beams using 6" wide CFRP sheets only developed 80% ~ 85% of their capacity. More large-scale and full-scale tests will shed more light on the size-effect or width-effect of the CFRP reinforcement.

REFERENCES

1. Saadehvaziri, M. A., Spillers, W. R., and Yin, L., "Improvement of Continuity Connections over Fixed Piers" Interim Report to New Jersey Department of Transportation, Aug. 2002, 25 pp.
2. Kaar, P. H., Kriz, L. B., and Hognestad, E., "Precast-Prestressed Concrete Bridges, 1. Pilot Tests of Continuous Girders." J. PCA Res. and Dev. Laboratories, Vol. 2, No. 2, May 1960, pp. 21-37.
3. Hanson, N. W., "Precast-Prestressed Concrete Bridges, 2. Horizontal Shear Connections." J. PCA Res. and Dev. Laboratories, Vol. 2, No. 2, May 1960, pp. 38-58.
4. Mattock, A. H., and Kaar, P. H., "Precast-Prestressed Concrete Bridges, 3. Further Tests of Continuous Girders." J. PCA Res. and Dev. Laboratories, Vol. 2, No. 3, Sep. 1960, pp. 51-78.
5. Kaar, P. H., and Mattock, A. H., "Precast-Prestressed Concrete Bridges, 4. Shear Tests of Continuous Girders." J. PCA Res. and Dev. Laboratories, Vol. 3, No. 1, Jan. 1961, pp. 19-46.
6. Mattock, A. H., "Precast-Prestressed Concrete Bridges, 5. Creep and Shrinkage Studies." J. PCA Res. and Dev. Laboratories, Vol. 3, No. 2, May 1961, pp. 32-66.
7. Mattock, A. H., and Kaar, P. H., "Precast-Prestressed Concrete Bridges, 6. Tests of a Half-Scale Highway Bridge Continuous over Two Spans." J. PCA Res. and Dev. Laboratories, Vol. 3, No. 3, Sep. 1961, pp. 30-70.
8. Freyermuth, C. L., "Design of Continuous Highway Bridges with Precast, Prestressed Concrete Girders." Journal of Prestressed Concrete Institute, Apr. 1969, pp. 14-39.
9. Suttikan, C., "A Generalized Solution for Time-dependent Response and Strength of Noncomposite and Composite Prestressed Concrete Beams". Ph.D. Dissertation, Univ. of Texas at Austin, 1978.
10. Oesterle, R. G., Glikin, J. D., and Larson, S. C., "Design of Precast Prestressed Bridge Girders Made Continuous". National Cooperative Highway Research Program-Report 322, Nov. 1989, 97 pp .

11. Mirmiran, A., Kulkarni, S., Castrodale, R., Miller, R., and Hastak, M., "Nonlinear Continuity Analysis of Precast, Prestressed Concrete Girders with Cast-in-place Decks and Diaphragms." J. PCI, Sep.-Oct. 2001, pp. 60-80.
12. Bishara, A. G. and Mahmoud, M. H., "Continuous Prestressed Concrete Girders With Keyed Scarf Connections" ACI Journal, Sep. 1972, pp. 569-577.
13. Bishop, E. D., "Continuity Connection for Precast Prestressed Concrete Bridges". ACI Journal, Apr. 1962, pp. 585-599.
14. Saleh, M. A., Einea, A., and Tadros, M. K., "Creating Continuity in Precast Prestressed Girder Bridges". Concrete International, Aug. 1995, pp. 27-32.
15. Tadros, M. K., Ficenec, J. A., Einea, A., and Holdsworth, S., "A New Technique to Create Continuity in Prestressed Concrete Members". PCI Journal, Sep.-Oct. 1993, pp. 30-37.
16. Ma, Z., Huo, X., Tadros, M. K., and Baishya, M., "Restraint Moments in Precast Prestressed Concrete Continuous Bridges." PCI Journal, Nov.-Dec. 1998, pp. 40-57.
17. Englekirk, R. E., "An innovative Design Solution for Precast Prestressed Concrete Buildings in High Seismic Zones". PCI Journal, July-Aug. 1996, pp. 44-53.
18. American Association of State Highway and Transportation Officials, "Standard Specifications for Highway Bridges" 15th Edition, 1992.
19. American Association of State Highway and Transportation Officials, "LRFD Bridge Design Specifications" 1st Edition, 1994.
20. New Jersey Dept. of Transportation, "Design Manual – Bridges and Structures" 3rd Edition, 1998.
21. The Market Development Alliance of the FRP Composites Industry, "Product Selection Guide: FRP Composite Products for Bridge Applications", First Edition, 2000.
22. M. Tavakkolizadeh, and H. Saadatmanesh, "Strengthening of Steel-Concrete Composite Girders Using Carbon Fiber Reinforced Polymers Sheets." Journal of Structural Engineering, Jan. 2003, pp. 30-40.
23. American Concrete Institute Committee 440, Guide for the Design and Construction of Externally Bonded FRP Systems for Strengthening Concrete Structures, 2002, 45 pp.

24. American Concrete Institute Committee 440, State-of-the-Art Report on Fiber Reinforced Plastic (FRP) Reinforcement for Concrete Structures, 1996, 67 pp.
25. De Lorenzis, L., Miller, B. and Nanni, A., "Bond of FRP Laminates to Concrete", ACI Materials Journal, Vol.98, No. 3, May-June 2001, pp. 256-264.
26. Muller, H. S., "New Prediction Models for Creep and Shrinkage of Concrete", Creep and Shrinkage of Concrete: Effect of Materials and Environment, ACI SP-135, 1992, pp. 1-18.
27. Dilger W. H., and Wang, C., "Creep and Shrinkage of High-Performance Concrete", The Adam Neville Symposium: Creep and Shrinkage – Structural Design Effects, ACI SP-194, 2000, pp. 361-379.
28. Miller, R. A., Castrodale, R., Mirmiran, A. and Hastak, M., Connection between Simple Span Precast Concrete Girders Made Continuous, Final Report, National Cooperative Highway Research Program, Project 12-53, Oct. 2003, 97 pp.
29. Chandrupatla, T. R. and Belegundu, A. D., Introduction to Finite Elements in Engineering, 2nd Edition, Prentice Hall, 1997, 461 pp.
30. Sika Corporation, Retrieved Aug. 24, 2003 from the World Wide Web: <http://www.sikaconstruction.com/con/con-prod.htm>.
31. Thorenfeldt, E., Tomaszewicz, A., and Jensen, J.J., "Mechanical Properties of High-Strength Concrete and Application in Design," Proceedings of the Symposium "Utilization of High Strength Concrete," Stavanger, Norway, June 1987, pp. 149-159.
32. PCI Committee on Prestress Losses, "Recommendation for Estimating Prestress Losses." J. Prestressed Concrete Institute, Vol. 20, No. 4 (July-Aug. 1975) pp. 44-75.